

## **The SAS4A/SASSYS-1 Safety Analysis Code System**

---

**Nuclear Engineering Division**

### **About Argonne National Laboratory**

Argonne is a U.S. Department of Energy laboratory managed by UChicago Argonne, LLC under contract DE-AC02-06CH11357. The Laboratory's main facility is outside Chicago, at 9700 South Cass Avenue, Argonne, Illinois 60439. For information about Argonne, see <http://www.anl.gov>.

### **Availability of This Report**

This report is available, at no cost, at <http://www.osti.gov/bridge>. It is also available on paper to the U.S. Department of Energy and its contractors, for a processing fee, from:

U.S. Department of Energy  
Office of Scientific and Technical Information  
P.O. Box 62  
Oak Ridge, TN 37831-0062  
phone (865) 576-8401  
fax (865) 576-5728  
[reports@adonis.osti.gov](mailto:reports@adonis.osti.gov)

### **Disclaimer**

This report was prepared as an account of work sponsored by an agency of the United States Government. Neither the United States Government nor any agency thereof, nor UChicago Argonne, LLC, nor any of their employees or officers, makes any warranty, express or implied, or assumes any legal liability or responsibility for the accuracy, completeness, or usefulness of any information, apparatus, product, or process disclosed, or represents that its use would not infringe privately owned rights. Reference herein to any specific commercial product, process, or service by trade name, trademark, manufacturer, or otherwise, does not necessarily constitute or imply its endorsement, recommendation, or favoring by the United States Government or any agency thereof. The views and opinions of document authors expressed herein do not necessarily state or reflect those of the United States Government or any agency thereof, Argonne National Laboratory, or UChicago Argonne, LLC.

## **The SAS4A/SASSYS-1 Safety Analysis Code System**

### **Chapter 8:**

### **DEFORM-4: Steady-State and Transient Pre-Failure Pin Behavior**

---

Nuclear Engineering Division  
Argonne National Laboratory

January 31, 2012



## TABLE OF CONTENTS

	<u>Page</u>
NOMENCLATURE .....	8-vii
<b>8.0 DEFORM-4: STEADY-STATE AND TRANSIENT PRE-FAILURE PIN BEHAVIOR</b> .....	<b>8-1</b>
8.1 Overview and General Background .....	8-1
8.1.1 Objectives, General Background, and General Physical Description .....	8-1
8.1.2 Interaction with other SAS4A Models .....	8-9
8.2 Fuel-pin Mechanics .....	8-11
8.2.1 Solid Fuel and Cladding Thermoelastic Solution .....	8-13
8.2.2 Cracked Fuel Thermoelastic Solution and Crack Volume .....	8-21
8.2.3 Fully Cracked Fuel .....	8-26
8.2.4 Axial Expansion Solution .....	8-28
8.3 Fuel-pin Phenomenology .....	8-33
8.3.1 As-fabricated Porosity Migration .....	8-33
8.3.2 Grain Growth .....	8-39
8.3.2.1 Unlimited Grain Growth - Equiaxed Region .....	8-40
8.3.2.2 Limited Grain Growth - Equiaxed Region .....	8-42
8.3.2.3 Columnar Grain Size and Region Boundaries .....	8-44
8.3.3 Fission-gas Release .....	8-45
8.3.3.1 Fission-gas Generation .....	8-46
8.3.3.2 Isotropic Fission-gas Release .....	8-50
8.3.3.3 Fission-gas Trap-release Model .....	8-51
8.3.4 Fuel Swelling .....	8-54
8.3.4.1 Nonequilibrium Fission-gas Bubbles .....	8-55
8.3.4.2 Solid Fission-product Swelling .....	8-63
8.3.5 Irradiation-induced Cladding Swelling .....	8-64
8.3.6 Fission-gas Plenum Pressure .....	8-68
8.3.7 Molten Cavity Pressurization .....	8-72
8.3.7.1 Incremental Melt Fraction Ratio .....	8-73
8.3.7.2 Gas Release on Melting .....	8-77
8.3.7.2.1 Central Void Considerations .....	8-77
8.3.7.2.2 Grain Boundary Gas .....	8-77
8.3.7.2.3 Intra-Granular Gas .....	8-79
8.3.7.2.4 As-Fabricated Gas .....	8-82
8.3.7.2.5 Fuel Crack Gas .....	8-83
8.3.7.3 Fuel Volume Changes .....	8-84
8.3.7.4 Molten Cavity Pressure .....	8-86
8.3.7.5 Fuel Vapor Pressure .....	8-88

TABLE OF CONTENTS (Cont'd)

	<u>Page</u>
8.3.8 Fuel-cladding Gap Conductance . . . . .	8-89
8.3.8.1 Modified Ross-Stoute Gap Conductance Model . . . . .	8-89
8.3.8.1.1 Radiative Heat Transfer . . . . .	8-90
8.3.8.1.2 Conduction Heat Transfer . . . . .	8-92
8.3.8.1.3 Solid-to-solid Heat Transfer . . . . .	8-96
8.3.8.1.4 Total Gap Heat-transfer Coefficient . . . . .	8-98
8.3.8.2 SAS3D Parametric Model . . . . .	8-99
8.3.8.3 SAS3D Simple Model . . . . .	8-100
8.3.9 Fuel Axial Expansion Reactivity Model . . . . .	8-101
8.3.9.1 Free Fuel Expansion Controlled Feedback . . . . .	8-102
8.3.9.2 Free Cladding Expansion Controlled Feedback . . . . .	8-102
8.3.9.3 Constrained Fuel/Cladding Expansion Controlled Feedback . . . . .	8-103
8.3.10 Metal Fuel Modeling . . . . .	8-104
8.3.10.1 Fission Gas Behavior . . . . .	8-104
8.3.10.1.1 Closed and Connected Porosity Description . . . . .	8-105
8.3.10.1.2 Fission Gas Release . . . . .	8-106
8.3.10.2 Metal Fuel Behavior During Melting . . . . .	8-108
8.3.10.2.1 Molten Cavity . . . . .	8-108
8.3.10.2.2 Connected Porosity . . . . .	8-109
8.3.10.2.3 Closed Porosity . . . . .	8-109
8.3.10.3 Axial Extrusion in Solid Fuel . . . . .	8-110
8.3.10.3.1 Fission Gas Induced Swelling . . . . .	8-110
8.3.10.3.2 Axial Swelling Fraction . . . . .	8-112
8.3.10.4 Sodium Bond . . . . .	8-113
8.4 Fuel-pin Failure Criteria . . . . .	8-115
8.4.1 Input Specified Failure Criteria . . . . .	8-116
8.4.2 Calculated Failure Correlations . . . . .	8-117
8.4.2.1 Biaxial Stress Rupture . . . . .	8-117
8.4.2.2 Burst Pressure . . . . .	8-118
8.4.2.3 Transient Burst Temperature . . . . .	8-119
8.4.2.4 Larson-Miller Life Fraction . . . . .	8-119
8.4.3 Preliminary Metal Fuel Failure Criteria . . . . .	8-121
8.4.4 Failure Modeling Coupling to Fuel Motion Models . . . . .	8-123
8.4.5 Time-step Control on Approach to Failure . . . . .	8-126
8.5 General Method of Solution . . . . .	8-128
8.5.1 Thermal-mechanical Solution . . . . .	8-133
8.5.2 Plastic Fuel Deformation Solution . . . . .	8-139
8.5.3 Final DEFORM-4 Calculations . . . . .	8-140
8.6 Computer Code Implementation . . . . .	8-140
8.6.1 Subroutine and Function List . . . . .	8-141
8.6.2 Input Variables . . . . .	8-142

## TABLE OF CONTENTS (Cont'd)

		<u>Page</u>
	8.6.3 Output Specific to DEFORM-4 .....	8-149
8.7	Material Properties .....	8-151
	8.7.1 Mixed Oxide Fuel Density .....	8-151
	8.7.2 Mixed Oxide Fuel Thermal Expansion Coefficient .....	8-165
	8.7.3 Mixed Oxide Fuel Modulus of Elasticity .....	8-167
	8.7.4 Mixed Oxide Fuel Thermal Conductivity .....	8-168
	8.7.5 Mixed Oxide Fuel Fracture Strength .....	8-171
	8.7.6 Mixed Oxide Fuel Creep Rate .....	8-171
	8.7.7 Cladding Thermal Expansion Coefficient .....	8-172
	8.7.8 Cladding Modulus of Elasticity .....	8-173
	8.7.9 Cladding Ultimate Tensile Strength .....	8-173
	8.7.10 Cladding Flow Stress .....	8-174
	8.7.11 Thermal Conductivity of Helium .....	8-179
	8.7.12 Thermal Conductivity of Fission Gas .....	8-180
	8.7.13 Mixed Oxide Fuel Hardness .....	8-180
	8.7.14 Cladding Hardness .....	8-181
	8.7.15 Cladding Fast Creep .....	8-181
	8.7.16 Material Properties of Metal Alloy Fuel .....	8-182
	8.7.16.1 Modulus of Elasticity .....	8-182
	8.7.16.2 Poisson's Ratio .....	8-182
	8.7.16.3 Fracture Strength .....	8-183
	8.7.16.4 Fuel Creep Rate .....	8-183
	REFERENCES .....	8-185

## LIST OF FIGURES

		<u>Page</u>
8.1-1	Schematic of SAS4A Channel Discretization . . . . .	8-3
8.1-2	DEFORM-4 Axial Segmentation with Possible Fuel-cladding Interactions . . . . .	8-4
8.1-3	Radial Cell Construction Options . . . . .	8-5
8.1-4	Relationship Between SAS4A and DEFORM-4 Cells and Cell-boundaries . . . . .	8-6
8.1-5	DEFORM-4 Mechanical and Phenomenological Considerations and Their Interactions . . . . .	8-7
8.2-1	DEFORM-4 Radial Zones . . . . .	8-12
8.3-1	DEFORM-4 Fission Gas Parameter FGMIN . . . . .	8-57
8.3-2	Geometry of the Fuel-cladding Gap . . . . .	8-91
8.3-3	Effect of Fuel Swelling on Fission Gas Release in Metal Fuels . . . . .	8-107
8.5-1	DEFORM-4 - SAS4A Time Step Interaction Scheme . . . . .	8-129
8.5-2	Pretransient DEFORM-4 Driver (SSFUEL) Flow Chart . . . . .	8-130
8.5-3	Transient DEFORM-4 Driver (DEFORM3) Flow Chart . . . . .	8-131
8.5-4	DEFORM-4 Mechanics Driver (DEFORM) Flow Chart . . . . .	8-134
8.5-5	DEFORM-4 Mechanics Interaction Solutions (SOLID) Flow Chart . . . . .	8-135
8.5-6	DEFORM-4 Mechanics Interaction Solution with Fully Cracked Fuel (MKDRIV) Flow Chart . . . . .	8-138
8.6-1	SAS4A Steady-state Coolant Condition Output . . . . .	8-152
8.6-2	SAS4A Fuel Temperature and Node Location Map . . . . .	8-153
8.6-3	SAS4A Fuel-pin Condition Summary Output . . . . .	8-154
8.6-4	DEFORM-4 Radial Stress Map . . . . .	8-155
8.6-5	DEFORM-4 Circumferential Stress Map . . . . .	8-156
8.6-6	DEFORM-4 Axial Stress Map . . . . .	8-157
8.6-7	DEFORM-4 Fission-gas Retention Fraction Map . . . . .	8-158
8.6-8	DEFORM-4 Total Porosity Fraction Map . . . . .	8-159
8.6-9	DEFORM-4 Fission-gas-induced Porosity Fraction Map . . . . .	8-160
8.6-10	DEFORM-4 Fuel Grain Size Map . . . . .	8-161
8.6-11	DEFORM-4 Fuel Crack Volume Fraction Map . . . . .	8-162
8.6-12	DEFORM-4 Radial Node Locations . . . . .	8-163
8.6-13	DEFORM-4 Short Form Pin Summary Output . . . . .	8-164

## LIST OF TABLES

		<u>Page</u>
8.3-1	Comparison Between Oxide and Metal Fuel Models for Fission Gas Porosity Behavior . . . . .	8-109
8.4-1	Failure Initiation Options . . . . .	8-116
8.6-1	DEFORM-4 Associated Subroutines and Functions . . . . .	8-141
8.6-2	DEFORM-4 Input Variables . . . . .	8-142

## NOMENCLATURE

<u>Symbols</u>	<u>Definition</u>	<u>Units</u>
A, A <sub>h</sub>	Axial segment length	m
B	Burnup	atom %
C <sub>r</sub>	Calibration constant for metal fuel bubble radius	
D	Grain size	m
E	Modulus of elasticity	Pa
E <sub>c</sub>	Energy of the cladding J/kg	
E <sub>f</sub>	Modulus of Elasticity of the fuel	Pa
F	Force	N
F <sub>as</sub>	Fraction of volume change occurring axially	
F <sub>f</sub>	Failure fraction	
f	Mole fraction	
G <sub>f</sub>	Fission gas retained in fuel cell	kg
G <sub>r</sub>	Fission gas released from fuel cell	kg
G <sub>t</sub>	Total fission gas produced in fuel cell	kg
g	Thermal jump distance	m
H	Hardness of cladding	Pa
H <sub>sp</sub>	Height of sodium in the plenum	m
h	Heat-transfer coefficient	W m <sup>-2</sup> K <sup>-1</sup>
K	Bulk modulus	Pa
k	Thermal conductivity	W m <sup>-1</sup> K <sup>-1</sup>
M	Molecular weight, g mole, or Mass	kg
M <sub>s,j</sub>	Mass of sodium in fuel-cladding gap in axial segment j	kg
M <sub>s,l</sub>	Mass of sodium loaded into the fuel pin	kg
M <sub>sp</sub>	Mass of sodium in the plenum region	kg
M <sub>st</sub>	Total mass of sodium in the fuel-cladding gap	kg
n	Number of moles	
P	Pressure	Pa
P <sub>cav</sub>	Molten cavity pressure	Pa

## NOMENCLATURE (Cont'd)

<u>Symbols</u>	<u>Definition</u>	<u>Units</u>
$P_{ext}$	Coolant channel pressure	Pa
$P_{fci}$	Fuel-cladding interface pressure	Pa
$p$	Porosity fraction	
$R$	Universal gas constant	$J K^{-1}g\text{-mole}^{-1}$
$R_B$	Fission gas bubble radius	m
$R_c$	Fuel creep rate	$s^{-1}$
$R_f$	Fission gas release fraction	
$r$	Radius	m
$r_{cav}$	Radius of central molten cavity	m
$r_{ci}$	Inner radius of the cladding	m
$r_{co}$	Outer cladding radius	m
$r_{c1}$	Outer boundary of SAS4A inner cladding cell	m
$r_{c2}$	Outer boundary of SAS4A central cladding cell	m
$r_{fo}$	Outer fuel radius	m
$r_p$	Inner cladding radius in the plenum	m
$S_f$	Volumetric swelling fraction	
$T$	Temperature	K
$T_a$	Average temperature	K
$T_{cc}$	Temperature of cladding center	K
$T_{ci}$	Inner cladding temperature	K
$T_{co}$	Outer cladding temperature	K
$T_{c1}$	Temperature of PLUTO2/LEVITATE inner cladding node	K
$T_{eut}$	Eutectic temperature	$^{\circ}C$
$T_f$	Time to failure	s
$t$	Time	s
$U$	Velocity	$m s^{-1}$
$U_{ts}$	Ultimate tensile strength	Pa
$u$	Radial displacement	m

## NOMENCLATURE (Cont'd)

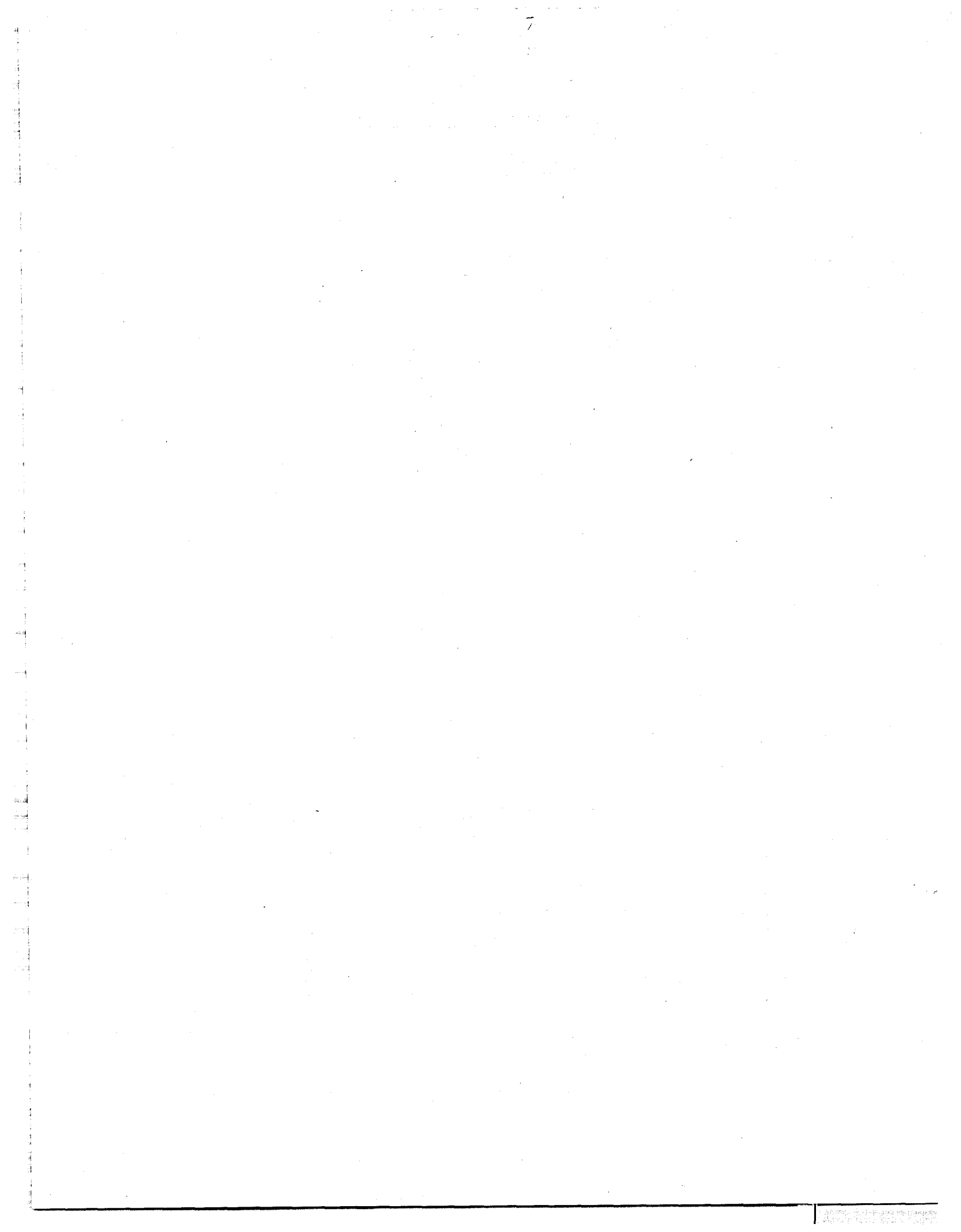
<u>Symbols</u>	<u>Definition</u>	<u>Units</u>
V	Volume	m <sup>3</sup>
V <sub>c</sub>	Volume of a cell	m <sup>3</sup>
V <sub>f</sub>	Volume of fission gas in closed porosity	m <sup>3</sup>
V <sub>r</sub>	Volume of fission gas moved from closed to open porosity	m <sup>3</sup>
ΔV <sub>a</sub>	Axial volume change	m <sup>3</sup>
ΔV <sub>exc</sub>	Volume of excess radial fuel swelling	m <sup>3</sup>
ΔV <sub>r</sub>	Radial volume change	m <sup>3</sup>
V <sub>th</sub>	Theoretical volume of material in a cell	m <sup>3</sup>
v	Circumferential displacement	m
W	Weighting factor	
z <sub>o</sub>	Radially constant axial strain	
Z	Axial elevation	m
α	Thermal-expansion coefficient	K <sup>-1</sup>
γ	Surface tension	N m <sup>-1</sup>
Δt	Time-step length	s
δ	Mean surface roughness	m
ε	Strain or emissivity	
η	Outer radius of solid fuel annulus	m
ρ	Inner radius of solid fuel annulus or density	m kg m <sup>-3</sup>
ρ <sub>s,j</sub>	Density of sodium in fuel-cladding gap in axial segment j	kg m <sup>-3</sup>
ρ <sub>sp</sub>	Density of sodium in the plenum	kg m <sup>-3</sup>
ν	Poisson's ratio	
φ	Neutron flux	n m <sup>-2</sup> s <sup>-1</sup>
σ	Stress, Pa, or Stefan-Boltzmann constant	J s <sup>-1</sup> m <sup>-2</sup> k <sup>-4</sup>
σ <sub>c</sub>	Circumferential stress in cladding	Pa
Y	Time constant, s <sup>-1</sup> , or incubation parameter	n/m <sup>2</sup>
Σ	Negative fractional density change in the cladding	

## NOMENCLATURE (Cont'd)

<u>Symbols</u>	<u>Definition</u>	<u>Units</u>
<u>Superscripts</u>		
f	Force component	
th	Thermal component	
p	Plenum	
v	Central fuel void	
<u>Subscripts</u>		
r	Radial or reference	
$\theta$	Circumferential	
z	Axial	
f	Force or fuel	
th	Thermal	
$\rho$	Inner radius of the solid fuel annulus	
$\eta$	Outer radius of the solid fuel annulus	
g	Plenum gas or fuel-cladding gap	
FC	Fuel-cladding interface	
c	Cladding	
m	Maximum	
k	Iteration counter	
i	Time step or radial node	
j	Axial node	
B	Bubble	
fg	Fission gas	
s	Swelling	
v	Central fuel void	
p	Plenum or pore	
He	Helium	
T	Total	
R	Reference	

## NOMENCLATURE (Cont'd)

<u>Symbols</u>	<u>Definition</u>	<u>Units</u>
cav	Molten cavity	
mc	Melting of cladding	



## 8.0 DEFORM-4: STEADY-STATE AND TRANSIENT PRE-FAILURE PIN BEHAVIOR

### 8.1 Overview and General Background

#### 8.1.1 Objectives, General Background, and General Physical Description

The response of LMFBR fuel pins to transient accident conditions is an important safety concern. For transients leading to pin failure, the failure modes and initial fuel disruption depend in part on pre-transient irradiation effects, such as restructuring, fission-gas retention, fuel-cladding gap, central void size and makeup. As the transient fuel-pin models develop, an increasingly rigorous pre-transient characterization of the fuel pin is also required. For this reason, an effort has been made to integrate a detailed treatment of the pre-transient fuel-pin characterization into SAS4A. At the same time, an attempt has been made to assure that the models are consistent with the transient calculation and, where possible, to develop models in such a manner that they can be used in both the pre-transient and transient calculations.

Because the phenomena affecting fuel-pin integrity are not all well understood, most performance codes use one of two methods to predict the pin characterization: (1) empirical correlations derived from a data base of experimentally determined information, or (2) a phenomenological description of the process that contains parameters that need to be calibrated to experiments or the information data base. Care must be exercised with both approaches, but especially with the former method, because unrealistic values can be obtained if the pin conditions fall outside the correlation data base. In the phenomenological (or mechanistic) approach the attempt is made to model the physical process taking place and then calibrate this to available data. Since the model attempts to describe the physical processes, it is possible to extrapolate the response to conditions outside the calibration data base with greater assurance than with the correlation approach. It was, therefore, decided that this mechanistic approach would be adopted wherever possible in the DEFORM-4 module of SAS4A.

This approach is different from that used by earlier versions of the SAS codes [8-1 - 8-4]. The former versions contained a very brief steady-state calculation of one time step at constant power and used correlations to determine the parameters necessary to start the transient

calculation. The DEFORM-4 module simulates the pre-transient irradiation with a series of power changes and power levels of various time lengths. This provides the means to account for the reactor operating history and its effect on the physical state of the fuel pin, and leads to a more realistic description of the fuel pins subjected to the transient.

The pin is divided into a number of axial segments ( $\leq 24$ ) of arbitrary length. If either the PLUTO2 or LEVITATE failed pin modeling is used, then there will be restrictions on the "arbitrariness" of these lengths (see Chapters 14 and 16). The fuel and cladding are assumed to occupy the same axial segment. Figure 8.1-1 shows an example of the axial and radial discretization for a fuel pin with an upper fission-gas plenum. The DEFORM-4 module is concerned with the axial region containing the driver fuel, axial blankets, and the fission-gas plenum. The core region, i.e., driver and axial blanket fuel segments, is shown in Fig. 8.1-2. Illustrated are the three fuel-cladding gap conditions considered: (1) no contact between the fuel and cladding, (2) the fuel elastically straining the cladding, and (3) the fuel plastically straining the cladding. Also illustrated is a central cavity that formed in the hotter regions of the driver fuel.

The fuel in an axial segment is divided into a series of radial cells ( $\leq 11$ ). The radial cell boundaries may be determined on the basis of equal mass in each, except the inner and outer cells which contain half the mass of a regular cell, or with each cell thickness being equal, again except for the inner and outer cell which have half the nominal thickness (see Fig. 8.1-3). The cladding is divided into two radial cells. The relationship between the general SAS4A cell structure and temperature locations and those used in DEFORM-4 is indicated in Fig. 8.1-4. In the fuel region, the temperatures used by some DEFORM-4 calculations (refer to the specific models described below) are obtained by averaging the two SAS4A temperatures on either side of the radial cell boundary. Where the property being considered is an average over the annular cell, such as porosity, modulus of elasticity, conductivity, etc., the actual temperatures calculated by the thermal models in SAS4A are used.

A number of phenomena are treated in the pre-transient irradiation calculation. These are shown in Fig. 8.1-5. Detailed descriptions are given in the following sections, but a brief outline is presented here. These major models include:

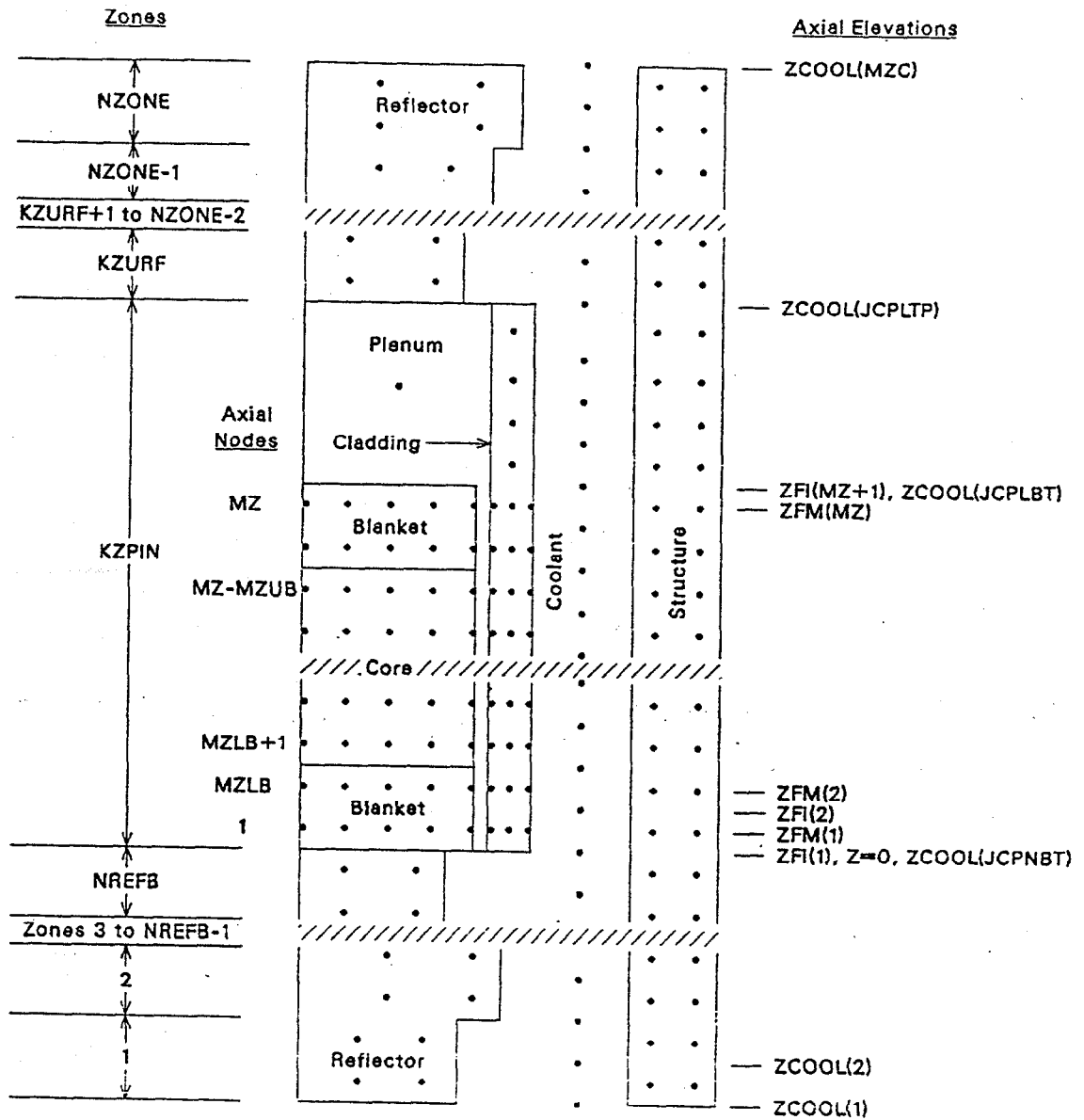


Fig. 8.1-1. Schematic of SAS4A Channel Discretization

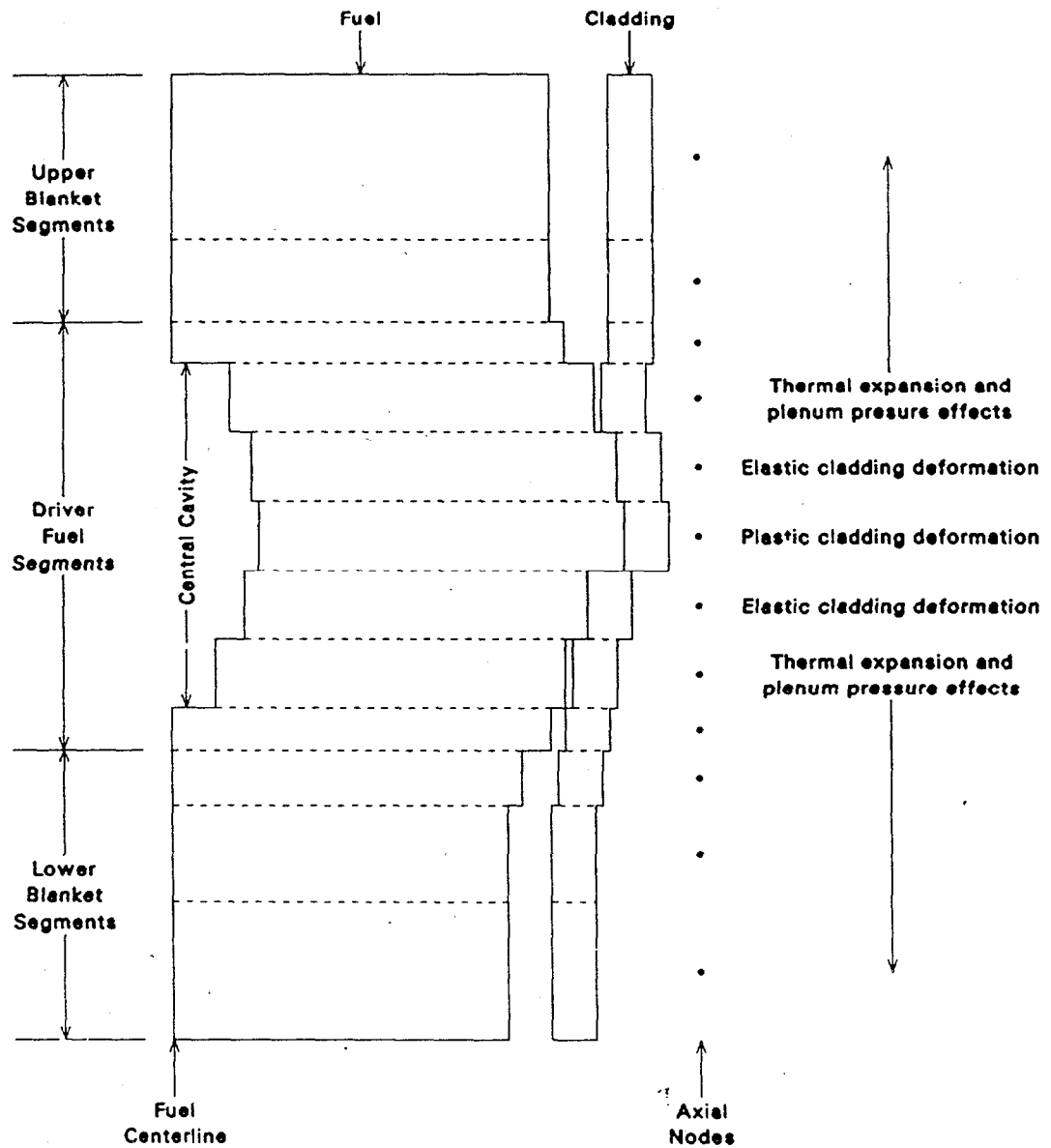
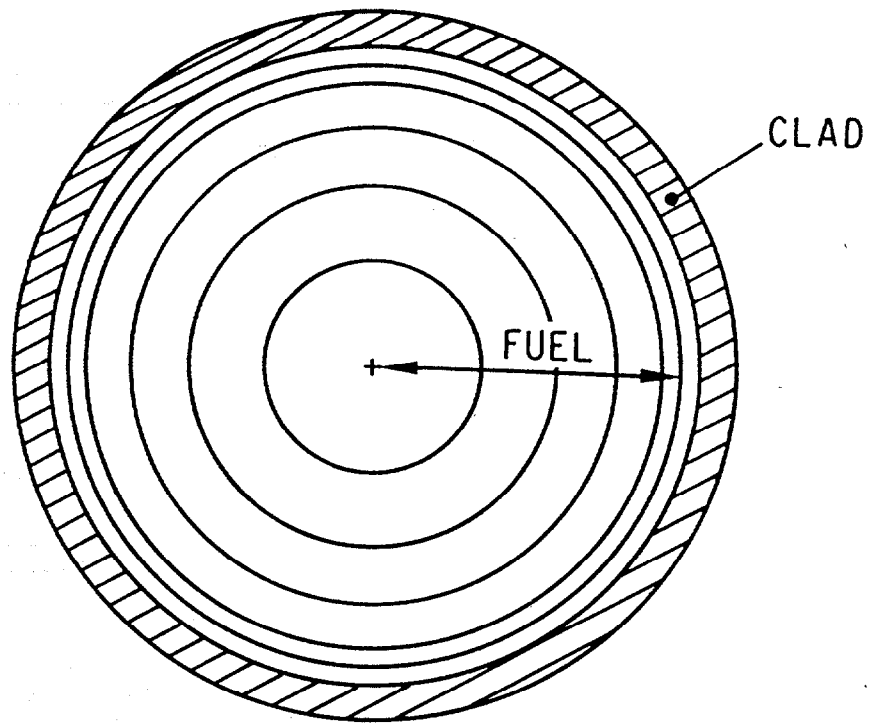
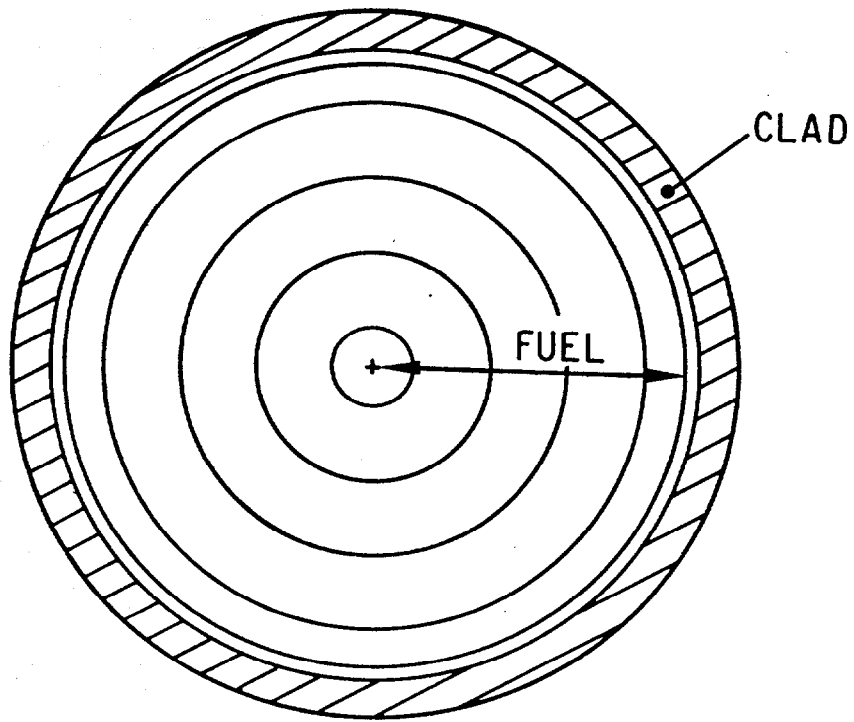


Fig. 8.1-2. DEFORM-4 Axial Segmentation with Possible Fuel-cladding Interactions



EQUAL MASS NODES



EQUAL  $\Delta r$  NODES

Fig. 8.1-3. Radial Cell Construction Options

EXAMPLE OF SAS4A AND DEFORM NODE STRUCTURE WITH NT = 5

9-8

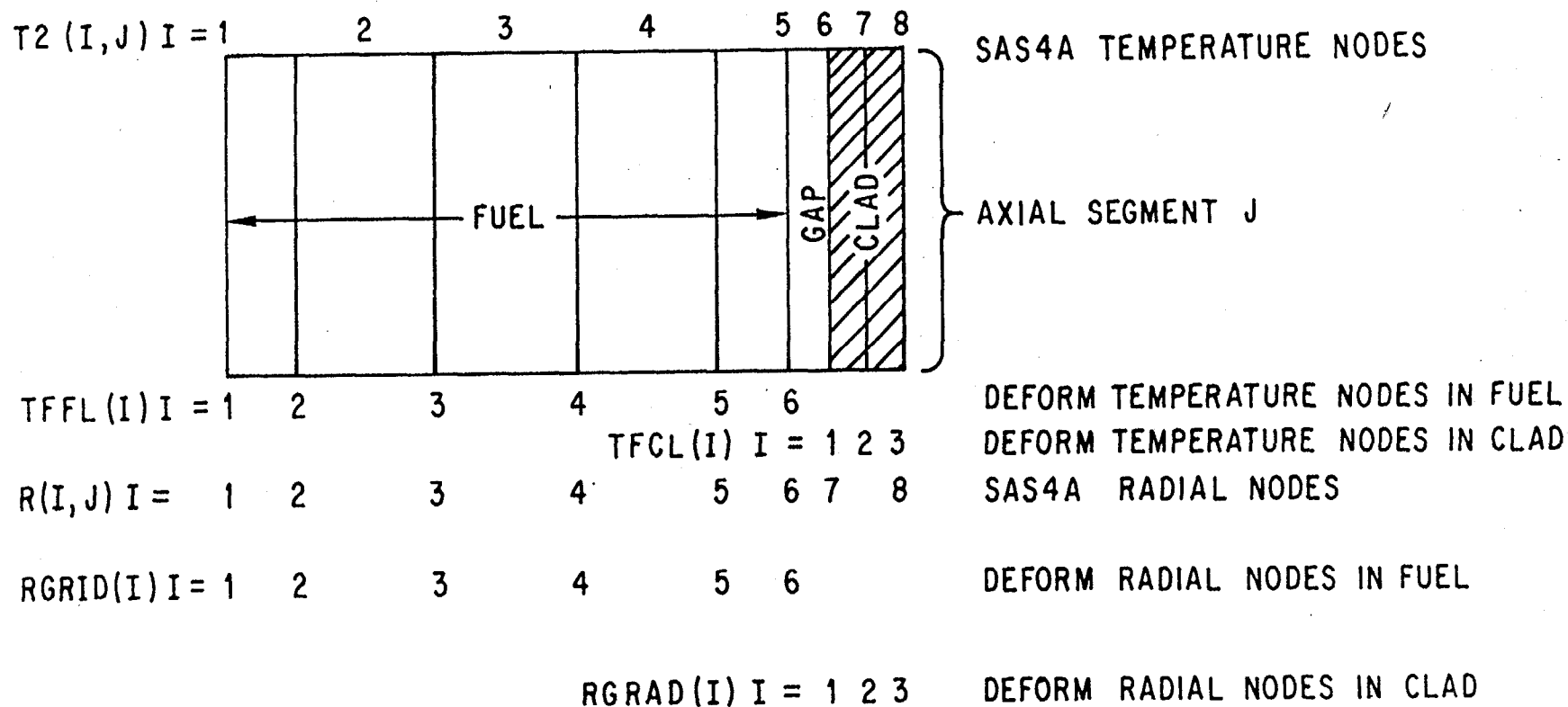


Fig. 8.1-4. Relationship Between SAS4A and DEFORM-4 Cells and Cell-boundaries

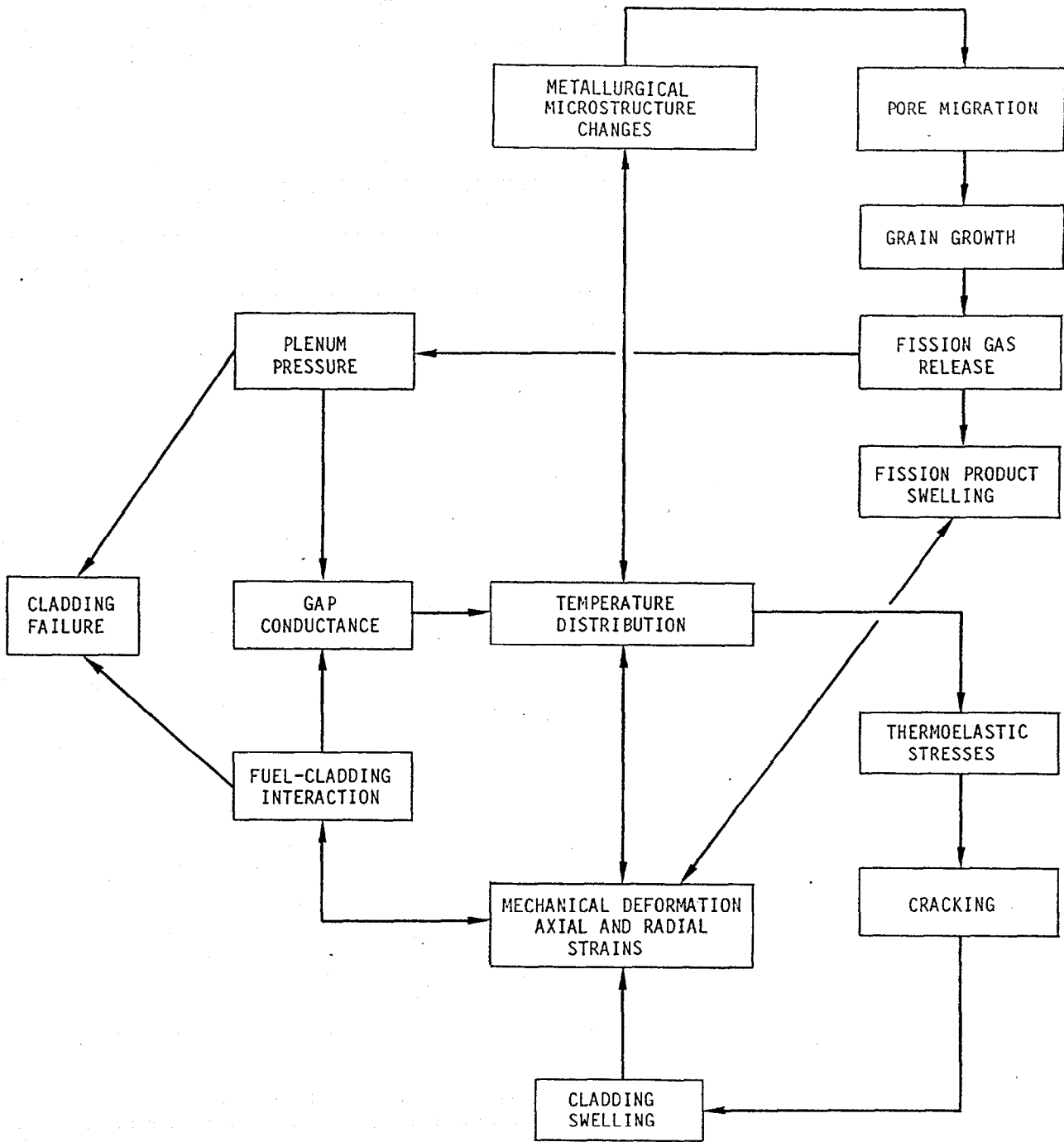


Fig. 8.1-5. DEFORM-4 Mechanical and Phenomenological Considerations and Their Interactions

(1) As-fabricated porosity migration by vapor transport (Section 8.3.1), which is responsible for the formation of the central void and provides a radial distribution of the remaining as-fabricated porosity that affects thermal conductivity;

(2) Grain growth (Section 8.3.2), which affects the fission-gas release and fuel creep characteristics;

(3) Fission-gas release (Section 8.3.3), which affects the radial distribution of total porosity and fission-gas-bubble-induced fuel swelling;

(4) Fission-product swelling (Section 8.3.4), which includes solid fission product and fission-gas bubble swelling, and affects the radial porosity profile and fuel dimensions; and

(5) Irradiation-induced cladding swelling (Section 8.3.5), which affects the cladding dimensions and density.

Since the transient calculation covers seconds and minutes rather than days and years, as in the pre-transient irradiation, the phenomena listed above are not considered, except for the fission-product swelling. Transient fission-gas release is assumed to occur only on fuel melting and is treated in the molten cavity routine, Section 8.3.7.

The thermoelastic mechanical calculations for the fuel and cladding are identical in both the pre-transient and transient. The cladding is treated as an elastic-perfectly-plastic material, although one of the options for the flow stress is dependent on strain and strain rate, and this introduces a type of work-hardening effect. In addition, the cladding is allowed to plastically creep in response to temperature and stress conditions. Axial and radial deformations result from thermal expansion and mechanical interactions. The effects of fuel-cladding interaction are also considered in the fission product swelling calculation.

The fuel is allowed to crack radially whenever the circumferential stress exceeds a temperature-dependent fracture strength. The crack volume varies due to thermal and swelling effects. In the transient, the volume associated with the cracks, the fission gas, and the remaining as-fabricated porosity can be important in accommodating the thermal expansion on melting and determining the molten cavity pressure.

Fuel-pin failure can be initiated by a number of criteria. These include the following;

- (1) Time,
- (2) Fuel temperature,
- (3) Melt fraction,
- (4) Molten cavity pressure,
- (5) Cladding stress,
- (6) Eutectic penetration for U-5FS fuel,
- (7) Cladding reaching conditions equivalent to PLUTO2/LEVITATE failure propagation model,
- (8) Eutectic penetration with cladding stress for metal fuel, and
- (9) Melt fraction for time and failure propagation for location.

Also included are a number of life-fraction correlations based on Larson-Miller and Dorn parameters, but these have not been tied into the automatic failure initiation. The use of these to initiate failure is through observation of the life fractions and then selection of a time and location to be used in a subsequent restart calculation.

#### 8.1.2 Interaction with other SAS4A Models

Because the DEFORM-4 module performs all the fuel-pin characterization and mechanics calculations for SAS4A, it must be capable of exchanging data with the rest of the code. This is done through the use of COMMON blocks accessible by other modules. In the pre-transient and pre-failure transient calculations, DEFORM-4 communicates with the thermal hydraulic models in SAS4A and PINACLE. Once failure has occurred and CLAP, PLUTO2, or LEVITATE become activated, DEFORM-4 is no longer used for that channel, but still performs the calculations for any remaining unfailed channels.

In the initiation of CLAP, LEVITATE, or PLUTO2, the main responsibility of DEFORM-4 is to assure that the necessary information is available for these modules to continue the calculation. If the user has so specified by appropriate input options, then DEFORM-4 will determine when the failure has occurred and initiate the activation of the appropriate module for fuel motion. If it is not being used, failure can still be initiated, but important parameters, such

as fission gas distributions and molten cavity pressures, will not be available for PLUTO2 and LEVITATE. This will cause significant problems in the computations carried out by these modules. The CLAP module does not depend on DEFORM-4 results in its calculations for cladding motion, except for the initial pin dimensions.

The main communication with the rest of SAS4A on an interactive basis is through the core temperatures and pressures supplied by the thermal hydraulic models and then the radii, axial lengths, porosity distributions which affect thermal conductivities, and gap conductances which are returned from DEFORM-4. In order to avoid time-consuming iterations between the thermal hydraulic models and DEFORM-4, the calculations are performed serially. The thermal hydraulic models use the geometry they have at the beginning of a time step with the power, flow, and time-step length to determine temperatures at the end of the time step (see Chapter 3). These final temperatures and the initial temperatures are then used by DEFORM-4 to determine the thermal mechanical changes that take place during the same interval. The new conditions are then transferred back to the thermal hydraulic routines as the initial conditions for the next time step.

This method of interaction with the SAS4A thermal hydraulic models has been employed to avoid the resource-consuming iterations that could occur between the thermal hydraulic and pin characterization routines. These iterations would assure complete consistency between the temperatures and the characterization state of the pin, but at a price in computational effort that would preclude the use of the code for many of the multiple channel, extended pre-transient and transient cases of interest in initiating-phase accident analysis. Instead of iterations, there is control over the length of the computational time step. In the early pre-transient irradiation where pore migration and initial fission-gas release cause changes in the geometry and heat-transfer properties that would greatly affect the temperatures, time intervals on the order of one to two days should be used. During power changes it may be necessary to cut these further, especially during the initial startup to full power. In later stages, the time steps can be on the order of ten to 30 days. During the transient where the time steps are controlled by a variety of restrictions, such as maximum reactivity change, maximum temperature change, etc., the heat-transfer time steps are small enough, on the order of less than a second, to remove any problems with inconsistencies. DEFORM-4 would be able to handle considerably longer time

steps without problems. In practice, these types of limits have resulted in excellent results with minimum computational effort.

## 8.2 Fuel-pin Mechanics

In the treatment adopted in DEFORM-4, the fuel pin in an axial segment is divided into 6 radial zones, not all of which need exist. These are (1) the central void, (2) the molten fuel zone, (3) the solid, continuous fuel zone, (4) the cracked fuel zone, (5) the fuel-cladding gap, and (6) the fuel-pin cladding. The zones are illustrated in Fig. 8.2-1. Each zone may consist of one or more cells. These zones will be explained in detail in the following sections.

The approach used is to divide the calculation into the thermoelastic solution, and then superimpose on this the plastic deformation resulting from fuel swelling or cladding stress induced plastic creep and irradiation swelling

$$\epsilon_T = \epsilon_e + \epsilon_{th} + \epsilon_s \quad (8.2-1)$$

where

- $\epsilon_T$  = Total strain at the cell boundary
- $\epsilon_e$  = Elastic strain from applied boundary forces
- $\epsilon_{th}$  = Thermal expansion induced strain
- $\epsilon_s$  = Swelling strains from the solid and volatile fission products in the fuel, or irradiation induced void formation and stress induced plastic creep in the cladding.

These terms are discussed in the following sections.

The cladding is assumed to be an elastic-perfectly-plastic material. Several functions are available as options to provide the flow stress of the cladding. Once the fuel-cladding interface pressure produces a circumferential stress exceeding the flow stress, the interface pressure is limited to that necessary to achieve the flow stress and the cladding will follow the fuel

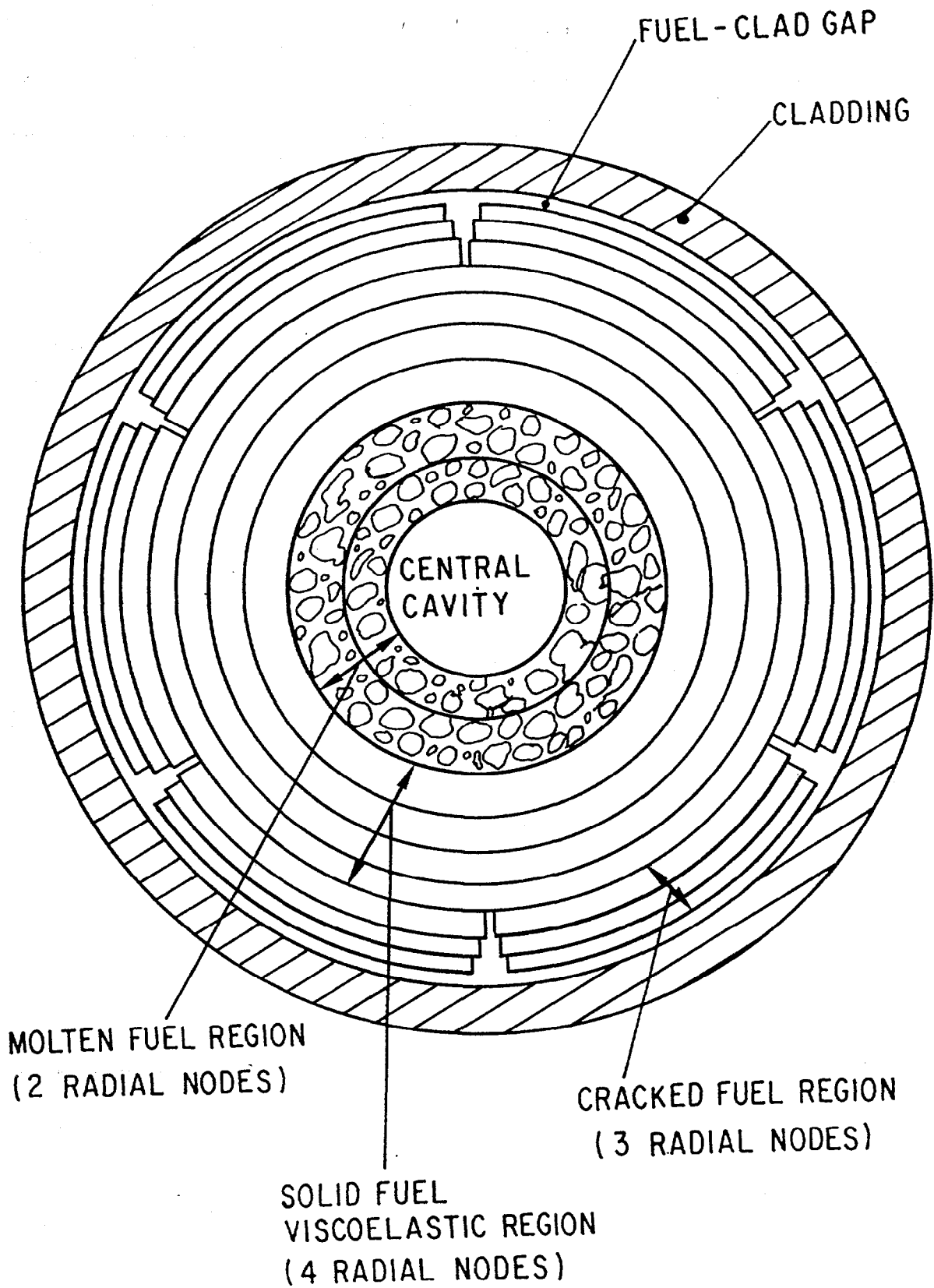


Fig. 8.2-1. DEFORM-4 Radial Zones

deformation until the conditions bring the cladding back into the elastic behavior region. One of the options for flow stress includes the effects of previous strain, strain rate, temperature, and irradiation history. When this option is used, the flow stress changes as these parameters change, providing a work hardening and strain-rate dependence. Besides this perfectly plastic behavior, there is plastic creep of the cladding at conditions below the flow stress. This strain is calculated and added to the accumulated strain.

### 8.2.1 Solid Fuel and Cladding Thermoelastic Solution

In the solid fuel and cladding, the material is assumed to be continuous, isotropic, elastic, and axisymmetric. Because of the axisymmetry, all shear stresses and strains are assumed to be zero. The generalization of Hooke's Law to three dimensions is used to provide the linear elastic relationship between the stresses and strains. The thermal expansion strains are included through the principle of superposition of linear equations. These considerations therefore yield the following set of constitutive equations.

$$\epsilon_r = \frac{1}{E} [\sigma_r - \nu(\sigma_\theta + \sigma_z)] + \Delta(\alpha T) \quad (8.2-2)$$

$$\epsilon_\theta = \frac{1}{E} [\sigma_\theta - \nu(\sigma_r + \sigma_z)] + \Delta(\alpha T) \quad (8.2-3)$$

$$\epsilon_z = \frac{1}{E} [\sigma_z - \nu(\sigma_r + \sigma_\theta)] + \Delta(\alpha T) \quad (8.2-4)$$

$$\Delta(\alpha T) = \alpha(T_2) (T_2 - T_r) - \alpha(T_1) (T_1 - T_r) \quad (8.2-5)$$

where

$\epsilon_r, \epsilon_\theta, \epsilon_z$  = Strain in the radial, circumferential, and axial directions, respectively

$\sigma_r, \sigma_\theta, \sigma_z$  = Stress in the radial, circumferential, and axial directions, respectively

$\nu$  = Poisson's ratio for the material

$\alpha(T)$  = Mean linear thermal expansion coefficient

$E$  = Modulus of elasticity

$T_2, T_1$  = Temperature at the final and initial states, respectively,  
 $T_r$  = Reference temperature

The strains are related to the displacements through geometrical considerations. In the cylindrical coordinate system used in SAS4A, these kinematic equations are as follows:

$$\epsilon_r = \frac{du}{dr} \quad (8.2-6)$$

$$\epsilon_\theta = \frac{u}{r} + \frac{1}{r} \frac{dv}{d\theta} \quad (8.2-7)$$

$$\epsilon_z = \frac{dw}{dz} \quad (8.2-8)$$

where

$u$  = Displacement in the radial direction  $r$   
 $v$  = Displacement in the circumferential direction  $\theta$   
 $w$  = Displacement in the axial direction  $z$

Since material is assumed to be axisymmetric, there is no variation of  $v$  circumferentially, so Eq. 8.2-7 reduces to

$$\epsilon_\theta = \frac{u}{r} \quad (8.2-9)$$

In order to be able to obtain simple analytical solutions with the above equations, a generalized plane strain approximation has been employed. Each axial segment is assumed to elongate uniformly over the cross section to maintain a plane interface between segments. Equation 8.2-8 can therefore be rewritten as

$$\epsilon_z = z_0 \quad (8.2-10)$$

where

$z_0$  = Axial plane strain for the segment

Since the cells under consideration are assumed to be at rest, with no shear stresses, mechanical considerations provide the following equation of equilibrium.

$$\frac{d\sigma_r}{dr} + \frac{\sigma_r - \sigma_\theta}{r} = 0 \quad (8.2-11)$$

Equations 8.2-2 through 8.2-6, and 8.2-9 through 8.2-11 form the set of equations solved by DEFORM-4 for the thermoelastic response. Equation 8.2-10 is substituted into 8.2-4 and this is solved for the axial stress,  $\sigma_z$ . This result is then substituted along with Eqs. 8.2-6 and 8.2-9 in Eqs. 8.2-2 and 8.2-3 to yield

$$\sigma_r = \frac{E}{(1+\nu)(1-2\nu)} \left[ (1-\nu) \frac{du}{dr} + \nu \frac{u}{r} + \nu z_0 - (1+\nu)\Delta(\alpha T) \right] \quad (8.2-12)$$

$$\sigma_\theta = \frac{E}{(1+\nu)(1-2\nu)} \left[ \nu \frac{du}{dr} + (1-\nu) \frac{u}{r} + \nu z_0 - (1+\nu)\Delta(\alpha T) \right] \quad (8.2-13)$$

The stresses are expressed in terms of the radial displacement function  $u(r)$ . When these equations are used in the equilibrium Eq. 8.2-11, the following is obtained, assuming the modulus of elasticity,  $E$ , is constant over the region of interest. The value for the modulus of elasticity is the mass-weighted average of all those cells in this zone.

$$\frac{1}{r} \frac{d}{dr} \left( r \frac{du}{dr} \right) - \frac{u}{r^2} = \frac{(1+\nu)}{(1-\nu)} \frac{d}{dr} [\Delta(\alpha T)] \quad (8.2-14)$$

The solution to this differential equation may be obtained as

$$u(r) = \left[ \frac{1+\nu}{1-\nu} \right] r I(r) + C_1 r + \frac{C_2}{r} \quad (8.2-15)$$

where

$C_1, C_2 =$  Constants of integration

The function  $I(r)$  is defined as

$$I(r) = \frac{1}{r^2} \int_{\rho}^r \Delta(\alpha T) r' dr' \quad (8.2-16)$$

where

$\rho =$  Inner radius of the zone under consideration

If Eq. 8.2-15 is used to rewrite Eqs. 8.2-12 and 8.2-13, the radial and circumferential stresses as functions of  $r$ ,  $C_1$ , and  $C_2$  may be obtained.

$$\frac{\sigma_r(r)}{E} = - \frac{I(r)}{(1-\nu)} + \frac{1}{(1+\nu)(1-2\nu)} \left[ C_1 - \frac{(1-2\nu)C_2}{r^2} + \nu Z_0 \right] \quad (8.2-17)$$

$$\frac{\sigma_{\theta}(r)}{E} = \frac{I(r)}{(1-\nu)} + \frac{1}{(1+\nu)(1-2\nu)} \left[ C_1 - \frac{(1-2\nu)C_2}{r^2} + \nu Z_0 \right] - \frac{\Delta(\alpha T)}{(1-\nu)} \quad (8.2-18)$$

The constants of integration,  $C_1$  and  $C_2$ , may be determined by the following boundary conditions:

$$\sigma_r(r=\rho) = \sigma_\rho \quad (8.2-19)$$

$$\sigma_r(r=\eta) = \sigma_\eta \quad (8.2-20)$$

where

$\eta$  = Outer radius of the zone under consideration

$\sigma_\rho$  = Stress at the inner surface of the zone

$\sigma_\eta$  = Stress at the outer surface of the zone

For the fuel,  $\rho$  and  $\eta$  would correspond to the inner solid and outer uncracked cell boundaries, respectively. For the cladding, they would correspond to the inner and outer surfaces, respectively.

The constants may then be determined by substituting Eqs. 8.2-19 and 8.2-20 into Eqs. 8.2-17 and 8.2-18 and solving them simultaneously for  $C_1$  and  $C_2$ .

$$C_1 = \frac{(1+\nu)(1-2\nu)}{(\eta^2-\rho^2)} \left[ \frac{I(\eta)\eta^2}{(1-\nu)} - \frac{1}{E}(\rho^2\sigma_\rho - \eta^2\sigma_\eta) \right] - \nu Z_0 \quad (8.2-21)$$

$$C_2 = \frac{(1+\nu)\rho^2\eta^2}{(\eta^2-\rho^2)} \left[ \frac{I(\eta)}{(1-\nu)} - \frac{(\sigma_\rho - \sigma_\eta)}{E} \right] \quad (8.2-22)$$

These constants may then be used in Eqs. 8.2-15, 8.2-17, and 8.2-18 to determine the radial displacement and stresses due to externally applied forces and thermal expansion.

$$u(r) = u_f(r) + u_{th}(r) \quad (8.2-23)$$

$$\begin{aligned}
u_f(r) &= \text{Elastic displacement due to externally applied stress } \sigma_\rho \text{ and } \sigma_\eta \\
&= \frac{(1+\nu)}{(\eta^2-\rho^2)E} \left\{ \eta^2\sigma_\eta \left[ (1-2\nu)r + \frac{\rho^2}{r} \right] - \rho^2\sigma_\rho \left[ (1-2\nu)r + \frac{\eta^2}{r} \right] \right\} - \nu z_o^f r
\end{aligned} \tag{8.2-24}$$

$$\begin{aligned}
u_{th}(r) &= \text{Displacements due to thermal expansion} \\
&= \left[ \frac{1+\nu}{1-\nu} \right] \left\{ rI(r) + \frac{I(\eta)\eta^2}{(\eta^2-\rho^2)} \left[ (1-2\nu)r + \frac{\rho^2}{r} \right] \right\} - \nu z_o^{th} r
\end{aligned} \tag{8.2-25}$$

where  $z_o$  has been divided into its thermal and boundary force components,  $z_o^{th}$  and  $z_o^f$ , respectively (see Section 8.2.4).

The stresses are similarly divided into their thermal and externally applied force components.

$$\sigma_r(r) = \sigma_r^f(r) + \sigma_r^{th}(r) \tag{8.2-26}$$

$$\begin{aligned}
\sigma_r^f(r) &= \text{Radial stress from externally applied forces} \\
&= \frac{1}{(\eta^2-\rho^2)} \left[ \eta^2\sigma_\eta \left( 1 - \frac{\rho^2}{r^2} \right) - \rho^2\sigma_\rho \left( 1 - \frac{\eta^2}{r^2} \right) \right]
\end{aligned} \tag{8.2-27}$$

$$\begin{aligned}
\sigma_r^{th}(r) &= \text{Radial stress from thermal expansion} \\
&= \frac{E}{(1-\nu)} \left[ \frac{\eta^2 I(\eta)}{(\eta^2-\rho^2)} \left( 1 - \frac{\rho^2}{r^2} \right) - I(r) \right]
\end{aligned} \tag{8.2-28}$$

$$\sigma_\theta(r) = \sigma_\theta^f(r) + \sigma_\theta^{th}(r) \tag{8.2-29}$$

$$\begin{aligned}\sigma_{\theta}^f(r) &= \text{Circumferential stress from externally applied forces} \\ &= \frac{1}{(\eta^2 - \rho^2)} \left[ \eta^2 \sigma_{\eta} \left(1 + \frac{\rho^2}{r^2}\right) - \rho^2 \sigma_{\rho} \left(1 + \frac{\eta^2}{r^2}\right) \right]\end{aligned}\quad (8.2-30)$$

$$\begin{aligned}\sigma_{\theta}^{th}(r) &= \text{Circumferential stress from thermal expansion} \\ &= \frac{E}{(1-\nu)} \left[ \frac{\eta^2 I(\eta)}{(\eta^2 - \rho^2)} \left(1 + \frac{\rho^2}{r^2}\right) + I(r) - \Delta(\alpha T) \right]\end{aligned}\quad (8.2-31)$$

Throughout the derivation given above, only the thermal components contain the explicit reference to a change from one state to another, i.e., reliance on temperatures  $T_2$  and  $T_1$  of Eq. 8.2-5. All the force components are based on a change from a zero stress state to some state created by the imposition of the external force boundary conditions. In the calculational procedure used in SAS4A, there are a series of time steps with different conditions at the beginning and end of the step. As mentioned above, the SAS4A thermal hydraulic routines generate temperatures at the beginning and end of the time step and then DEFORM-4 determines the changes in dimensions, stress state, and characterization that occur during the time step. In order to use this natural, incremental approach, Eqs. 8.2-24, 8.2-27, and 8.2-30 must be changed to represent the changes from the beginning of the time step to the end.

Equation 8.2-27 gives the radial stress state set up by the externally applied stresses  $\sigma_{\eta}$  and  $\sigma_{\rho}$  when the material was initially in an unstressed condition. If a different set of conditions existed, then a different stress state is set up. The change from one state to the next can be found by using Eq. 8.2-27 twice, once with each external stress boundary condition, and then subtracting.

$$\begin{aligned}\Delta\sigma_{r,i}^f(r) &= \frac{1}{(\eta^2 - \rho^2)} \left[ \eta^2 \left(1 - \frac{\rho^2}{r^2}\right) (\sigma_{\eta,i} - \sigma_{\eta,i-1}) \right. \\ &\quad \left. - \rho^2 \left(1 - \frac{\eta^2}{r^2}\right) (\sigma_{\rho,i} - \sigma_{\rho,i-1}) \right]\end{aligned}\quad (8.2-32)$$

where

- $\sigma_{\rho,i}, \sigma_{\eta,i}$  = Inner and outer externally applied stresses at the end of time step  $i$ , respectively
- $\sigma_{\rho,i-1}, \sigma_{\eta,i-1}$  = Inner and outer externally applied stresses at the beginning of time step  $i$  (end of time step  $i-1$ ), respectively
- $\Delta\sigma_{r,i}^f(r)$  = Incremental change in the radial stress due to changes in the externally applied stresses  $\sigma_{\rho}$  and  $\sigma_{\eta}$

In a like manner, Eqs. 8.2-24 and 8.2-30 can be used to provide the changes occurring during the computational time step.

$$\Delta u_{f,i}(r) = \frac{(1 + \nu)}{(\eta^2 - \rho^2)E} \left\{ \eta^2 (\sigma_{\eta,i} - \sigma_{\eta,i-1}) \left[ (1-2\nu) r + \frac{\rho^2}{r} \right] - \rho^2 (\sigma_{\rho,i} - \sigma_{\rho,i-1}) \left[ (1-2\nu) r + \frac{\eta^2}{r} \right] \right\} - \nu \Delta z_{o,i}^f r \quad (8.2-33)$$

$$\Delta \sigma_{\theta,i}^f(r) = \frac{1}{(\eta^2 - \rho^2)} \left[ \eta^2 \left( 1 + \frac{\rho^2}{r^2} \right) (\sigma_{\eta,i} - \sigma_{\eta,i-1}) - \rho^2 \left( 1 + \frac{\eta^2}{r^2} \right) (\sigma_{\rho,i} - \sigma_{\rho,i-1}) \right] \quad (8.2-34)$$

where

- $\Delta u_{f,i}(r)$  = Incremental elastic displacement due to changes in the externally applied stresses  $\sigma_{\rho}$  and  $\sigma_{\eta}$
- $\Delta \sigma_{\theta,i}^f(r)$  = Incremental change in the circumferential stress due to changes in the externally applied stresses  $\sigma_{\rho}$  and  $\sigma_{\eta}$
- $\Delta z_{o,i}^f$  = Incremental change in the axial plane strain due to changes in the external applied stresses  $\sigma_{\rho}$  and  $\sigma_{\eta}$

As mentioned above, this same procedure is not required for the thermally induced stresses and strains, since they are derived from explicit temperature changes. With the initial and final temperatures in Eq. 8.2-5 defined as the temperatures at the beginning and end of the current time step, respectively, the incremental changes in the stresses and strains are determined.

Equations 8.2-25, 8.2-28, and 8.2-31, define the incremental changes in the deformation, radial stress, and circumferential stress in response to a temperature change during the time step. Equations 8.2-32 through 8.2-34 define the changes in response to changes in the externally applied forces. The incremental changes in the axial stresses can be found from Eq. 8.2-4, once the axial plane strain is determined. The separation of the stresses into the thermal and force components makes it possible to implement thermal stress relaxation in a straightforward manner.

The subroutine FSIGMA solves the equations for the fuel and the subroutine CSIGMA solves them for the cladding.

### 8.2.2 Cracked Fuel Thermoelastic Solution and Crack Volume

If the circumferential stress at a cell boundary exceeds the fracture strength of the fuel, the cell immediately inside that boundary is assumed to crack. The new outer solid fuel boundary is then studied to determine if it will also crack. This process is repeated until a stable solid boundary is reached, or cracking occurs to the central void or molten fuel boundary. This procedure is carried out in the subroutine FSIGMA. The treatment for the solid zone was presented previously and the solution in the cracked zone is given below.

In the cracked zone, it is assumed that numerous radial and transverse cracks exist and extend inward to the same radial position. Under these conditions the circumferential and axial stress,  $\sigma_\theta$  and  $\sigma_z$ , respectively, are both set equal to the negative of the plenum gas pressure,  $P_g$ , since it is assumed that communication exists with the plenum.

$$\sigma_{\theta} = \sigma_z = -P_g \quad (8.2-35)$$

If these values are substituted into the equilibrium Eq. 8.2-11, and the integration performed from the outer fuel radius,  $R_f$ , to a radius  $r$ , the radial stress at any point in the cracked region results:

$$\sigma_r(r) = -P_g + \frac{R_f}{r} (P_g + \sigma_{FC}) \quad (8.2-36)$$

where

$\sigma_{FC}$  = Fuel-cladding interface stress, the negative of the interface pressure

If the integration is performed outward from the boundary between the continuous and the cracked fuel,  $\eta$ , to a radius  $r$ , then the stress in the cracked fuel is of the form:

$$\sigma_r(r) = -P_g + \frac{\eta}{r} (P_g + \sigma_{\eta}) \quad (8.2-37)$$

where

$\sigma_{\eta}$  = Stress at the outer boundary of the solid fuel

Since Eqs. 8.2-36 and 8.2-37 must define the same stress at a given radius, the relationship between the stress at the solid-cracked boundary and the fuel-cladding interface may be determined as

$$\sigma_{\eta} = -P_g + \frac{R_f}{\eta} (P_g + \sigma_{FC}) \quad (8.2-38)$$

It should be noted that the radial stress in the cracked region contains no dependence on the thermal expansion of the region.

To obtain the radial displacement,  $u_r$ , Eqs. 8.2-35 and 8.2-36 are substituted into Eq. 8.2-2 and the result used in Eq. 8.2-6. Upon integration, the radial displacement is given by

$$u_r = u_\eta + (2\nu-1)(r-\eta) \frac{P_g}{E_c} + \frac{(P_g + \sigma_\eta)}{E_c} \eta \ln\left(\frac{r}{\eta}\right) + \int_\eta^r \Delta(\alpha T) dr' \quad (8.2-39)$$

where

$u_r$  = Displacement at radius  $r$  in the cracked fuel zone

$u_\eta$  = Displacement of the outer surface of the continuous fuel zone

$E_c$  = Mass averaged modulus of elasticity in the cracked fuel zone

As in the section on solid fuel or cladding, the above derivations contain the implicit assumption that the cells start out in an unexpanded, stress free state. This is not what exists at the beginning of the time step. Equations 8.2-35 through 8.2-39 can be used to obtain the changes that occur from the beginning of the time step to the end.

$$\Delta\sigma_{\theta,i} = \Delta\sigma_{z,i} = -\Delta P_{g,i} \quad (8.2-40)$$

$$\begin{aligned} \Delta\sigma_{r,i} &= -\Delta P_{g,i} + \frac{R_f}{r} (\Delta P_{g,i} + \Delta\sigma_{FC,i}) \\ &= -\Delta P_{g,i} + \frac{\eta}{r} (\Delta P_{g,i} + \Delta\sigma_{n,i}) \end{aligned} \quad (8.2-41)$$

$$\Delta\sigma_{n,i} = -\Delta P_{g,i} + \frac{R_f}{\eta} (\Delta P_{g,i} + \Delta\sigma_{FC,i}) \quad (8.2-42)$$

where

$\Delta P_{g,i}$  = Change in plenum pressure during time step i

$\Delta \sigma_{FC,i}$  = Change in fuel-cladding interface stress during time step i

$\Delta \sigma_{n,i}$  = Change in stress at solid fuel-cracked fuel boundary during time step i

The displacement calculated in Eq. 8.2-39 contains two parts, that due to forces and that due to temperature changes. As with the solid fuel, the thermal effects are already handled in an incremental fashion, so no changes are required. However, the force effects have to be modified to handle the changes during the time step. Using the solid fuel results for incremental changes, the value of outer solid fuel displacement,  $u_{\eta}$ , will be an incremental change. The force effects can be made incremental in the manner used above.

$$u_{r,i} = u_{\eta,i} + (2\nu-1) (r-\eta) \frac{\Delta P_{g,i}}{E_c} + \frac{(\Delta P_{g,i} + \Delta \sigma_{n,i})}{E_c} \eta \ln \left( \frac{r}{\eta} \right) + \int_{\eta}^r \Delta (\alpha T) dr' \quad (8.2-43)$$

Equation 8.2-43 gives the displacements of the cracked fuel nodes in the incremental manner desired. These equations are solved in the subroutine FSIGMA.

As the dimensions of a cracked fuel cell change, so will the fraction of the volume which is associated with the cracks. These changes are calculated in the subroutine CRAKER. In the current version of DEFORM-4, the volume associated with transverse, or axial, cracking is neglected. The radial crack volume fraction is affected by three factors: (1) changes in the cell boundary locations, (2) circumferential strain, and (3) fission-product-induced fuel swelling. The first two processes are treated in the subroutine CRAKER, whereas the third is treated in the subroutine FSWELL.

$$\Delta_{VCRK} = \Delta_V(u) - \epsilon_{\theta}^c - \Delta_{VS} \quad (8.2-44)$$

where

$\Delta_{VCRK}$  = Fractional volume change due to radial cracks

$\Delta_V(u)$  = Fractional volume change associated with the changes in the radial boundaries of the cell by the constant displacement  $u$

$\epsilon_\theta^c$  = Circumferential strain of the cracked fuel cell

$\Delta_{VS}$  = Fractional volume change associated with fission-product swelling in the cell

The first term in Eq. 8.2-44 is based on purely geometric considerations. If an annulus with inner radius  $r_i$  and outer radius  $r_o$  is moved radially by an amount  $u$ , the new inner and outer radius become  $r_i + u$  and  $r_o + u$ , respectively. This new annulus has a different volume from the original configuration. The change in volume fraction is assumed to be contained in the cracks in the fuel cell.

$$\Delta_V(u) = \frac{[(r_o + u)^2 - (r_i + u)^2] - [r_o^2 - r_i^2]}{r_o^2 - r_i^2} \quad (8.2-45)$$

Equation 8.2-45 reduces to

$$\Delta_V(u) = \frac{2u}{r_o + r_i} \quad (8.2-46)$$

In the determination of the circumferential strain in a cracked fuel cell, it is assumed that the fuel continues to act as linear elastic material obeying Eq. 8.2-3. With the circumferential and axial stresses set to the negative of the plenum pressure, Eq. 8.2-35, and the radial stress as given in Eq. 8.2-36, the circumferential strain in the cracked zone can be determined as the sum of the force and thermal components to the strain  $\epsilon_{\theta,f}^c$  and  $\epsilon_{\theta,th}^c$ , respectively.

$$\epsilon_\theta^c = \epsilon_{\theta,f}^c + \epsilon_{\theta,th}^c \quad (8.2-47)$$

$$\epsilon_{\theta,r}^c = - (1 - 2\nu) \frac{\Delta P_{g,i}}{E_c} - \frac{\nu R_f}{E_c r} (\Delta P_{g,i} + \Delta \sigma_{FC,i}) \quad (8.2-48)$$

$$\epsilon_{\theta,th}^c = \Delta(\alpha T) \quad (8.2-49)$$

The value of the force strain used in determining the strain of a particular cell is the average of the strain at the cell boundaries and is based on the changes occurring during the time step. The thermal component is evaluated from the change in the cell temperature during the time step.

### 8.2.3 Fully Cracked Fuel

In some pretransient situations and many transient cases, it is possible for the solid fuel to become fully cracked, i.e., there is no solid fuel annulus. Being fully cracked, there would be no resistance to radial relocation outward, until the cladding is reached, or radially inward, until the crack volume is closed in the central solid regions of the fuel. If the pressure in the cracks remains the plenum pressure, Eq. 8.2-38 then represents the necessary equilibrium condition that must be satisfied. However, if the crack pressure is assumed to reach a level equivalent to the central cavity pressure, the substitution in Eq. 8.2-11 yields a constant pressure, equivalent to the cavity pressure, throughout the fuel and as the fuel-cladding interface pressure. Both options are available within DEFORM-4.

The movement of the cracked fuel is controlled by the two external forces applied: (1) the central cavity pressure, and (2) the fuel-cladding interface pressure. If no molten cavity exists with a pressure greater than the plenum pressure, the cracked fuel cannot relocate radially outward to remove the fuel-cladding gap that may exist. Under these conditions the maximum fuel-cladding interface pressure is equivalent to the plenum pressure. If the previous time step contained a solid fuel annulus which had produced an interface pressure greater than the plenum pressure, once full cracking is achieved the interface pressure will drop to the plenum pressure, and the fuel may be relocated inward in response to the alleviation of previous elastic strains in the cladding.

If a pressurized molten cavity does exist at the time the cracked region reaches the melt boundary, or melting proceeds to the cracked boundary, then radial relocation to the cladding surface will take place if a gap existed. If no gap existed, then the relocation could occur either outward or inward depending on the previous interface pressure, the cavity pressure, and the option used for the pressure of the gas in the cracks.

When the crack pressure is assumed to remain at the plenum pressure, the new interface pressure is determined from Eq. 8.2-38.

$$\sigma_{FC} = -P_g + \frac{R_{cav}}{R_f} (\sigma_{cav} + P_g) \quad (8.2-50)$$

where

- $\sigma_{cav}$  = Molten central cavity pressure
- $R_{cav}$  = Outer radius of the molten central cavity

If this new interface pressure is less than the previous time step, removal of the previous elastic strain will take place, moving the cracked fuel toward the center. If it is greater than the previous interface pressure, more elastic strain will be produced, and the fuel and cladding will move outward. If this new pressure produces a circumferential stress larger than the cladding flow stress, the cladding will strain plastically to provide enough volume to reduce the cavity pressure to a value that produces an interface pressure equal to that necessary to produce a circumferential stress equal to the flow stress.

These conditions are all handled by the fully crack fuel solution driver subroutine MKDRIV.

With these considerations it is possible for the cladding stress to build up while solid fuel exists, then become alleviated when the fuel becomes fully cracked with a low molten cavity pressure, and then again build up as the molten cavity pressure and melt radius increase. The

timing of such behavior and the magnitude reached will depend on the particular transient being studied.

#### 8.2.4 Axial Expansion Solution

As discussed in Section 8.2.1, the analytical solution to the mechanics equations is produced through a generalized plane strain assumption. The axial interfaces between segments are assumed to remain parallel, and a segment expands or contracts with a uniform strain,  $z_0$ , over its entire radius. Since this axial strain exists in the equations which represent the radial displacement function, it is necessary to find the axial strain prior to the radial strain results. The calculation for the axial strain of a segment is performed in the subroutine EXPAND.

The axial force in the fuel segment,  $F_f$ , is found by integrating the axial stress,  $\sigma_z$ , over the cylindrical fuel geometry,

$$F_f = 2\pi \int_{\rho}^{\eta} \sigma_z r dr. \quad (8.2-51)$$

Substituting Eqs. 8.2-27, -28, -30, -31 and -10 into Eq. 8.2-4 and solving for the axial stress function, yields:

$$\sigma_z = \frac{2\nu E}{(\eta^2 - \rho^2)} \left[ \frac{I(\eta)\eta^2}{(1-\nu)} - \frac{(\rho^2\sigma_\rho - \eta^2\sigma_\eta)}{E} \right] - \frac{E\Delta(\alpha T)}{(1-\nu)} + Ez_0 \quad (8.2-52)$$

This is then used in Eq. 8.2-51 and integrated to yield

$$F_f = -2\pi E\eta^2 I(n) + 2\pi\nu(\eta^2\sigma_\eta - \rho^2\sigma_\rho) + \pi E z_0(\eta^2 - \rho^2) \quad (8.2-53)$$

In order to find the axial plane strain, a total force balance is performed. The state of the fuel-cladding gap can influence the terms in the force summation. If the fuel-cladding gap is open, or the free axial expansion option is chosen through the input parameter NAXOP, then the force summation contains no term for the cladding effects. If, however, the fuel and cladding are in contact, then cladding terms must be included in the force balance. The following is the general equation for the force balance.

$$F_f = F_{cav} + F_{ax} + F_c \quad (8.2-54)$$

where

- $F_{cav}$  = Force in the central void or molten fuel cavity
- $F_{ax}$  = Force applied axially to the fuel column, usually from the plenum gas pressure
- $F_f$  = Force from the solid fuel zone
- $F_c$  = Force from the cladding, which is 0 with free axial expansion

In the central void or molten cavity, the force is given by

$$F_{cav} = \pi \rho^2 P_{cav} \quad (8.2-55)$$

where

- $P_{cav}$  = The pressure in the molten cavity or central void
- $\rho$  = The radial extent of melting or the central void radius

The axial force from the plenum pressure is given by

$$F_{ax} = \pi r_p^2 P_{gas} \quad (8.2-56)$$

where

$P_{\text{gas}}$  = Fission-gas plenum pressure

$r_p$  = Radius of the plenum

For the cladding, the force is either zero or the same as Eq. 8.2-53 but with cladding properties, thermal expansion, and inner and outer boundary forces.

If free axial expansion is assumed, then Eqs. 8.2-53, -55, and -56 can be used in Eq. 8.2-54. This is then solved for the uniform axial strain.

$$z_o = [z_o \text{ (thermal)} + z_o \text{ (forces)}] A_f \quad (8.2-57)$$

$$z_o \text{ (thermal)} = \frac{2\eta^2 I(\eta)}{(\eta^2 - \rho^2)} \quad (8.2-58)$$

$$z_o \text{ (forces)} = \frac{-2\nu}{(\eta^2 - \rho^2)} \frac{(\eta^2 \sigma_\eta - \rho^2 \sigma_\rho)}{E} - \frac{(\rho^2 P_{\text{cav}} + r_p^2 P_{\text{gas}})}{E(\eta^2 - \rho^2)} \quad (8.2-59)$$

where

$A_f$  = Fraction of axial expansion to be used

All properties in the above two equations refer to the fuel, and the modulus of elasticity,  $E$ , is a mass-averaged value.

Since this equation assumes an initial stress free state, it must be modified to account for the changes which take place during the specific time step. The time step changes occur in the inner and outer boundary conditions,  $\sigma_\rho$  and  $\rho_\eta$ , and the cavity and plenum pressures,  $P_{\text{CAV}}$  and  $P_{\text{gas}}$ .

$$z_o \text{ (forces)} = \frac{-2\nu}{(\eta^2 - \rho^2)} \frac{(\eta^2 \Delta\sigma_{n,i} - \rho^2 \Delta\sigma_{p,i})}{E} - \frac{(\rho^2 \Delta P_{CAV} + r_p^2 \Delta P_{gas})}{E (\eta^2 - \rho^2)} \quad (8.2-60)$$

Equation 8.2-60 together with Eq. 8.2-58 define the axial strain occurring during the time step due to force and thermal considerations, respectively.

For the case where the fuel and cladding are considered "constrained", the fuel and cladding surfaces are assumed to be locked to each other. Equation 8.2-54 is used with Eq. 8.2-53 (used twice, once with fuel properties, once with cladding properties), and Eqs. 8.2-55 and -56. The result is again solved for the axial strain

$$z_o \text{ (thermal)} = \frac{2 [E_f \eta_f^2 I(\eta_f) + E_c \eta_c^2 I(\eta_c)]}{[E_c (\eta_c^2 - \rho_c^2) + E_f (\eta_f^2 - \rho_f^2)]} \quad (8.2-61)$$

$$z_o \text{ (forces)} = \left\{ -2 [\nu_f (\eta_f^2 \sigma_{\eta,f} - \rho_f^2 \sigma_{\rho,f}) + \nu_c (\eta_c^2 \sigma_{\eta,c} - \rho_c^2 \sigma_{\rho,c})] - (\rho_f^2 P_{cav} + r_p^2 P_{gas}) \right\} \div [E_c (\eta_c^2 - \rho_c^2) + E_f (\eta_f^2 - \rho_f^2)] \quad (8.2-62)$$

The subscript "f" refers to fuel properties and dimensions and the subscript "c" refers to the cladding properties and dimensions. Again, Eq. 8.2-62 must be transformed to consider the changes from one time step to the next.

$$z_o \text{ (forces)} = \left\{ -2 [\nu_f (\eta_f^2 \Delta\sigma_{\eta,f,i} - \rho_f^2 \Delta\sigma_{\rho,f,i}) + \nu_c (\eta_c^2 \Delta\sigma_{\eta,c,i} - \rho_c^2 \Delta\sigma_{\rho,c,i})] - (\rho_f^2 \Delta P_{CAV} + r_p^2 \Delta P_{gas}) \right\} \div [E_c (\eta_c^2 - \rho_c^2) + E_f (\eta_f^2 - \rho_f^2)] \quad (8.2-63)$$

Equation 8.2-63 together with Eq. 8.2-61 defines the axial strain for the time step when the fuel and cladding are locked together.

The axial strain is separated into its thermal and force components to allow for the option to use only thermal effects or both thermal and force effects through the input parameter IAXTHF. There are also four options available which concern the treatment of the fuel-cladding locking. The axial expansion can be set to the free axial expansion of the fuel or the cladding, to always be constrained expansion, or to be a combination depending on the actual interface conditions. In the fourth option, all axial segments below the top locked segment are assumed to be in the constrained state. These options are controlled through the input parameter NAXOP. The most realistic options are both thermal and force components with the mixed free/constrained state. The other options are available to facilitate the study of axial expansion assumptions on accident sequences.

There also may be a third fuel-cladding boundary condition which does not currently exist in DEFORM-4. This is the "slip" condition where, at some level of mismatch between the fuel and cladding forces, the fuel would slide along the cladding. This is noted for possible inclusion in the future.

In the equations given above, the implicit assumption is present that the fuel in the region under consideration is both solid and uncracked. In the current version of DEFORM-4, the entire solid fuel zone is used in the calculation, both continuous and cracked. The result is to provide average axial expansion effects in a generalized plane strain framework. If transverse crack volumes are instituted in the cracking model, then the expansion effects in the cracked fuel region will be restudied. In order to provide a conservative assumption, when the melting reaches the cracked fuel boundary, axial expansion of that node is stopped. This is used to handle the necessity of expanding into transverse crack volume, before additional reactivity effects are treated.

### 8.3 Fuel-pin Phenomenology

In addition to the area of investigation termed "mechanics" that was described in Section 8.2, there is another area which is broadly termed "phenomenology". This includes those elements of fuel performance that are not necessarily considered in a structural/mechanical sense, but are generally of a microscopic nature resulting in macroscopic effects. Examples would include as-fabricated porosity migration, grain growth, fission-gas generation and release, and fuel swelling induced by solid and volatile fission products. Since these produce effects on various time scales, some are not considered in the transient calculation. However, all models have been coded so that they could be incorporated in the transient calculation if appropriate.

#### 8.3.1 As-Fabricated Porosity Migration

When cylindrical oxide fuel pins are placed in a neutron flux, the volumetric heating rates and low thermal conductivity of the fuel combine to produce high temperatures and very steep radial thermal gradients. These conditions can lead to the phenomenon commonly referred to as restructuring. The most distinct macroscopic aspects are divided into the columnar, equiaxed, and as-fabricated fuel zones. The basic physical processes that produce these zones have been identified as grain growth kinetics for the equiaxed zone, and porosity migration for the columnar zone. In this section, the phenomenon of porosity migration will be discussed.

Sintered fuel pellets contain residual pores on the grain boundaries. At the high temperatures commonly experienced in a nuclear fuel pin, the mobility of the constituent atoms can become important since this activity is usually related to the internal energy, which is represented in an Arrhenius equation form. However, if the temperature was uniform, there would be no macroscopic movement because there is no driving force. The large thermal gradients that exist in a fuel pin act as the driving force for atomic movement. This mobility and driving force cause the pores to migrate up the thermal gradient. This movement of porosity is important because the thermal conductivity of the fuel depends on its local porosity. If there is a large amount of pore migration a central hole will be formed. This change in geometry affects the heat transfer characteristics of the pin.

The process begins with the coalescence of the irregularly shaped pores in the as-fabricated fuel. The coalescence and movement of these pores results in the formation of characteristic lenticular pores, with a long axis parallel to the fuel isotherms and the short axis in the direction of the thermal gradient. This initial step of becoming lenticular is not included in DEFORM-4; only the movement of the pores up the thermal gradient.

There are three mechanisms that could lead to pore motion: (1) evaporation condensation across the pore, (2) pore surface diffusion, and (3) mass diffusion around the pores. The mass diffusion process is assumed to be negligible because of the high activation energy required to make atoms in a solid sufficiently mobile to produce appreciable mass transport. The evaporation-condensation process is expected to be the dominant process if the as-fabricated pores are large and temperatures are high. If the pores are small and at lower temperatures, the surface diffusion process would be expected to dominate. When the LIFE-III [8-5] code was in the process of thermal calibration, it was found that the available data made it impossible to determine the thermal dependences of these last two processes, so the evaporation-condensation process was chosen as the dominant mechanism. This same approach has been employed in DEFORM-4.

The large radial thermal gradient existing in reactor fuel pins at power produces a gradient across the pore. The atoms on the hotter surface evaporate, move across the pore, and condense on the cooler surface. This causes the pore to move up the thermal gradient. Bober and Schumacher [8-6] developed the following form for the velocity of the pore due to this process.

$$U = \frac{A_p}{T^A} e^{-[Q_p/RT]} \frac{dT}{dr} \quad (8.3-1)$$

where

U = Pore velocity, m/s

T = Temperature, K

- r = Radius, m
- $A_p$  = Pre-exponential factor,  $m^2 T^{(A-1)} s^{-1}$
- $Q_p$  = Evaporation-condensation activation energy, J g-mole<sup>-1</sup>
- R = Universal gas constant, J K<sup>-1</sup> g-mole<sup>-1</sup>
- A = Temperature exponent

Theoretical values for  $Q_p$ ,  $A_p$ , and A were obtained by Clement [8-7] and compare well with experimental values. Values have also been determined through the thermal calibration of the LIFE-III code [8-5].

In a cylindrical fuel rod with an axisymmetric power distribution, the thermal gradient is zero at the center of the pin, or inner surface if a central void exists. The direct application of Eq. 8.3-1 would result in an accumulation of porosity in the innermost cell. To avoid this nonphysical situation, the thermal gradient at the inner fuel cell boundary is assumed to be the average value across the central cell. This treatment simulates the diffusion of the pores and the formation of channels open to the central void.

In DEFORM-4, each fuel cell is assumed to have a uniform porosity. The change in cell porosity is determined from the initial porosity, the porosity moving into the cell from a neighboring cell, and the porosity moving out of the cell to a neighboring cell.

$$P_i(t+\Delta t) = P_i(t) + P_{in}(\Delta t) - P_{out}(\Delta t) \quad (8.3-2)$$

where

- $P_i(t+\Delta t)$  = Porosity in cell i at the end of the time step
- $P_i(t)$  = Porosity in cell i at the beginning of the time step
- $P_{in}(\Delta t)$  = Porosity moving into cell i from cell i+1
- $P_{out}(\Delta t)$  = Porosity moving out of cell i and entering cell i-1
- $\Delta t$  = Time-step length

Lackey, et al. [8-8] developed the amount of porosity crossing a cell boundary, based on the velocity of the pores and the length of the time step. The porosity in the annulus from  $r_i$  to  $r_i + U_i \Delta t$  would be expected to cross the cell boundary at  $r_i$  during the time step,  $\Delta t$ . These considerations result in the following definitions for  $P_{in}$  and  $P_{out}$ .

$$P_{in}(\Delta t) = \frac{\pi P_{i+1}(t)}{A_{i+1}} [(r_{i+1} + U_{i+1} \Delta t)^2 - r_{i+1}^2] \quad (8.3-3)$$

$$P_{out}(\Delta t) = \frac{\pi P_i(t)}{A_i} [(r_i + U_i \Delta T)^2 - r_i^2] \quad (8.3-4)$$

where

- $P_{i+1}(t), P_i(t)$  = Initial porosity in fuel cells  $i+1$  and  $i$ , respectively
- $r_{i+1}, r_i$  = Outer and inner radial boundaries of fuel cell  $i$
- $U_{i+1}, U_i$  = Pore velocity at radial locations  $r_{i+1}$  and  $r_i$ , respectively
- $A_{i+1}, A_i$  = Cross-sectional area of radial fuel cells  $i+1$  and  $i$ , respectively

The application of Eqs. 8.3-2 through 8.3-4 could lead to a situation in which more porosity leaves a cell than exists originally and enters from the neighboring cell. This is clearly a nonphysical result of the equations. It is also unlikely that the porosity in any cell would become zero because porosity can become trapped behind dislocations, impurities, and fission products. A parameter, PRSMIN, is available to allow input of the minimum porosity allowed in a cell. If application of Eq. 8.3-2 would cause the new cell porosity to fall below PRSMIN,  $P_{out}$  is reduced to the amount which would make the cell porosity equal to the allowed minimum. This treatment assumes that the total porosity is conserved.

At the fuel surface, the influx of porosity is assumed to be zero. Because of the strong temperature dependence of the Arrhenius term in Eq. 8.3-1, the pore velocity is very small even with the thermal gradient at its maximum. This, combined with the surface tension, makes it extremely unlikely to have significant porosity introduced at the fuel surface.

The above equations are solved in the subroutine PORMIG. In the solution, it is assumed that all pores in the vicinity of the boundary  $r_i$  travel at the velocity  $U_i$ . Therefore, the maximum travel of a pore is directly related to the time-step length.

$$\Delta r_v = U_i \Delta t \quad (8.3-5)$$

where

$$\Delta r_v = \text{Maximum distance traveled by pores}$$

In order to maintain accuracy, it has been found that the time step length should be restricted so that the maximum distance traveled by the fastest pores is less than a fourth of the cell width.

$$\Delta t_m = \frac{\Delta r_m}{4U_m} \quad (8.3-6)$$

where

$$\Delta t_m = \text{Maximum time-step length}$$

$$\Delta r_m = \text{Extent of the fuel cell outside the fastest velocity boundary}$$

$$U_m = \text{Maximum pore velocity}$$

There is a second reason for limiting the size of the computational time step. As discussed in Section 8.1.2, the thermal hydraulic calculations in SAS4A are performed separately from the mechanical/phenomenological calculations in DEFORM-4. Since porosity migration changes the geometry of the fuel pin and the radial porosity distribution, which changes the conductivities, it is necessary to limit the time step so the geometric and property changes can be fed back into the thermal calculation. It has been found that the criterion given in Eq. 8.3-6 is quite adequate for this purpose.

When the porosity migrates up the thermal gradient, it can pull the grain boundaries along with it, producing the characteristic columnar grains seen in restructured fuel. If enough porosity has migrated out of a cell, the grains in the cell are assumed to be columnar. In DEFORM-4, the mechanism for determining if a cell contains columnar grains is the checking of the current porosity against the initial value in the as-fabricated fuel.

$$P_i(t+\Delta t) \leq R_{eq} P_o \quad (8.3-7)$$

where

$R_{eq}$  = Fraction, input parameter

$P_o$  = Initial as-fabricated porosity

If the inequality in Eq. 8.3-7 is satisfied, the cell is assumed to contain columnar grains. All cells inside the outermost cell which satisfy the inequality are also assumed to be columnar. This determination does not affect any calculations, but is used for comparisons with the results from the destructive examination of pins used in calibration exercises.

The movement of these as-fabricated pores causes a movement of gas to the central void, and release to the plenum. In order to achieve a strict conservation of gases within the pin, the effect must be considered. At the as-fabricated conditions, the porosity is assumed to contain helium in equilibrium with the reference conditions. This, therefore, defines the amount of gas associated with each radial cell. As the porosity changes in the cell, the associated gas is also changed under the assumption that the gas content change is directly related to the porosity change.

$$G_{af,i}(t + \Delta t) + G_{af,i}(t) \frac{P_i(t + \Delta t)}{P_i(t)} \quad (8.3-8)$$

where

$G_{af,i}(t+At)$  = As-fabricated gas in radial cell i at end of the time step, kg

$G_{af,i}(t)$  = As-fabricated gas in radial cell i at end of the time step, kg

Once the changes have been determined for all radial cells, the amount of gas released to the central void, and hence the plenum, is determined and added to the total helium inventory.

While this gas accountability may have a very small effect on the actual plenum pressure during the pretransient calculations, it can be significant under transient conditions. Since melting of a radial cell is assumed to release the as-fabricated porosity and its associated gas into the molten cavity immediately, there can arise situations where this addition can affect the molten cavity pressure. With the conservation of this material considered in DEFORM-4, a better representation of the molten cavity pressurization is provided, no matter the transient under study.

### 8.3.2 Grain Growth

At the relatively low temperatures in the outer fuel region, the as-fabricated porosity is unable to migrate despite the large thermal gradient, because the atomic mobility is too low. However, the atoms may be active enough to cross the grain boundaries. The larger grains grow at the expense of the smaller, due to the tendency of atoms to jump from a convex (higher energy) to a concave (lower energy) surface. The net effect is to reduce the surface area, and thereby, the surface energy associated with the grains. This grain growth is a strong function of atomic activity, i.e., temperature. In nuclear fuels, the surface temperature is usually below the "threshold" temperature where activity is great enough to cause redistribution at the grain surfaces. Due to the strong temperature dependence and the steep thermal gradient, a distinct region usually develops where the grains grow isotropically, irrespective of the large gradient. This "equiaxed" zone extends inward to the region where pore migration becomes active and produces the "columnar" grains by dragging the boundaries during migration.

The grain-size distribution is important because the fission-gas release and fuel-creep functions depend on this parameter. The calculation of this clearly visible zone also offers a simple experimental calibration region which can be used in the validation process.

Two grain-growth models are available in the GRGROW subroutines and are selected through the input variable NGRAIN. If NGRAIN is greater than 0, the unlimited grain-growth option is used and the value of NGRAIN is the grain diameter exponent; see Section 8.3.2.1 below. If NGRAIN is zero, a limited grain-growth model is used. In this model the grain sizes are limited to an experimentally determined value; see Section 8.3.2.2 below. Both models give very similar results in the lower temperature regions associated with the equiaxed region where the grains are usually two to ten times the initial size. At higher temperatures, the first model results in larger grains because of the unconstrained growth. However, in these regions, porosity migration also produces the columnar grain structure which uses a separate method for determining the effective grain size for use in the fission-gas release and fuel-creep calculations; see Section 8.3.2.3 below. Because the unlimited growth model offers more flexibility to model mechanistic behavior, it is suggested for use prior to the validation of the integral code.

### 8.3.2.1 Unlimited Grain Growth - Equiaxed Region

The growth phenomenon may be characterized by a simple kinetic equation, with the growth rate given as

$$\frac{1}{D} \frac{dD}{dt} = \frac{1}{D^n} A_g \exp(-Q_v/RT) \quad (8.3-9)$$

where

D = Grain diameter, m

n = Growth mechanism input parameter

A<sub>g</sub> = Pre-exponential constant

Q<sub>v</sub> = Activation energy for the growth mechanism related to n, J g-mole<sup>-1</sup>

- $t$  = Time, s  
 $R$  = Universal gas constant,  $J K^{-1} g\text{-mole}^{-1}$   
 $T$  = Temperature, K

The value of the parameter  $n$  is related to the grain-growth mechanism and depends on the driving and retarding forces being considered. Nichols [8-9] developed theoretical meanings for the values usually associated with  $n$ . If the grain boundaries are assumed to move toward their center of curvature at a rate proportional to the curvature,  $n$  would be 2. If the mechanism is through the evaporation-condensation process across pores on the boundaries, with the pressure in the pores inversely proportional to their radius, the value of  $n$  is 3. If boundaries are shifted by volume diffusion moving material around the pores or the evaporation-condensation process with the internal pore pressure constant, the value of  $n$  is 4. If the mechanism is surface or interface diffusion in the pores, the value of  $n$  is 5. In all cases where  $n$  is 3 through 5, it is assumed that the pores remain on the grain boundaries.

If the temperature is assumed constant for a time period  $\Delta t$ , Eq. 8.3-9 can be integrated to yield

$$D^n(t+\Delta t) = D^n(t) + n A_g \Delta t \exp(-Q_v/RT) \quad (8.3-10)$$

The term  $(n A_g)$  is usually combined when determining the constants by comparison with experimental data, so Eq. 8.3-10 is rewritten as

$$D^n(t+\Delta t) = D^n(t) + G_k \Delta t \exp(-Q_v/RT) \quad (8.3-11)$$

which is in the form coded in the GRGROW subroutine. In all cases, the values for the parameters  $G_k$  and  $Q_v$  depend strongly on the value of  $n$  used in Eq. 8.3-11.

R.N. Singh [8-10] conducted an investigation into the grain-growth kinetics for sintered  $UO_2$  pellets at temperatures between 1800 and 2100°C. His conclusions suggested that the cubic form of Eq. 8.3-10 was most accurate, and appropriate constants were determined. When the

MATPRO-10 [8-11] materials properties package was developed, the available experimental evidence was collected, and curve fits were applied for exponents of 2 through 4. In this study, it was found that an exponent of 4 gave the best fit with 3 giving very similar results. In the GRGROW subroutine, the input variables for the exponent, pre-exponential constant, and activation energy are used to provide maximum flexibility for the user.

### 8.3.2.2 Limited Grain Growth - Equiaxed Region

In a study of grain sizes in irradiated fuel by Ainscough, et al. [8-12], a kinetics equation for grain growth was developed that included a maximum grain size. As the grains grow, the boundaries are retarded by the effects of intergranular pores, solid fission products, and gas bubbles. After the grains reach a certain size, they are stopped from additional growth. It was postulated that the maximum grain size could be represented by the form

$$D_m = G_m \exp (-Q_m/RT) \quad (8.3-12)$$

where

$D_m$  = Maximum grain size, m

$G_m$  = Pre-exponential constant, m

$Q_m$  = Maximum grain size activation energy, J (g-mole)<sup>-1</sup>

$R$  = Universal gas constant, J k<sup>-1</sup> g-mole<sup>-1</sup>

$T$  = Temperature, K

The temperature dependence of Eq. 8.3-12 results from the higher mobility of the retardants and the resultant reduction in grain-boundary drag as the temperature increases.

The kinetic equation developed is then given by

$$\frac{dD}{dt} = G \left[ \frac{1}{D} - \frac{1}{D_m} \right] \exp (-Q/RT) \quad (8.3-13)$$

where

$D$  = Grain diameter, m

$G$  = Pre-exponential grain growth constant,  $m^2 s^{-1}$

$Q$  = Grain-growth activation energy,  $J g\text{-mole}^{-1}$

If the temperature is assumed to be constant over the time step,  $\Delta t$ , the integration of Eq. 8.3-13 produces the following transcendental equation:

$$f(D(t+\Delta t)) = D_m^2 \ln \left[ \frac{D_m - D(t)}{D_m - D(t+\Delta t)} \right] - G \Delta t \exp(-Q/RT) + D_m (D(t) - D(t+\Delta t)) = 0 \quad (8.3-14)$$

The solution for  $D(t+\Delta t)$  is obtained through the Newton's Method iterative scheme.

$$D_{k+1} = D_k - \frac{f(D_k(t+\Delta t))}{f'(D_k(t+\Delta t))} \quad (8.3-15)$$

where

$D_k$  = The  $k$ -th estimate of the grain diameter to satisfy Eq. 8.3-14, m

$$f'(D_k(t+\Delta t)) = \frac{df(D_k)}{dD_k} \quad (8.3-16)$$

Since the grain size at the beginning of the time step,  $D(t)$ , and the maximum grain size,  $D_m$ , are known constants, the differentiation in Eq. 8.3-16 may be performed on Eq. 8.3-14 after expanding the log term to the difference of two log terms:

$$f'(D_k(t+\Delta t)) = \frac{D_m^2}{D_m - D_k(t+\Delta t)} - D_m \quad (8.3-17)$$

Equation 8.3-17 is reduced to

$$f'(D_k(t+\Delta t)) = \frac{D_m D_k(t+\Delta t)}{D_m - D_k(t+\Delta t)} \quad (8.3-18)$$

and this is substituted into Eq. 8.3-15 to produce the final form for the next estimate,  $k+1$ , of the grain size to satisfy Eq. 8.3-14.

$$D_{k+1}(t+\Delta t) = D_k(t+\Delta t) - f(D_k(t+\Delta t)) \frac{(D_m - D_k(t+\Delta t))}{D_m D_k(t+\Delta t)} \quad (8.3-19)$$

This iteration is continued until a consistent value is determined.

If the maximum grain size,  $D_m$ , is smaller than the size at the beginning of the time step,  $D(t)$ , due to power or temperature reductions, the current grain size,  $D(t+\Delta t)$ , is maintained at its previous value.

### 8.3.2.3 Columnar Grain Size and Region Boundaries

The extent of the columnar region boundary is found as was discussed in Section 8.3.1. The effective grain size in this region is determined by the equiaxed grain size at the columnar/equiaxed boundary and the extent of the columnar boundary.

$$D_{col} = \sqrt{\Delta r_{col} D_b} \quad (8.3-20)$$

where

- $D_{col}$  = Effective grain size in the columnar region, m
- $\Delta r_{col}$  = Radial extent of the columnar region, m
- $D_b$  = Equiaxed grain size at the columnar/equiaxed boundary, m

The boundary between the equiaxed and as-fabricated region is based on the amount of grain growth. The grain size in each radial cell is compared to the initial grain size and if suitable growth has occurred, the region is classified as equiaxed.

$$D_i(t + \Delta t) \geq R_{ueq} D_o \quad (8.3-21)$$

where

- $D_i(t + \Delta t)$  = Grain size in radial cell  $i$  at the end of the time step, m
- $R_{ueq}$  = Input factor
- $D_o$  = As-fabricated grain size, m

The check is started at the outer fuel surface and once the inequality in Eq. 8.3-21 is satisfied, that determines the equiaxed/as-fabricated boundary.

### 8.3.3 Fission-gas Release

The nuclear fission processes occurring in the fuel during the irradiation produce both solid and gaseous fission products. The gaseous products are primarily xenon and krypton. The model currently used in DEFORM-4 assumes that the gaseous products either precipitate as gas-filled bubbles on the grain boundaries, are contained in microbubbles within the fuel matrix, or are released to the available free volume in the pin plenum and fuel central void. Formation of grain boundary bubbles leads to fuel swelling and reduces the fuel-cladding gap size. The intra-granular gas is assumed to play no part in fuel swelling but becomes important upon fuel melting. Release to the free volume changes the gas mixture and reduces the thermal

conductivity of the gas in the gap. Fission-gas release, fuel swelling, and the fuel-pin temperature distribution are therefore closely interrelated. The migration of fission-gas bubbles up the thermal gradient is not treated.

Fission gases can be released when they reach any open porosity such as cracks, the fuel-cladding gap, the central void, or the fission-gas plenum. At temperatures below about 1300 K, the mobility of the gas atoms is too low for diffusion, so they are released only by collisions with fission fragments near the fuel surface. This fraction is very small and can be neglected. At temperatures between about 1300 and 1900 K, the atomic motion is high enough to allow diffusion to the grain surfaces. At temperatures above 1900 K, the gas bubbles become mobile and may escape by migration up the temperature gradient.

The mechanistic approach to the problem of gas release has been employed in codes such as GRASS-SST [8-13] and FRAS [8-14]. A complete modeling of the fission-gas behavior is attempted in these codes, describing the migration and coalescence of fission-gas bubbles in the grain and on grain boundaries. Gas release from the grains and grain boundaries to the exterior of the fuel are modeled. Detailed bubble-size distributions are calculated and grain-boundary channel formation is treated. The parameters involved have been studied and extensively calibrated.

Such a complete and detailed modeling effort is not currently envisioned for SAS4A. Because of the requirements that the SAS4A code size and running time be minimized, considerably simpler, less-mechanistic models have been incorporated into SAS4A. These models relate the release rate to escape probabilities. These probabilities are modeled as functions of temperature and density. They should also be related to grain size, but are not in the current version. The calculations are performed in the subroutine RELGAS.

#### 8.3.3.1 Fission-gas Generation

The total amount of fission gas generated in a fuel cell is related to the power of that cell. As the fission process proceeds, a number of isotopes result. Some of these fission products are

volatile gases which may coalesce to form fission-gas bubbles. It is assumed that each fission produces a constant fraction of fission-gas atoms.

$$G_a = F \times f_g \quad (8.3-22)$$

where

- $G_a$  = Number of gas atoms generated
- $F$  = Number of fissions during the time step
- $f_g$  = Fractional gas atoms generated per fission

While this model is not true of a single fission event, it does accurately represent the macroscopic results of a large number of fissions.

The number of fissions in an axial segment is related to the power generated.

$$F = \frac{P_j \Delta t}{1.603 \times 10^{-13} E_f} \quad (8.3-23)$$

where

- $P_j$  = Power generated by axial fuel segment j, w
- $\Delta t$  = Time-step length, s
- $E_f$  = Energy generated per fission, MeV

The numeric constant in Eq. 8.3-23 is the conversion factor from MeV to W-s. The code uses the amount of gas in units of mass, so Eq. 8.3-22 is rewritten as

$$G_m = \frac{F \times f_g \times MW_{fg} \times 10^{-3}}{N_a} \quad (8.3-24)$$

where

- $G_m$  = Mass of fission gas, kg  
 $MW_{fg}$  = Molecular weight of the fission gas, amu  
 $N_a$  = Avogadro number,  $0.6025 \times 10^{24}$  atoms/g-mole

The numeric constant in Eq. 8.3-24 converts g to kg. Combining Eq. 8.3-24 with 8.3-23 results in the mass of fission gas generated in the axial segment during the time step.

$$G_m = \frac{P_j \Delta t f_g MW_{fg}}{9.658 \times 10^{13} E_f} \quad (8.3-25)$$

If the radial power shape was flat, the total fission-gas mass could be divided between the radial fuel cells on the basis of cell mass. However, it is possible to have a radial power shape. The fission-gas mass in a radial fuel cell is determined by multiplying the fission gas generated by the whole segment by a radial factor.

$$G_i = G_m f_i \quad (8.3-26)$$

where

- $G_i$  = Fission-gas mass generated in radial fuel cell i, kg  
 $f_i$  = Fraction of total mass generated in radial cell i

The radial factor is based on the radial power shape factors and the radial fuel cell masses.

$$f_i = \frac{S_i M_i}{\sum_{k=1}^N (S_k M_k)} \quad (8.3-27)$$

where

- $S_i$  = Radial power shape factor for radial cell  $i$
- $M_i$  = Fuel mass in radial cell  $i$ , kg
- $N$  = Number of radial fuel cells

Substituting Eqs. 8.3-27 and 8.3-25 into Eq. 8.3-26 results in the fission-gas mass generated in the radial cell.

$$G_i = \frac{P_j \Delta t f_g MW_{fg} S_i M_i}{9.658 \times 10^{13} E_f \sum_{k=1}^N (S_k M_k)} \quad (8.3-28)$$

The amount of this gas located on the grain boundaries vs the amount retained in the fuel matrix is controlled through the input parameter FIFNGB. At each time step the new gas generated is divided between these two locations

$$G_{gb,i} = G_i f_{gb} \quad (8.3-29)$$

$$G_{fm,i} = G_i (1 - f_{gb}) \quad (8.3-30)$$

where

- $G_{gb,i}$  = Mass of generated fission gas assumed to be on grain boundaries in radial cell  $i$ , kg
- $G_{fm,i}$  = Mass of generated fission gas assumed to be in the fuel matrix in radial cell  $i$ , kg
- $f_{gb}$  = Fraction of fission gas generated that is on the grain boundaries, input parameter FIFNGB

Currently, release from these two regions is treated in the same manner, as described below. However, with this type of split in DEFORM-4, it would be possible to develop different release mechanisms, and even provide for a radially dependent value of  $f_{gb}$ . These considerations have been identified for possible future work if their effects were to become important.

This split in the gas location is significant because of the interactions with two other models: (1) the molten cavity pressure (Section 8.3.7), and (2) fission gas swelling (Section 8.3.4). Upon melting, all grain boundary gas is released immediately while the intra-granular gas has a delayed coalescence. In fuel swelling, only the grain boundary gas is assumed to produce fuel swelling.

#### 8.3.3.2 Isotropic Fission-gas Release

In the isotropic fission-gas release model, the release is treated as a function of a single release rate fraction,  $f$ , which is a function of temperature. This is the probability per unit time that a retained gas atom would be released. The basic rate equation governing the amount of retained gas in the fuel, at all locations, can be given by

$$\frac{dS}{dt} = -Sf + G \quad (8.3-31)$$

where

$S$  = Amount of fission-gas retained in the fuel, kg

$f$  = Fractional release rate of the retained gas,  $(\text{kg} \cdot \text{s})^{-1}$

$G$  = Fission-gas production rate,  $\text{kg s}^{-1}$

Assuming that  $f$  and  $G$  are constant within the time step,  $\Delta t$ , Eq. 8.3-31 may be integrated over the time step to yield the amount of retained gas at the end of the interval.

$$S(t + \Delta t) = S(t)\exp(-f\Delta t) + \frac{G}{f} [1 - \exp(-f\Delta t)] \quad (8.3-32)$$

Since the mobility of the gas atoms is a thermally activated process, it is assumed that the fractional release rate can be represented by

$$f = A_{\alpha} \exp(-Q_{\alpha}/RT) \quad (8.3-33)$$

where

$A_{\alpha}$  = Pre-exponential input constant

$Q_{\alpha}$  = Activation energy for release, input constant

The constants  $A_{\alpha}$  and  $Q_{\alpha}$  are determined through comparisons with experimentally determined values of the retained fission-gas from the destructive examination of irradiated fuel pellets and through comparisons with more sophisticated fission-gas release codes. Preliminary constants have been determined, but the validation exercises will be used to refine them.

### 8.3.3.3 Fission-gas Trap-release Model

A slightly more complex model that includes a more mechanistic treatment of fission-gas release was developed by Weisman et al. [8-15]. In this model the gas is assumed to be released in two ways: (1) direct release to the fuel surface, and (2) entrapment in the fuel matrix and subsequent release to the surface.

The amount of gas generated that is released directly is given by the following:

$$dn_i = k' G dt \quad (8.3-34)$$

where

- $dn_1$  = Amount of gas released in time increment  $dt$ , kg
- $k'$  = Fraction of the free gas that escapes to the surface without becoming trapped
- $G$  = Fission-gas production rate,  $\text{kg s}^{-1}$
- $dt$  = Time increment, s

The amount of gas trapped in the fuel matrix is given by the total amount generated minus the total released.

$$c = Gt - n \quad (8.3-35)$$

where

- $c$  = Amount of gas trapped in the fuel matrix, kg
- $t$  = Time, s
- $n$  = Amount of gas released, kg

If  $k$  is the probability that trapped gas will be released per unit time, then the amount of trapped gas which is released is given by

$$dn_f = k c dt \quad (8.3-36)$$

where

- $dn_f$  = Amount of trapped gas which is freed, kg

Of this gas, only a fraction  $k'$  is released to the surface without becoming retrapped

$$dn_2 = k' k c dt \quad (8.3-37)$$

where

$dn_2$  = Amount of trapped gas that is released to the fuel surface

The total amount of released gas,  $dn$ , is therefore given by

$$dn = dn_1 + dn_2 \quad (8.3-38)$$

or upon substitution of Eqs. 8.3-34, 8.3-35, and 8.3-37 into Eq. 8.3-38,

$$dn = k' G dt + k' k (Gt - n) dt \quad (8.3-39)$$

Integration of Eq. 8.3-39 is performed to give

$$n = G \left\{ t - \frac{1-k'}{K} [1 - \exp(-Kt)] \right\} \quad (8.3-40)$$

where

$K = k'k$  = Probability that trapped gas is released from the fuel matrix to the fuel surface

Assuming that the reactor power history is described by a series of constant power steps, the amount of gas released during a constant power time step is given by

$$\begin{aligned} \Delta n_i &= n_i - n_{i-1} \\ &= G_i \left\{ \Delta t_i - \frac{1-k'_i}{K_i} [1 - \exp(-K_i \Delta t_i)] \right\} \\ &\quad + c_{i-1} [1 - \exp(-K_i \Delta t_i)] \end{aligned} \quad (8.3-41)$$

where

- $\Delta n_i$  = Amount of gas released during time step  $\Delta t_i$ , kg
- $G_i$  = Fission-gas generation rate during time step  $\Delta t_i$ , kg s<sup>-1</sup>
- $\Delta t_i$  = Time-step duration, s
- $c_{i-1}$  = Amount of trapped gas at beginning of time step, kg
- $k'_i, K_i$  = Defined above, but evaluated for the time step  $\Delta t_i$

Equations for the terms  $k'$  and  $K$  were developed during the calibration of the FRAP-S2 computer code [8-16].

$$k' = \exp (-Q_{A1}/T + Q_{A2} - Q_{A3} d) \quad (8.3-42)$$

$$K = \exp (-Q_{A4}/T + Q_{A5}) \quad (8.3-43)$$

where

- $T$  = Temperature, K
- $d$  = Percent theoretical density of the fuel
- $Q_{A1}, Q_{A2}, Q_{A3}, Q_{A4}, Q_{A5}$  = Input constants

#### 8.3.4 Fuel Swelling

In DEFORM-4, the as-fabricated porosity and the fission-gas-generated porosity are treated separately. The migration of the as-fabricated porosity can lead to either densification or swelling of the fuel depending on local conditions (see Section 8.3.1). The newly formed porosity arising from fission-gas bubbles introduces additional porosity that may be in a nonequilibrium condition, depending on the amount of gas in the bubbles, the local hydrostatic pressure, and the fuel surface tension. This fission-gas porosity may increase or decrease as a function of time, producing changes in the fuel dimensions through swelling or densification. These changes in fuel porosity also affect the fuel thermal conductivity, since both the

as-fabricated and fission-gas porosity are considered in the porosity terms. In addition to this gas effect, the solid fission products locate themselves interstitially in the fuel matrix, causing strains that produce swelling. Both these effects are accounted for by DEFORM-4.

Swelling strains may occur both axially and radially. In general, the axial swelling strains in oxide fuels are relatively small compared to the thermal expansion effects. However, in some transients the differences caused by including the axial swelling can be enough to modify the accident scenario. For this reason, and to provide the basis for future versatility, axial swelling has been incorporated into DEFORM-4. Radial swelling is important because of the effects on fuel-cladding gap size and mechanical interaction. Both effects can produce large differences in the prediction of cladding failure, so radial swelling is also included in DEFORM-4. These fuel swelling considerations are treated in the subroutine FSWELL.

#### 8.3.4.1 Nonequilibrium Fission-gas Bubbles

The swelling rate due to fission gas depends on the release of the gas to grain boundaries and formation of fission-gas bubbles. Detailed treatments for this process can be found in codes such as FRAS [8-14] and GRASS-SST [8-13]. The current model in DEFORM-4 is much simpler and phenomenological on a more macroscopic level. While fission gas exists in both the fuel matrix and on grain boundaries, it is the bubbles on the grain boundaries that produce the significant swelling in oxide fuels. If these bubbles are underpressurized, a reduction in the bubble volume due to the fuel hydrostatic pressure will reduce the volume of a fuel cell. If the bubbles are overpressurized, an increase in bubble size, and thereby fuel cell volume can result. To determine the rate of swelling, or densification, the mechanical stresses (Section 8.2), internal gas pressure, pressure due to surface tension, and the creep properties of the fuel (Section 8.7.6) must be known.

While fission gas exists in both the fuel matrix and on the grain boundaries, it is the bubbles on the grain boundaries that produces significant swelling in oxide fuels. However, the actual amount of gas involved and its distribution changes with burnup. As discussed in Section 8.3.3.1, DEFORM-4 uses a fixed factor to distribute the generated fission gas between the fuel

matrix and grain boundaries. However, this type of approach does not fully represent the gas mass associated with fuel swelling. Therefore, DEFORM-4 uses a burnup dependent parameter, FGMIN, to specify the amount of fuel matrix retained gas to associate with the fission gas induced swelling. Figure 8.3-1 shows the recommended curve for this fission gas parameter.

The treatment of the bubble gas pressure and surface tension follows that found in the LIFE code [8-7]. This approach is macroscopic in nature and the constants used are based on the calibration of LIFE. The swelling rate of these bubbles is estimated from the fuel creep function. Swelling causes changes in the stress state of the fuel because the changes in geometry produce changes in the boundary conditions. But changes in stress states also produce changes in the swelling through changes in hydrostatic pressures. The swelling and mechanical response are closely coupled. For this reason, the swelling calculation in DEFORM-4 has been incorporated within the iterations to find the set of conditions that bring about consistency between the fuel and cladding. Swelling and mechanical strains are stored separately, but calculated considering mutual influences. The strains due to swelling/hot pressing of the fuel are added to the total mechanical deformation at the end of each time step.

The pressure in the bubble necessary to balance the surface tension is parameterized as

$$P_{\gamma} = A_{pg} e^{(Q_{pg}/RT)} \quad (8.3-44)$$

where

$P_{\gamma}$  = Pressure due to surface tension effects, Pa

$A_{pg}$  = Pre-exponential calibration constant, Pa

$Q_{pg}$  = Exponential calibration constant, J(g-mole)<sup>-1</sup>

$T$  = Temperature, K

$R$  = Ideal-gas constant, J k<sup>-1</sup>(g-mole)<sup>-1</sup>

If the bubbles are assumed to be spherical, the relationship between surface tension pressure and bubble radius can be determined.

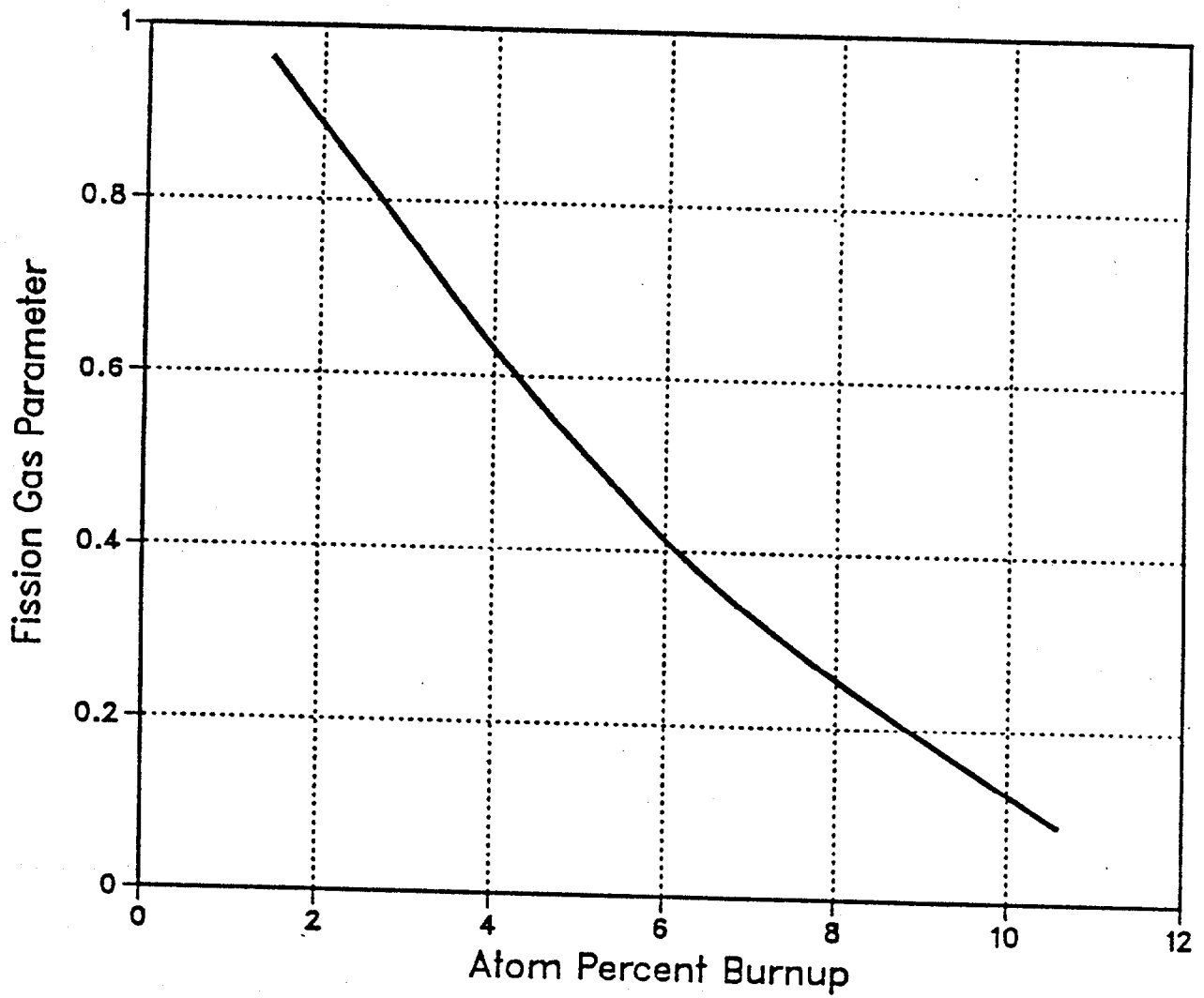


Fig. 8.3-1. DEFORM-4 Fission Gas Parameter FGMIN

$$r_B = \frac{2\gamma}{P_\gamma} \quad (8.3-45)$$

where

- $r_B$  = Average fission-gas bubble radius, m  
 $\gamma$  = Surface tension, N/m

The internal fission-gas bubble pressure,  $P_{fg}$ , is determined by the ideal-gas law.

$$P_{fg} = M_{fg} RT/V_{fg} \quad (8.3-46)$$

where

- $P_{fg}$  = Pressure inside the fission gas-bubble, Pa  
 $M_{fg}$  = Moles of fission gas in the bubbles  
 $R$  = Ideal-gas constant  
 $T$  = Temperature, K  
 $V_{fg}$  = Volume of fission-gas bubbles in the cell, m<sup>3</sup>

The hydrostatic pressure of the fuel,  $P_\sigma$ , is determined from the stress state in the fuel cell. The input parameter IPSIG determines the assumption used to define this pressure according to the following table.

<u>IPSIG</u>	<u>Definition of <math>P_\sigma</math></u>
1	$-\sigma_r$
2	$-1/2 (\sigma_r + \sigma_\theta)$
3	$-1/3 (\sigma_r + \sigma_\theta + \sigma_z)$

The imbalance between the bubble pressure and the external pressures is used to determine the effective creep rate of the fuel for swelling effects.

$$\Delta P = P_{fg} - P_{\gamma} - P_{\sigma} \quad (8.3-47)$$

where

- $\Delta P$  = Pressure differential
- $P_{fg}$  = Pressure in the bubbles
- $P_{\gamma}$  = Surface tension pressure
- $P_{\sigma}$  = Hydrostatic pressure

If the differential is positive, the bubbles will expand, swelling the fuel cell. If it is negative, the bubbles will contract, densifying the fuel cell. The process assumed to control the rate of these volume changes is the creep properties of the fuel in the cell.

There is a bubble volume that would cause Eq. 8.3-47 to become zero. The equilibrium volume,  $V_e$ , is found by assuming the pressure differential is zero. To achieve this, the bubble pressure must balance the surface tension and hydrostatic pressures.

$$P_{fg} = P_{\gamma} + P_{\sigma} \quad (8.3-48)$$

Equation 8.3-46 is substituted into Eq. 8.3-48 and the result rearranged to determine the fission-gas bubble equilibrium volume,  $V_e$ .

$$V_e = \frac{M_{fg} RT}{(P_{\gamma} + P_{\sigma})} \quad (8.3-49)$$

If all volume changes took place instantaneously, this would be the fission-gas bubble volume. However, it is assumed that the fuel creep properties define the rate of change of the volume and the driving force is the pressure differential. The following equation is therefore assumed to define the bubble volume rate of change.

$$\frac{dV_g}{dt} = \frac{(V_e - V_g)}{\tau_c} \quad (8.3-50)$$

where

- $V_g$  = Fission-gas bubble volume,  $m^3$
- $V_e$  = Equilibrium fission-gas bubble volume,  $m^3$
- $\tau_c$  = Fuel creep time constant, s
- $t$  = Time, s

The fuel creep time constant,  $\tau_c$ , is defined as the inverse of the fuel creep rate in the fuel cell under consideration with the pressure differential as the driving force. Integrating Eq. 8.3-50 over the time step,  $\Delta t$ , and rearranging to find the fission-gas bubble volume at the end of the time step results in the following.

$$V_g(t + \Delta t) = V_e [1 - e^{-\Delta t/\tau_c}] + V_g(t)e^{-\Delta t/\tau_c} \quad (8.3-51)$$

The change in volume over the time step,  $\Delta V_s(\Delta t)$ , is found by subtracting the volume at the beginning of the time step,  $V_g(t)$  from both sides of Eq. 8.3-51.

$$\Delta V_s(\Delta t) = [V_e - V_g(t)] [1 - e^{-\Delta t/\tau_c}] \quad (8.3-52)$$

Equation 8.3-52 gives the total volume change for a particular radial cell during the time step. When this change in volume takes place, part of it is radial volume expansion, typically 2/3, and the rest takes place axially. The radial component is handled nominally through the redefinition of the cell boundaries. The axial component requires special consideration because of the assumption of generalized plane strain. Each radial cell will produce a different axial strain due to the swelling process. A plane strain is determined that moves the same mass of fuel across the original axial segment boundary.

$$\Delta V_{s,i} = f_a \Delta V_s \quad (8.3-53)$$

where

- $\Delta V_{s,i}$  = Volume change due to swelling for radial node  $i$ ,  $m^3$ .  
 $f_a$  = Fraction of total swelling taking place axially.

This change would result in a new axial segment length.

$$\Delta V_{s,i} = \Delta h_{s,i} \pi (r_{i+1}^2 - r_i^2) \quad (8.3-54)$$

where

- $\Delta h_{s,i}$  = Axial segment length change from swelling,  $m$   
 $r_{i+1}$  = Outer radius of radial cell  $i$  after swelling is included,  $m$   
 $r_i$  = Inner radius of radial cell  $i$  after swelling is included,  $m$ .

Combining Eqs. 8.3-53 and 8.3-54, the segment length change for radial cell  $i$  can be found

$$\Delta h_{s,i} = \frac{f_a \Delta V_s}{\pi (r_{i+1}^2 - r_i^2)} \quad (8.3-55)$$

The axial strain for the cell can then be found

$$Z_{s,i} = \frac{\Delta h_{s,i}}{h} \quad (8.3-56)$$

where

- $h$  = Axial segment length at beginning of time step,  $m$

The fraction of the fuel mass that has moved from the original segment length,  $h$ , into the additional length,  $\Delta h_{s,i}$ , is the ratio of the length change to the new length, assuming uniform mass distribution within the segment

$$F_i = \frac{\Delta h_{s,i}}{h + \Delta h_{s,i}} \quad (8.3-57)$$

where

$F_i$  = Fraction of original cell mass moved into length  $\Delta h_{s,i}$ .

Using Eqs. 8.3-56 and 8.3-57, this mass fraction can be defined in terms of the axial strain

$$F_i = \frac{z_{s,i}}{1 + z_{s,i}} \quad (8.3-58)$$

The total mass movement across the original boundary can therefore be determined

$$M_{aT} = \sum_{i=1}^{N_t} F_i M_i \quad (8.3-59)$$

where

$M_{aT}$  = Total fuel mass moved out of original segment length, kg

$M_i$  = Fuel mass in radial cell  $i$

$N_t$  = Total number of radial cells

A generalized axial swelling strain using Eqs. 8.3-58 and 8.3-59 can now be defined that gives this same mass transfer.

$$M_{aT} = \frac{z_{s,a}}{1 + z_{s,a}} M_T \quad (8.3-60)$$

where

$z_{s,a}$  = Generalized axial swelling strain

$M_T$  = Total mass in the axial segment

Solving Eq. 8.3-60 yields the desired result of an axial strain that is uniform over the radial cross section, but produces the same mass movement as the sum of the individual radial cell components

$$z_{s,a} = \frac{M_{aT}}{M_T - M_{aT}} \quad (8.3-61)$$

These fission gas bubble swelling considerations are handled by the subroutine FSWELL.

#### 8.3.4.2 Solid Fission-product Swelling

In addition to the gaseous fission-product swelling, there is solid fission-product swelling from products such as zirconium, niobium, molybdenum, the rare earths, yttrium, etc. A detailed treatment of these solid fission products, which considered their physical and chemical state to determine the partial volumes, would yield the lattice strain created. This, together with the isotopic yields from fission, would result in a mechanistic estimate of solid product swelling. This type of treatment requires more computational resources than are warranted for the magnitude of the phenomenon.

A simpler model is assumed which relates the fractional volume change to the fuel burnup.

$$\left[ \frac{\Delta V}{V} \right]_{SP} = \dot{\epsilon}_{sfp} B \quad (8.3-62)$$

where

$$\left[ \frac{\Delta V}{V} \right]_{SP} = \text{Fractional volume change due to solid fission products}$$

$$\dot{\epsilon}_{sfp} = \text{Solid fission-product swelling rate parameter, } (\Delta V/V) (\text{atom \% burnup})^{-1}$$

$$B = \text{Fuel burnup, atom \%}$$

Due to uncertainties in the thermodynamic state and migration characteristics of the products, the value of  $\dot{\epsilon}_{sfp}$  is specified by an input parameter.

The volume changes from solid product changes are included with those of the volatile products when determining the changes in fuel volume that may change the fuel-cladding interface conditions. However, this volume change is not affected by the local hydrostatic pressure and therefore remains a constant through the iterations mentioned in the previous section and discussed at length in Section 8.5.

### 8.3.5 Irradiation-induced Cladding Swelling

When 20% cold-worked 316 stainless steel material is irradiated in a fast neutron flux, there is a temperature- and flux-dependent reduction in density through the formation of irradiation-induced voids. The model in DEFORM-4 is based on an empirical correlation corresponding to stress-free swelling in the Nuclear Systems Material Handbook [8-17]. The volume change is represented by

$$\frac{\Delta V}{V} = \frac{\Sigma}{1-\Sigma} \quad (8.3-63)$$

where

$$\begin{aligned}\Sigma &= \text{Negative fractional density change} \\ &= - \frac{(\rho_f - \rho_o)}{\rho_o}\end{aligned}\tag{8.3-64}$$

$\rho_f$  = Final immersion density

$\rho_o$  = Initial immersion density

To find the change during the time step, the derivative of Eq. 8.3-63 is

$$\frac{d \left( \frac{\Delta V}{V} \right)}{dt} = \frac{1}{(1-\Sigma)^2} \left( \frac{d\Sigma}{dt} \right)\tag{8.3-65}$$

The correlation represents two characteristics of irradiation-induced swelling based on experimental findings. First, the rate of swelling for 20% cold-worked 316 stainless steel is temperature sensitive. Second, there appears to be an incubation period during which little change in density is observed. The form given in the NSMH for the negative fractional density change is

$$\Sigma = R(T) \left\{ \phi t + \frac{1}{\alpha} \ln \left[ \frac{1 + \exp [\alpha(\tau - \phi t)]}{1 + \exp (\alpha\tau)} \right] \right\}\tag{8.3-66}$$

where

$R(T)$  = Temperature-dependent rate parameter

$\phi$  = Fast neutron flux

$t$  = Time

$\alpha$  = Calibration constant

$\tau$  = Incubation parameter

The derivative of Eq. 8.3-66 gives

$$\frac{d\Sigma}{dt} = R(t) \phi \left[ 1 - \frac{1}{1 + \exp[-\alpha(\tau - \phi t)]} \right] \quad (8.3-67)$$

The fractional volume change is, therefore, determined from

$$\Delta \left[ \frac{\Delta V}{V} \right] = \frac{d \left[ \frac{\Delta V}{V} \right]}{dt} \Delta t = \frac{\Delta t}{(1-\Sigma)^2} \frac{d\Sigma}{dt} \quad (8.3-68)$$

The swelling is assumed to be isotropic and always outward. The new cross sectional area,  $A$ , is calculated assuming  $\frac{1}{3}$  of the volume change takes place axially.

$$A(t + \Delta t) = \pi[r_o^2(t + \Delta t) - r_i^2(t + \Delta t)] = \pi[r_o^2(t) - r_i^2(t)] \left[ 1 + \frac{2}{3} \left( \frac{\Delta V}{V} \right) \right] \quad (8.3-69)$$

where

- $A$  = Cross-sectional area
- $r_o(t), r_o(t+\Delta t)$  = Outer radius at the beginning and end of the time step
- $r_i(t), r_i(t+\Delta t)$  = Inner radius of the beginning and end of the time step

The new inner radius is calculated from

$$r_i(t + \Delta t) = r_i(t) \left[ 1 + \frac{1}{3} \left( \frac{\Delta V}{V} \right) \right] \quad (8.3-70)$$

The forms given for the rate and incubation parameter are given below.

$$R(T) = 0.01 [\exp (0.0419 + 1.498 \beta + 0.122\beta^2 - 0.332\beta^3 - 0.441\beta^4)] \quad (8.3-71)$$

$$\tau = 4.742 - 0.2326 \beta + 2.717 \beta^2 \quad (8.3-72)$$

$$\alpha = 0.75 \quad (8.3-73)$$

where

$$\beta = (T - 500)/1000$$

$$T = \text{Temperature, } ^\circ\text{C}$$

The rate, R, and incubation,  $\tau$ , parameters needed in Eq. 8.3-67 have several options which are controlled through the input parameters IRATE and ITAU. The confidence limits on the use of these equations suggest the use of upper and lower bounds on R and  $\tau$ . Nominal values are obtained with no multipliers to these parameters. The input parameters IRATE and ITAU can be used to select the specified bound as illustrated below. Input values of zero give the nominal parameters. If cladding swelling does not occur, the values of ITAU and IRATE can be set to bypass the swelling calculation.

Limits on steady-state swelling rate parameter, R:

Upper bound (IRATE = 1)

$$F = 1.3 + 2.5 \exp[-(T - 350)^2 \times 10^{-4}] + 1.7 \exp[-(T - 650)^2 \times 10^{-3}] \quad (8.3-74)$$

$$R_u = R \times F \quad (8.3-75)$$

$$T = \text{Temperature, } ^\circ\text{C}$$

Lower bound (IRATE = -1)

$$R_l = R \times 0.70 \quad (8.3-76)$$

No swelling (IRATE = -2)

Limits on incubation parameter  $\tau$ :

Upper bound (ITAU = 1)

$$\tau_u = \tau \times 1.30 \quad (8.3-77)$$

Lower bound (ITAU = -1)

$$\tau_l = \tau \times 0.70 \quad (8.3-78)$$

No swelling (ITAU = -2)

These equations are solved in the subroutine CLADSW.

### 8.3.6 Fission-gas Plenum Pressure

As the volatile fission products are released from the fuel, they enter the free volume associated with the fuel pin and are assumed to mix homogeneously with the gases already present. The free volumes considered are the fabricated fission gas plenum, the central fuel void not associated with a central molten fuel cavity, the fuel-cladding gap, and the crack volume within the fuel. A homogeneous ideal-gas mixture that is in pressure equilibrium is assumed to form.

The total number of moles of fission gas and helium is known prior to the pressure calculation, although the distribution is not known.

$$n_T = n_T^{fp} + n_T^{He} \quad (8.3-79)$$

where

$n_T$  = Total moles of gas

$n_T^{fp}$  = Moles of fission product gas

$n_T^{He}$  = Moles of helium

The amount of helium is known from the fill gas pressure, the fraction that is not helium, and the reference temperature geometry. The amount of helium also contains the amount released as porosity migration occurs (Section 8.3.1). The number of moles of fission gas is known from the fission gas release calculation (Section 8.3.3) and the non-helium initial fill gas.

If all the free volume exists at the same pressure,  $P_g$ , then the number of moles of gas at any specific free volume location can be determined from the ideal gas law.

$$n_i = \frac{P_g}{R} \left[ \frac{V_i}{T_i} \right] \quad (8.3-80)$$

where

- $n_i$  = Moles of gas in free volume  $i$
- $P_g$  = Pressure of the gas, Pa
- $R$  = Ideal-gas constant,  $J K^{-1} (g\text{-mole})^{-1}$
- $V_i$  = Volume of free volume  $i$ ,  $m^3$
- $T_i$  = Temperature of free volume  $i$ , K

This basic relationship can be used to determine the moles of gas associated with the types of free volumes listed above. For the plenum, there exists only one volume and temperature.

$$n_p = \frac{P_g}{R} \left[ \frac{V_p}{T_p} \right] \quad (8.3-81)$$

where

- $n_p$  = Total number of moles in the plenum
- $V_p$  = Volume of the fission gas plenum,  $m^3$
- $T_p$  = Temperature of the fission gas plenum, K

The central fuel void may exist over a number of axial segments due to as-fabricated porosity or the fuel initially fabricated with a central hole. Therefore, each axial segment contributes to the number of moles.

$$n_v = \frac{P_g}{R} \left[ \sum_{j=1}^{MZ} \frac{V_{v,j}}{T_{v,j}} \right] \quad (8.3-82)$$

where

- $n_v$  = Total number of moles in central void
- $V_{v,j}$  = Volume of central void in axial segment j, m<sup>3</sup>
- $T_{v,j}$  = Temperature of the central void in axial segment j, K
- MZ = Number of axial nodes

If an axial segment has a central void included as part of the molten cavity, its contribution is not included in Eq. 8.3-82.

The fuel-cladding gap can also contain the released gases. It also exists over a number of axial nodes, and its contribution to the total moles of gas is a summation over all axial segments.

$$n_g = \frac{P_g}{R} \left[ \sum_{j=1}^{MZ} \frac{V_{g,j}}{T_{g,j}} \right] \quad (8.3-83)$$

where

- $n_g$  = Total number of moles in fuel-cladding gap
- $V_{g,j}$  = Volume of fuel-cladding gap in axial segment j, m<sup>3</sup>
- $T_{g,j}$  = Temperature of the fuel-cladding gap, K
- = 0.5 (T<sub>f,j</sub> + T<sub>c,j</sub>)

$T_{f,j}$  = Fuel surface temperature in axial segment j, K

$T_{c,j}$  = Inner cladding surface temperature in axial segment j, K

The volume associated with the crack volume requires a summation over both the radial extent of cracking and the axial segments. In a given axial segment, the volumes and temperatures change with the radius.

$$n_k = \frac{P_g}{R} \left[ \sum_{j=1}^{MZ} \left( \sum_{i=IETA}^{NT} \frac{V_{k,i,j}}{T_{k,i,j}} \right) \right] \quad (8.3-84)$$

where

$n_k$  = Total number of moles in the crack volume

$V_{k,i,j}$  = Volume of cracks in radial cell i of axial segment j, m<sup>3</sup>

$T_{k,i,j}$  = Temperature of fuel in radial cell i of axial segment j, K

IETA = Innermost cracked fuel node

NT = Total number of radial fuel nodes

It is assumed that the gas in the cracks of the fuel is in thermal equilibrium with the fuel in the same cell.

Since the total number of moles must reside in the free volumes considered, Eq. 8.3-79 can be combined with Eqs. 8.3-81 through 8.3-84

$$n_T = \frac{P_g}{R} \left[ \frac{V_p}{T_p} + \sum_{j=1}^{MZ} \frac{V_{v,j}}{T_{v,j}} + \sum_{j=1}^{MZ} \frac{V_{g,j}}{T_{g,j}} + \sum_{j=1}^{MZ} \left( \sum_{i=IETA}^{NT} \frac{V_{k,i,j}}{T_{k,i,j}} \right) \right] \quad (8.3-85)$$

Everything in Eq. 8.3-85 is known except the gas pressure, therefore the equation can be solved to find the pressure.

$$P_g = \frac{n_T R}{\left[ \frac{V_p}{T_p} \sum_{j=1}^{MZ} \left( \frac{V_{v,j}}{T_{v,j}} + \frac{V_{g,j}}{T_{g,j}} + \sum_{i=IETA}^{NT} \frac{V_{k,i,j}}{T_{k,i,j}} \right) \right]} \quad (8.3-86)$$

Once the uniform pressure has been determined from Eq. 8.3-86, and using the known ratio of fission product moles to helium moles with Eq. 8.3-79, the number of moles of fission gas and helium can be found in any of the free volumes.

These calculations are performed in the subroutine PRESPL.

### 8.3.7 Molten Cavity Pressurization

Prior to fuel melting, the central void and plenum are assumed to be in pressure equilibrium. Once melting has begun, DEFORM-4 provides for three different methods for calculating the molten cavity pressure: (1) the cavity under consideration extends axially only over the range of segments where melting has occurred, (2) the cavity extends over all axial segments, and (3) each axial segment is considered a separate cavity. These options are controlled by the input variable IMELTV.

<u>IMELTV</u>	<u>Description</u>
0	Molten cavity extends only over the axial extent of fuel melting
1	Molten cavity extends over all axial segments
2	Each axial segment treated as a separate control volume

If a central void exists before fuel melting, then the first two options give similar results. The second option presents a more mechanistic approach to the molten cavity. As melting begins, it is expected that communication would exist all along the central void. As the available volume for the helium and fission gas associated with one axial segment is decreased because of fuel melting and thermal expansion, the excess gas would move to other segments to produce a balanced pressure all along the central void. This model assumes that the transient time scales are long enough to allow this redistribution process.

The third option is included for the study of extremely fast transients. If the time scale is short enough to preclude material redistribution, then each axial segment is assumed to act as a separate molten cavity. A separate pressure is calculated for each segment, and axial pressure differentials are produced. The effects of these axial differentials on the radial mechanics solution in the cladding can then be studied to determine the sensitivity of cladding failure location.

In addition to these options, the effects of fuel moving into the cracks and pressurizing them to the same level as the molten cavity can be studied through the input parameter IROR. If this parameter is set to 1, the crack volume is included in the molten cavity volume and the cavity pressure acts directly on the cladding, see Section 8.2.3. Because DEFORM-4 does not consider mass transport between axial segments or radial cells, the actual movement of fuel cannot take place. The consideration of the crack volume does allow the macroscopic effect of volume increase in the molten cavity by movement of molten fuel out of the cavity into crack volume to be considered.

When the PINACLE module is initiated, which describes the pre-failure in-pin molten fuel relocation, it provides the molten cavity pressure that is a boundary condition for the DEFORM calculation. This module replaces the CAVITY subroutine in DEFORM. DEFORM and PINACLE work interactively with PINACLE providing the temperatures and molten cavity pressures for DEFORM, and DEFORM determining the fuel pin thermal/mechanical response to changes in these conditions and returning to PINACLE the new axial and radial node locations.

The following calculations are performed in the subroutine CAVITE.

#### 8.3.7.1 Incremental Melt Fraction Ratio

The radial extent of the molten cavity is determined by the relationship between the radial cell temperature and the solidus temperature. Melting of the cell is assumed to begin when the solidus temperature is reached, and be complete when the liquidus temperature is attained.

$$f_{m,i}(t + \Delta t) = \frac{(T_{2,i} - T_s)}{(T_\ell - T_s)} \quad (8.3-87)$$

where

- $f_{m,i}$  = Melt fraction of radial cell i
- $t$  = Time at beginning of the time step, s
- $\Delta t$  = Time step length, s
- $T_{2,i}$  = Temperature of radial cell i at end of time step, K
- $T_s$  = Solidus temperature, K
- $T_\ell$  = Liquidus temperature, K

As the cell melts, the amount of material considered to be in the molten region of the cell is directly related to the melt fraction,  $f_{m,i}$ . However, the original fission gas content, etc., is not saved from one time step to the next, but the values at the end of the time step are determined, so a simple relationship between melt fraction change and material distribution between the molten state vs the solid state based on the current melt fraction cannot be used. It is necessary to develop an approach based on the solid fuel quantities at the beginning of the time step and the melt fraction change during the time step. This relationship is known as the incremental melt fraction ratio. With this approach, the cell can be considered to melt into the molten cavity in an incremental fashion rather than adding the node to the cavity all at one time when some arbitrary melt fraction has been reached.

Prior to melting, a radial cell contains some predetermined amount of a specific constituent which is important to the cavity pressurization, such as fission gas, as-fabricated gas and volume, crack gas and volume, etc. At the first step where melting occurs, some part of this is transferred from the solid region into the molten region.

$$F_{m,i}(1) = f_{m,i}(1) \times F_{o,i} \quad (8.3-88)$$

$$F_{s,i}(1) = F_{o,i} \times [1 - f_{m,i}(1)] \quad (8.3-89)$$

where

$F_{m,i}(1)$  = Amount of constituent in the molten region at end of time step 1 in radial cell  $i$

$F_{o,i}$  = Total amount of constituent in solid fuel prior to melting

$F_{s,i}(1)$  = Amount of constituent remaining in solid region at end of time step 1 in radial cell  $i$

At end of the second time step with melting, the amounts in the molten and solid regions are related to the new time step melt fraction

$$F_{m,i}(2) = F_{o,i} \times f_{m,i}(2) \quad (8.3-90)$$

$$F_{s,i}(2) = F_{o,i} \times [1 - f_{m,i}(2)] \quad (8.3-91)$$

Equations 8.3-90 and 8.3-91 can be rewritten in terms of the known quantities  $F_{m,i}(1)$  and  $F_{s,i}(1)$  rather than the now unknown,  $F_{o,i}$  by rearrangement of Eqs. 8.3-88 and 8.3-89.

$$F_{m,i}(2) = F_{s,i}(1) \frac{f_{m,i}(2)}{[1 - f_{m,i}(1)]} \quad (8.3-92)$$

$$F_{s,i}(2) = F_{s,i}(1) \frac{[1 - f_{m,i}(2)]}{[1 - f_{m,i}(1)]} \quad (8.3-93)$$

As the process continues, the relationship between the constituents and melt fractions at a specific time can be generalized.

$$F_{m,i}(t + \Delta t) = F_{s,i}(t) \frac{f_{m,i}(t + \Delta t)}{[1 - f_{m,i}(t)]} \quad (8.3-94)$$

$$F_{s,i}(t + \Delta t) = F_{s,i}(t) \frac{[1 - f_{m,i}(t + \Delta t)]}{[1 - f_{m,i}(t)]} \quad (8.3-95)$$

The change in the constituent during the time step can be determined by subtracting the results of two time steps and making use of the generalized form of Eq. 8.3-89.

$$\begin{aligned} \Delta F_{s,i} &= F_{s,i}(t + \Delta t) - F_{s,i}(t) \\ &= - F_{s,i}(t) \frac{[f_{m,i}(t + \Delta t) - f_{m,i}(t)]}{[1 - f_{m,i}(t)]} \end{aligned} \quad (8.3-96)$$

where

$\Delta F_{s,i}$  = Change in constituent in solid fuel in radial cell i that takes place during the time step

The same procedure applied to the change in the molten region constituent results in the negative of Eq. 8.3-96, as would be expected for conservation.

The considerations leading to Eq. 8.3-96 define what is known as the incremental melt fraction ratio.

$$R_{IMF} = \frac{[f_{m,i}(t + \Delta t) - f_{m,i}(t)]}{[1 - f_{m,i}(t)]} \quad (8.3-97)$$

where

$R_{IMF}$  = Incremental melt fraction ratio

This ratio is used in the considerations given below.

### 8.3.7.2 Gas Release on Melting

When melting begins in an axial segment, there are five constituents from which gas and volume may be moved into the molten cavity: (1) the initial central void, (2) the grain boundaries, (3) intragranular, (4) the as-fabricated porosity, and (5) the fuel cracks. Each of these can affect the molten cavity pressurization through the gas and volume associated with their inclusion and will be described below. In the discussion in the next five sections, each constituent is treated as a single adjustment to the cavity gas and volume consideration, while in actuality they are accumulated for the total change to the cavity.

#### 8.3.7.2.1 Central Void Considerations

Prior to melting, the central void is considered to be in equilibrium with the rest of the free volume within the pin. The number of moles of helium and fission gas associated with the central void in each axial segment varies depending on the volume, temperature, and pressure, and was discussed in Section 8.3.6. The amount of this gas, therefore, changes during each time step throughout the pretransient and transient up to fuel melting initiation.

Upon initial melting, the gas associated with the defined central molten cavity, see definition of IMELTV above, is fixed at its last value based on equilibrium with the plenum and associated free volume within the pin. This gas and its volume is then considered part of the molten cavity and is removed from the plenum pressure considerations. It is implicitly assumed that melting initiates the production on a molten cavity region which acts as a bottle that does not communicate with the plenum.

This central void consideration defines the initial state associated with the molten cavity.

#### 8.3.7.2.2 Grain Boundary Gas

As described in Section 8.3.3 and 8.3.4 above, the fission gas is assumed to exist in grain boundary bubbles that cause fuel swelling, and intragranular gas within the fuel matrix.

Upon fuel melting, the grain boundary gas and its volume is assumed to be released immediately into the molten cavity. Based on the discussion in Section 8.3.7.1, Eqs. 8.3-96 and 8.3-97 can be used to determine the gas released from the grain boundary to the molten cavity.

$$\Delta M_{gb,i,j}(\Delta t) = - M_{gb,i,j}(t) R_{IMF,i,j} \quad (8.3-98)$$

$$\Delta M_{c,gb}(\Delta t) = - \Delta M_{gb,i,j}(\Delta t) \quad (8.3-99)$$

where

$\Delta M_{gb,i,j}(\Delta t)$  = Change in moles of fission gas on the grain boundary during the time step in radial cell i of axial segment j

$M_{gb,i,j}(t)$  = Moles of fission gas on the grain boundary at beginning of the time step for radial cell i of axial segment j

$\Delta M_{c,gb}(\Delta t)$  = Moles of fission gas added to the molten cavity from the grain boundaries during the time step

$R_{IMF,i,j}$  = Incremental melt fraction ratio for radial cell i of axial node j

The volumes associated with the grain boundary gas is assumed to be moved to the molten cavity in the same proportion as the moles.

$$\Delta V_{gb,i,j}(\Delta t) = - V_{gb,i,j}(t) R_{IMF,i,j} \quad (8.3-100)$$

$$\Delta V_{c,gb}(\Delta t) = - \Delta V_{gb,i,j}(\Delta t) \quad (8.3-101)$$

where

$\Delta V_{gb,i,j}(\Delta t)$  = Change in volume of the fission gas on the grain boundaries during the time step in radial cell i of axial segment j, m<sup>3</sup>

$V_{gb,i,j}(t)$  = Volume of gas on grain boundaries at beginning of the time step for radial cell i of axial segment j, m<sup>3</sup>

$$\Delta V_{c,gb}(\Delta t) = \text{Volume added to molten cavity from grain boundaries during the time step, m}^3$$

As a cell progresses from initial melting to fully molten, all the grain boundary gas and volume is moved into the molten cavity.

Equations 8.3-98 through 8.3-101 all refer to a single radial node. The total amount of gas and volume moved into association with the molten cavity is found through a summation of these equations over all melting radial cells at all axial segments in the cavity. Combining Eqs. 8.3-98 and 8.3-99, and Eq. 8.3-100 and 8.3-101,

$$\Delta M_{c,gb}^T = \sum_{j=jcavb}^{jcavt} \left[ \sum_{i=1}^{iz-1} (M_{gb,i,j}(t) \times R_{IMF,i,j}) \right] \quad (8.3-102)$$

$$\Delta V_{c,gb}^T = \sum_{j=jcavb}^{jcavt} \left[ \sum_{i=1}^{iz-1} (V_{gb,i,j}(t) \times R_{IMF,i,j}) \right] \quad (8.3-103)$$

where

$\Delta M_{c,gb}^T$  = Total moles of gas added to molten cavity from the grain boundaries during the time step

$\Delta V_{c,gb}^T$  = Total volume of grain boundary gas added to molten cavity during the time step, m<sup>3</sup>

jcavb = Axial segment number at bottom of molten cavity

jcavt = Axial segment number at top of molten cavity

iz = Radial boundary number that defines the boundary between the molten and solid region

### 8.3.7.2.3 Intra-Granular Gas

While the grain boundary gas is assumed to move instantaneously into the molten cavity, the intragranular gas is assumed to be tied-up in very small bubbles or interstitially located, so

a time is required for the coalescence and buoyancy forces to release this gas into the cavity. Therefore, there can be gas in the molten fuel region which has not been released into the molten cavity.

The intra-granular gas is transferred from the solid fuel into the molten fuel based on the considerations presented in Section 8.3.7.1.

$$\Delta M_{m,ig}(\Delta t) = M_{ig,i,j}(t) R_{IMF,i,j} \quad (8.3-104)$$

$$M_{ig,i,j}(t + \Delta t) = M_{ig,i,j}(t) - \Delta M_{m,ig}(\Delta t) \quad (8.3-105)$$

$$M_{m,ig}(t + \Delta t) = M_{m,ig}(t) + \Delta M_{m,ig}(\Delta t) \quad (8.3-106)$$

where

- $\Delta M_{m,ig}(\Delta t)$  = Moles of intra-granular fission gas transferred from the solid to the molten fuel during the time step for the radial cell
- $M_{ig,i,j}(t)$  = Moles of intra-granular fission gas at beginning of the time step in radial cell  $i$  of axial segment  $j$
- $M_{ig,i,j}(t + \Delta t)$  = Moles of intra-granular fission gas at end of time step
- $M_{m,ig}(t + \Delta t)$  = Moles of gas retained in molten fuel at end of time step

The intra-granular gas is assumed to have no volume associated with it, so no volume movement occurs.

The release of the gas retained within the molten fuel to the molten cavity through coalescence and buoyancy effects is assumed to occur at a rate proportional to the amount of gas present.

$$\frac{dM_{m,ig}}{dt} = -\tau_g M_{m,ig} \quad (8.3-107)$$

where

$$\tau_g = \text{Time constant for coalescence release, s}^{-1}$$

Equation 8.3-107 is integrated over the time step to determine the release from the molten fuel to the molten cavity.

$$\Delta M_{c,ig}(\Delta t) = M_{m,ig}(t + \Delta t) [1 - \exp(-\Delta t \times \tau_g)] \quad (8.3-108)$$

$$M'_{m,ig}(t + \Delta t) = M_{m,ig}(t + \Delta t) - \Delta M_{c,ig}(\Delta t) \quad (8.3-109)$$

where

$\Delta M_{c,ig}(\Delta t)$  = Moles of intra-granular gas added to molten cavity during the time step

$M'_{m,ig}(t + \Delta t)$  = Moles of intra-granular gas remaining in the molten fuel at the end of the time step after both transfer from solid fuel and release to the cavity

Because this varies with each radial cell and axial segment, the total change is found through the double summation as with Eq. 8.3-102 above.

$$\Delta M_{c,ig}^T = \sum_{j=jcavb}^{jcavt} \left[ \sum_{i=1}^{iz-1} (\Delta M_{c,ig}) \right] \quad (8.3-110)$$

where

$\Delta M_{c,ig}^T$  = Total moles of gas added to molten cavity from the intragranular gas during the time step

#### 8.3.7.2.4 As-Fabricated Gas

Like the grain boundary gas, the gas and volume associated with any residual as-fabricated porosity, see Section 8.3.1, is assumed to be released to the molten cavity instantaneously upon melting.

$$\Delta M_{c,af}(\Delta t) = M_{af,ij}(t) R_{IMF,ij} \quad (8.3-111)$$

$$M_{af,ij}(t + \Delta t) = M_{af,ij}(t) - \Delta M_{c,af}(\Delta t) \quad (8.3-112)$$

$$\Delta V_{c,af}(\Delta t) = V_{af,ij}(t) R_{IMF,ij} \quad (8.3-113)$$

$$V_{af,ij}(t + \Delta t) = V_{af,ij}(t) - \Delta V_{c,af}(\Delta t) \quad (8.3-114)$$

where

$\Delta M_{c,af}$  = Moles of as-fabricated, retained helium added to the molten cavity

$M_{af,ij}$  = Moles of as-fabricated, retained helium that remains in the solid fuel of radial cell  $i$  of axial segment  $j$

$\Delta V_{c,af}$  = Volume of as-fabricated, retained porosity added to the molten cavity,  $m^3$

$V_{af,ij}$  = Volume of as-fabricated, retained porosity that remains in the solid fuel of radial cell  $i$  of axial segment  $j$

The contributions must be summed over all radial cells of all axial segments considered to be a part of the molten cavity.

$$\Delta M_{c,af}^T = \sum_{j=jcavb}^{jcavt} \left[ \sum_{i=1}^{iz-1} (M_{af,ij}(t) R_{IMF,ij}) \right] \quad (8.3-115)$$

$$\Delta V_{c,af}^T = \sum_{j=jcavb}^{jcavt} \left[ \sum_{i=1}^{iz-1} (V_{af,ij}(t) R_{IMF,ij}) \right] \quad (8.3-116)$$

where

$\Delta M_{c,af}^T$  = Total moles of gas added to molten cavity from the as-fabricated porosity during the time step

$\Delta V_{c,af}^T$  = Total volume added to the molten cavity from the as-fabricated porosity during the time step

### 8.3.7.2.5 Fuel Crack Gas

As the radial cell melts into the molten cavity, the gas and volume associated with cracks within the fuel are assumed to be added to the cavity instantaneously. The amount of gas within the cracks depends on the plenum pressure and the temperature of the cell, for all are assumed to be in equilibrium with the plenum.

$$M_{ck,i,j}(t) = \frac{P_g \times V_{ck,i,j}(t)}{R \times T_{i,j}} \quad (8.3-117)$$

where

$M_{ck,i,j}$  = Moles of gas (fission gas + helium) in the crack volume of radial cell i of axial segment j

$P_g$  = Plenum pressure, Pa

$V_{ck,i,j}$  = Volume of cracks of radial cell i of axial segment j, m<sup>3</sup>

$T_{i,j}$  = Temperature of radial cell i of axial segment j, m<sup>3</sup>

The amount of gas and volume moving into the molten cavity is again determined from the incremental melt fraction ratio and the initial conditions.

$$\Delta M_{c,ck}(\Delta t) = M_{ck,i,j}(t) R_{IMF,i,j} \quad (8.3-118)$$

$$M_{ck,i,j}(t+\Delta t) = M_{ck,i,j}(t) - \Delta M_{c,ck}(\Delta t) \quad (8.3-119)$$

$$\Delta V_{c,ck}(\Delta t) = V_{ck,i,j}(t) R_{IMF,i,j} \quad (8.3-120)$$

$$V_{ck,i,j}(t+\Delta t) = V_{ck,i,j}(t) - \Delta V_{c,ck}(\Delta t) \quad (8.3-121)$$

where

$\Delta M_{c,ck}$  = Moles of crack volume gas added to the molten cavity

$\Delta V_{c,ck}$  = Volume of cracks added to the molten cavity, m<sup>3</sup>

The total contributions are then summed over all melting radial cells of all axial segments in the molten cavity.

$$\Delta M_{c,ck}^T = \sum_{j=jcavb}^{jcavt} \left[ \sum_{i=1}^{iz-1} (M_{ck,i,j}(t) R_{IMF,i,j}) \right] \quad (8.3-122)$$

$$\Delta V_{c,ck}^T = \sum_{j=jcavb}^{jcavt} \left[ \sum_{i=1}^{iz-1} (V_{ck,i,j}(t) R_{IMF,i,j}) \right] \quad (8.3-123)$$

where

$\Delta M_{c,ck}^T$  = Total moles of crack volume gas added to the molten cavity during the time step

$\Delta V_{c,ck}^T$  = Total volume added to the molten cavity during the time step from cracks, m<sup>3</sup>

As crack volume gas is added to the molten cavity, it is removed from the plenum pressure calculation along with its associated volume, thereby maintaining conservation of gas.

### 8.3.7.3 Fuel Volume Changes

The discussion above covered the movement of gas and volume from various sources into the molten cavity. There are two other effects which will change the volume associated with

the molten cavity: (1) fuel volume change on melting, and (2) molten fuel thermal expansion. Any changes due to swelling or contraction of the remaining grain boundary fission gas bubbles are treated in the fuel swelling routine, see Section 8.3.4.

DEFORM-4 contains the function routine RHOF, which determines the theoretical density of the fuel at any given temperature, see Section 8.7.1. Since it is assumed that there is no mass transfer between radial cells or axial segments, the volume change for each cell can be determined

$$\Delta V_{th,i,j}(\Delta t) = \left[ \frac{1}{\rho(T_{2,i,j})} - \frac{1}{\rho(T_{1,i,j})} \right] F_{i,j} \quad (8.3-124)$$

where

- $\Delta V_{th,i,j}$  = Volume change caused by temperature changes during the time step for radial cell i of axial segment j, m<sup>3</sup>
- $\rho$  = Temperature dependent fuel theoretical density, kg/m<sup>3</sup>
- $T_{2,i,j}$  = Final temperature of radial cell i of axial segment j, K
- $T_{1,i,j}$  = Initial temperature of radial cell i of axial segment j, K
- $F_{i,j}$  = Mass of fuel in radial cell i of axial segment j, kg

Because the density function already incorporates the changes due to melting over the melting range, there is no need to use the incremental melt fraction ratio.

Summing over all radial cells and axial segments results in the total volume change due to thermal affects in the fuel

$$\Delta V_{c,th}^T = \sum_{j=jcavb}^{jcavt} \left[ \sum_{i=1}^{iz-1} (\Delta V_{th,i,j}(\Delta t)) \right] \quad (8.3-125)$$

where

$\Delta V_{c,th}^T$  = Total volume change in molten cavity due to changes in temperature in the fuel, m<sup>3</sup>

#### 8.3.7.4 Molten Cavity Pressure

The molten cavity pressure is determined from the ideal gas law.

$$P_{cav} = \frac{M_{cav} R T_{cav}}{V_{cav}} \quad (8.3-126)$$

where

$P_{cav}$  = Molten cavity pressure, Pa  
 $M_{cav}$  = Total moles of gas in molten cavity  
 $T_{cav}$  = Molten cavity temperature, K  
 $V_{cav}$  = Molten cavity volume, m<sup>3</sup>

The number of moles of gas in the cavity is determined by adding the changes discussed above to the amount present at the start of the time step. The volume is similarly determined.

$$M_{cav} = M_{c,i} + \Delta M_{c,gb}^T + \Delta M_{c,ig}^T + \Delta M_{c,af}^T + \Delta M_{c,ck}^T \quad (8.3-127)$$

$$V_{cav} = V_{c,i} + \Delta V_{c,gb}^T + \Delta V_{c,af}^T + \Delta V_{c,ck}^T + \Delta V_{c,th}^T \quad (8.3-128)$$

where

$M_{c,i}$  = Initial moles of gas present in the molten cavity  
 $V_{c,i}$  = Initial volume present in the molten cavity.

It is assumed that the boundary between the outer most cell that is melting and the solid fuel remains stationary during the time step. While this is not necessarily true, appropriate choice of the transient time step length will provide a close link between cavity pressurization and mechanical response to this force without the need to iterate between the cavity pressure and mechanical response parts of the code.

Because of the volume changes occurring as a transient progresses, it is possible for the central void to completely close. The case may even exist where there is more volume needed than exists inside the solid boundary. Because DEFORM-4 does not provide for relocation of fuel between axial segments, the additional material cannot be moved. However, to at least study the pressurization effects, when this situation arises, a volume deficit is calculated.

$$V_{d,j} = V_{f,j} - V_{sb,j} \quad (8.3-129)$$

where

$V_{d,j}$  = Volume deficit for axial segment  $j$ ,  $m^3$

$V_{f,j}$  = Volume the fuel would require at axial segment  $j$ ,  $m^3$

$V_{sb,j}$  = Volume available inside the solid fuel boundary,  $m^3$

These values are summed over all axial segments to provide the total volume mismatch.

$$V_d^T = \sum_{j=jcavb}^{jcavt} V_{s,i} \quad (8.3-130)$$

This value is then used to decrease the apparent volume given by Eq. 8.3-128.

$$V_{cav}^T = V_{cav} - V_d^T \quad (8.3-131)$$

The temperature used in Eq. 8.3-126 is an averaged value for the cavity. First the radially mass averaged temperature of the molten fuel for each axial segment is determined.

These temperatures are then weighted based on the volume available at each axial segment for gas to occupy.

$$T_{ma,j} = \frac{\sum_{i=1}^{iz-1} (T_{2,i,j} \times F_{i,j})}{\sum_{i=1}^{iz-1} (F_{i,j})} \quad (8.3-132)$$

$$T_{cav} = \frac{\sum_{j=jcavb}^{jcavt} (T_{ma,j} \times V_{c,j})}{\sum_{j=jcavb}^{jcavt} (V_{c,j})} \quad (8.3-133)$$

where

- $T_{ma,j}$  = Radially mass averaged fuel temperature over molten region, K
- $T_{2,i,j}$  = Temperature of radial cell i of axial segment j, K
- $F_{i,j}$  = Mass of radial cell i of axial segment j, kg
- $V_{c,j}$  = Volume of the central void at axial segment j, m<sup>3</sup>

Using the values determined from Eqs. 8.3-133, 8.3-131, and 8.3-127, the molten cavity pressure is calculated from 8.3-126. This procedure is carried out at the beginning of each time step, so the dimensional changes from the previous time step are used to calculate the molten cavity pressure to be used as the boundary condition for the current time step.

#### 8.3.7.5 Fuel Vapor Pressure

In addition to the pressure from the gases in the molten cavity, the fuel vapor pressure is included. The temperature used is the maximum radially mass-averaged temperature over the axial extent of the cavity. In the case where each axial segment is a separate cavity, the

mass-averaged temperature of the segment is used. The fuel vapor pressure terms are added to the gas induced pressure to obtain the total molten cavity pressure.

### 8.3.8 Fuel-cladding Gap Conductance

The thermal coupling between the cladding and the fuel is important because it affects the fuel and coolant temperatures and thereby, the swelling and thermal expansion of the fuel and cladding. The gap conductance provides this coupling. If the values are high, the fuel temperatures are lower, reducing the fuel swelling, thermal expansion, restructuring, fission-gas release, and stored energy. If the gap conductance is poor due to a large gap or a low conductivity gas mixture in the gap, then all fuel temperatures are raised, enhancing the phenomena mentioned previously. Because of the sensitivity of phenomena to temperature, and therefore gap conductance, it is best to describe the elements which contribute to the heat transfer between the fuel and cladding as mechanistically as possible.

SAS4A contains three options for calculating the gap conductances. In order of decreasing mechanistic consideration they are (1) a modified Ross-Stoute model [8-18], (2) a SAS3D parametric model, and (3) a simple SAS3D inverse-gap-size model. These are discussed below. It is recommended that the modified Ross-Stoute be used because of the more mechanistic nature of its formulation.

The gap conductance is determined at the end of each DEFORM-4 time step, and is used for the fuel-cladding thermal coupling when determining the temperatures at the end of the next time step. The modified Ross-Stoute model is coded in the function HGAP. The other two models are coded in the function HBFND. It is not possible to switch between models during the calculation because of modeling inconsistencies and the large changes that might result.

#### 8.3.8.1 Modified Ross-Stoute Gap Conductance Model

The recommended gap conductance model is a modified Ross-Stoute model [8-18]. This model has been used extensively in such codes as LIFE-III [8-5] and GAPCON [8-19] and is

considered the most mechanistic model currently available. The heat transfer through the fuel-cladding interface is considered to consist of three components: (1) conduction through the gas between the fuel and the cladding, (2) radiative transfer between the fuel and cladding surfaces, and (3) solid-to-solid heat transfer if the fuel and cladding are in contact. Even if contact does occur, the model still assumes the existence of a gas gap between the surfaces, a result of the effects of the surface roughnesses which are input parameters. If there is no contact, then the solid-to-solid component is set to zero. Figure 8.3-2 illustrates the fuel-cladding geometry and considerations for the open and closed gap cases.

#### 8.3.8.1.1 Radiative Heat Transfer

The radiative heat-transfer coefficient,  $h_r$ , is determined from

$$h_r = \frac{q_r/A_f}{(T_f - T_c)} \quad (8.3-134)$$

where

- $h_r$  = Radiative heat-transfer coefficient,  $W\ m^{-2}\ K^{-1}$
- $q_r$  = Heat transferred from the hotter to the colder surface,  $W$
- $A_f$  = Surface area of the fuel from which  $q_r$  is transferred,  $m^2$
- $T_f$  = Temperature of the fuel outer surface, the hotter one,  $K$
- $T_c$  = Temperature of the cladding inner surface, the colder one,  $K$

For radiative heat transfer between two surfaces,

$$\frac{q_r}{A_f} = \sigma \left[ \frac{1}{\epsilon_f} + \frac{A_f}{A_c} \left( \frac{1}{\epsilon_c} - 1 \right) \right]^{-1} [T_f^4 - T_c^4] \quad (8.3-135)$$

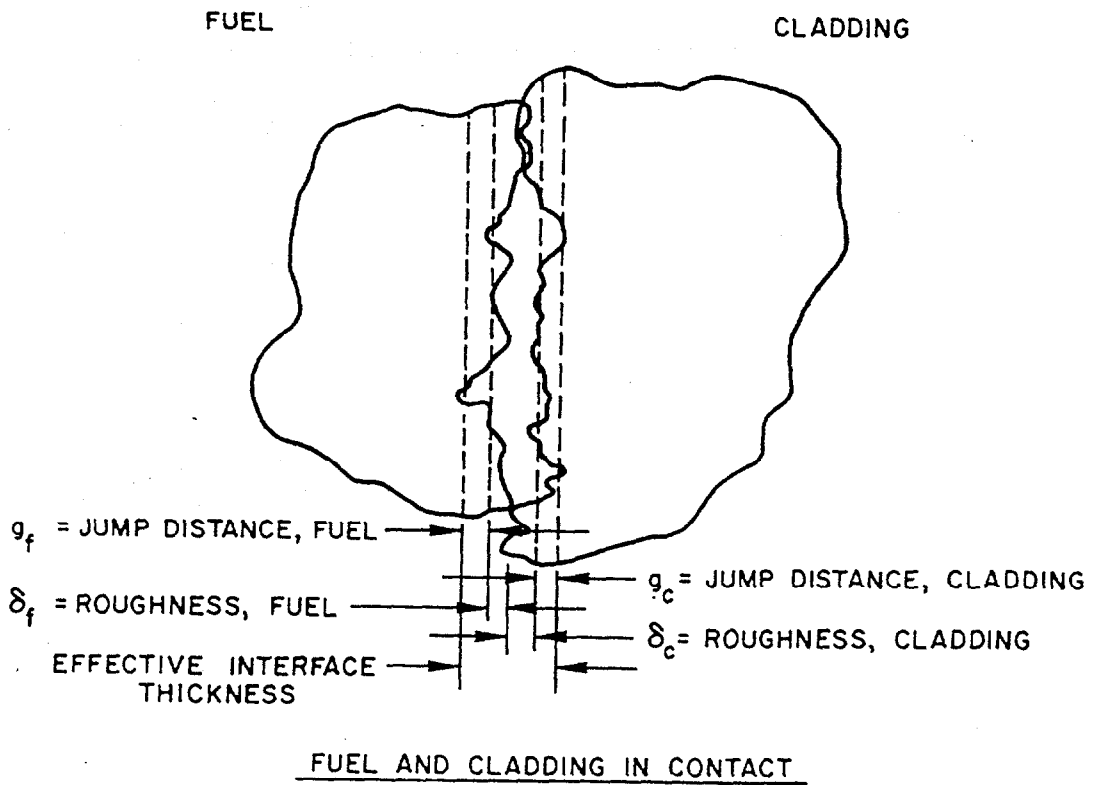
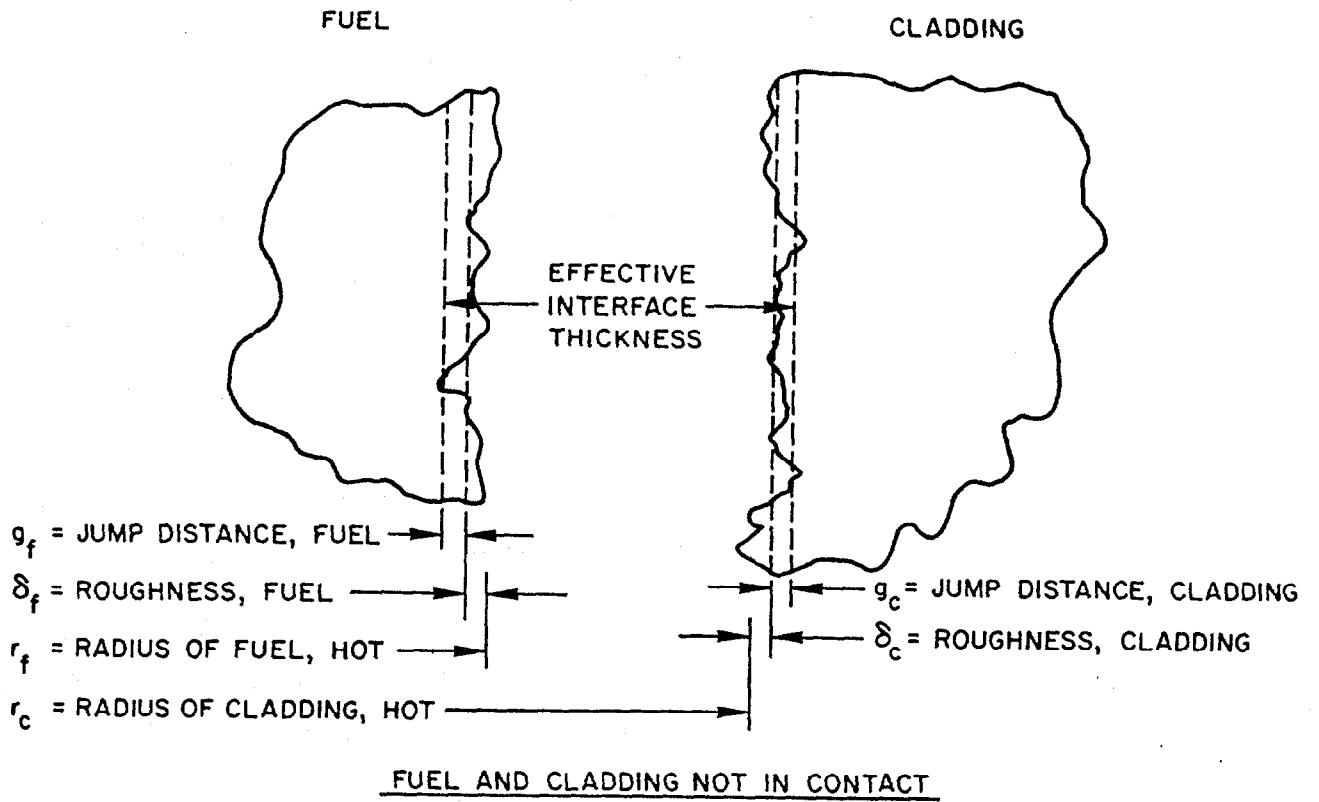


Fig. 8.3-2. Geometry of the Fuel-cladding Gap

where

- $\sigma$  = Stefan-Boltzmann constant,  $W\ m^{-2}\ K^{-4}$
- $\epsilon_f$  = Emissivity of the fuel surface
- $\epsilon_c$  = Emissivity of the cladding surface
- $A_c$  = Inner surface area of the cladding to which the heat is being transferred,  $m^2$

Combining Eqs. 8.3-134 and 8.3-135 provides the following result for the radiative heat-transfer coefficient.

$$h_r = \frac{\sigma (T_f^2 + T_c^2) (T_f + T_c)}{\left[ \frac{1}{\epsilon_f} + \frac{r_f}{r_c} \left( \frac{1}{\epsilon_c} - 1 \right) \right]} \quad (8.3-136)$$

where

- $r_f$  = Outer radius of the fuel, m
- $r_c$  = Inner radius of the cladding, m

#### 8.3.8.1.2 Conduction Heat Transfer

The heat-transfer coefficient for conduction through the gas in the fuel-cladding gap is given by

$$h_g = \frac{k_g}{(\Delta r)_g} \quad (8.3-137)$$

where

$h_g$  = Conduction heat-transfer coefficient,  $W m^{-2} K^{-1}$

$k_g$  = Thermal conductivity of the gas in the gap,  $W m^{-1} K^{-1}$

$(\Delta r)_g$  = Total effective fuel-cladding gap size, m

The conductivities of the helium and xenon gases that comprise the mixture in the fuel-cladding interface are given in Sections 8.7.11 and 8.7.12. The conductivity of this mixture of gas is derived from the kinetic theory of gases [8-20].

$$k_g = \sum_{i=1}^n \left[ K_i / \left( 1 + \sum_{\substack{j=1 \\ j \neq i}}^n G_{ij} X_j / X_i \right) \right] \quad (8.3-138)$$

$$G_{ij} = \frac{1.065}{\sqrt{8}} \left[ 1 + \frac{M_i}{M_j} \right]^{-1/2} \left[ 1 + \left[ \frac{k_i}{k_j} \right]^{1/2} \left[ \frac{M_i}{M_j} \right]^{1/4} \right]^2 \quad (8.3-139)$$

where

$k_g$  = Thermal conductivity of mixture of gases,  $W m^{-1} K^{-1}$

$k_i$  = Thermal conductivity of pure gas component i,  $W m^{-1} K^{-1}$

$X_i$  = Mole fraction of pure gas component i

$M_i$  = Atomic weight of pure gas component i

For the assumed binary mixture of helium and xenon, Eqs. 8.3-138 and 8.3-139 can be made specific with the subscripts h and x referring to the helium and xenon, respectively.

$$G_{hx} = \frac{1.065}{\sqrt{8}} \left[ 1 + \frac{M_h}{M_x} \right]^{-1/2} \left[ 1 + \left( \frac{k_h}{k_x} \right)^{1/2} \left( \frac{M_h}{M_x} \right)^{1/4} \right]^2 \quad (8.3-140)$$

$$G_{xh} = \frac{1.065}{\sqrt{8}} \left[ 1 + \frac{M_x}{M_h} \right]^{-1/2} \left[ 1 + \left( \frac{k_x}{k_h} \right)^{1/2} \left( \frac{M_x}{M_h} \right)^{1/4} \right]^2 \quad (8.3-141)$$

$$k_g = \frac{k_n}{\left[ 1 + G_{hx} \frac{X_x}{X_h} \right]} + \frac{k_x}{\left[ 1 + G_{xh} \frac{X_h}{X_x} \right]} \quad (8.3-142)$$

The effective gap size in Eq. 8.3-137 contains three elements based on the fuel-cladding gap considerations illustrated in Fig. 8.3-1. The first is the nominal fuel-cladding gap size. If the fuel and cladding are in contact this value goes to zero. The second consideration is derived from the incomplete energy exchange between the gas atoms and the solid surface of the fuel or cladding. This is modeled as an addition to the gap size. The third consideration is derived from the effects of surface roughnesses. Since the surfaces are not perfectly smooth, the roughness will produce a residual gap through which conduction takes place, as illustrated in Fig. 8.3-1.

$$(\Delta r)_g = (r_c - r_f) + (g_c + g_f) + C(\delta_c + \delta_f) \quad (8.3-143)$$

where

- $g_c$  = Thermal jump distance of the cladding surface, m
- $g_f$  = Thermal jump distance of the fuel surface, m
- $\delta_c$  = Mean surface roughness of the cladding, m

- $\delta_f$  = Mean surface roughness of the fuel, m  
 $C$  = Interface pressure dependent factor

The formulation for the temperature jump distances is derived from the kinetic theory of gases [8-20]. The jump distance is directly proportional to the mean free path of the gas in the gap. The extent to which energy exchange occurs when a gas atom strikes the solid surface is defined as the accommodation coefficient,  $a$ . This coefficient depends on the species present in the gas, and in the case of a mixture of monoatomic gases is determined from

$$a_{\text{mix}} = \frac{\sum a_i X_i M_i^{-1/2}}{\sum X_i M_i^{-1/2}} \quad (8.3-144)$$

where

- $a_{\text{mix}}$  = Accommodation coefficient of the gas mixture  
 $a_i$  = Accommodation coefficient of the  $i$ -th species of gas in the mixture  
 $X_i$  = Mole fraction of the  $i$ -th species of gas in the mixture  
 $M_i$  = Molecular weight of the  $i$ -th species of gas in the mixture

With the conductivity of the mixture,  $k_g$ , defined in Eq. 8.3-142, the jump distance,  $g$ , is determined from

$$g = \left[ \frac{2 - a_{\text{mix}}}{a_{\text{mix}}} \right] \frac{(2\pi R_m T)^{1/2} k_g}{(\gamma + 1) C_v P_g} \quad (8.3-145)$$

where

- $g$  = Jump distance of the surface under consideration, m  
 $R_m$  = Gas constant of the gas mixture,  $\text{J K}^{-1}$   
 $\gamma$  = Ratio of heat capacity at constant pressure to the heat capacity at constant volume

$C_v$  = Heat capacity at constant volume,  $J\ kg^{-1}\ K^{-1}$

$P_g$  = Gas pressure in the gap, Pa

From the above equation applied to the fuel and cladding surfaces, the second term in Eq. 8.3-143 can be determined.

The third term concerns the surface roughnesses of the cladding and fuel. The parameter,  $C$ , is assumed to depend exponentially on the interface pressure and is given by

$$C = C_o \exp(-1.23365 \times 10^{-8} P_i) \quad (8.3-146)$$

where

$C_o$  = Input pre-exponential constant,  $\sim 1.98$

$P_i$  = Fuel-cladding interface pressure, Pa

This formulation was determined for use in the GAPCON code [8-19] from the data from Ross and Stoute [8-18]. The value of  $C$  is then multiplied by the sum of the mean surface roughnesses of the cladding and the fuel to generate the component of the effective gap resulting from the mismatch of the surface roughnesses. As the interface pressure increases, this gap component becomes smaller because the increased pressure forces a more intimate contact between the surfaces.

#### 8.3.8.1.3 Solid-to-solid Heat Transfer

In addition to conduction through the gap and radiative heat transfer, heat can be passed directly through the solid-to-solid contact points when the gap is closed. Lassmann and Pazdera [8-21] suggest that the coefficient can be described by the following correlation:

$$h_s = \frac{Ak_s}{R^{2m-1}} \left[ \frac{P_i}{H} \right]^m \quad (8.3-147)$$

where

- $A, m$  = Constants determined through experimental comparisons
- $k_s$  = Effective thermal conductivity,  $W m^{-1} K^{-1}$
- $H$  = Hardness of the softer of the two materials, Pa
- $R$  = Square root of the mean squared roughnesses, m

The effective solid conductivity,  $k_s$ , is defined by

$$k_s = \frac{2 k_c k_f}{(k_c + k_f)} \quad (8.3-148)$$

where

- $k_c$  = Thermal conductivity of the cladding at the inner surface,  $W m^{-1} K^{-1}$
- $k_f$  = Thermal conductivity of the fuel at the outer surface,  $W m^{-1} K^{-1}$

The square root of the mean squared surface roughnesses,  $R$ , is defined by

$$R = \left[ \frac{\delta_f^2 + \delta_c^2}{2} \right]^{1/2} \quad (8.3-149)$$

The softer of the two materials is usually the cladding, however, depending on the transient conditions it could be either. Therefore, correlations for both the cladding and fuel have been incorporated, see Sections 8.7.13 and 8.7.14. The lower of the two values is used in Eq. 8.3-147.

The values of the constants  $A$  and  $m$  have been determined by Lassmann and Pazdera [8-21] through comparisons with experimental information to be 0.638 for  $A$  and 0.67 for  $m$ .

#### 8.3.8.1.4 Total Gap Heat-transfer Coefficient

The total heat-transfer coefficient across the fuel-cladding interface is the sum of the three components discussed above.

$$h_{\text{gap}} = h_g + h_r + h_s \quad (8.3-150)$$

If the fuel and cladding are not in contact, then the solid-to-solid term is set to zero.

The gap conductance is a parameter which both affects and is affected by changes in the temperatures, dimensions, and gas composition of the fuel-cladding gap. Because of this, the only way to achieve a fully consistent state between the gap conductance, dimensions, and temperatures is through a series of iterations. First an estimate of the gap conductance would be made. Second, the thermal changes for the time step would be calculated. Third, the dimensional and phenomenological changes over the time step would be determined. Fourth, the new state would be used to calculate a new gap conductance. If the initial estimate and the final value agreed within some predetermined error bound, the gap conductance is said to be consistent with the thermal/mechanical state. If the resultant gap conductance was outside the allowed error band, a new estimate would be determined and the entire calculation redone.

While this iteration method would achieve strict consistency, it can lead to long running times for a computer code. Because SAS4A must perform its calculations over many channels and long time periods, it is not possible to use the computational time necessary for the above scenario. Instead, two approximations are used. First, the effect of the new gap conductance estimate on the fuel surface gap temperature is considered. Within the function routine HGAP, iterations are performed over successive estimates of the conductance until the resulting gap conductance value is consistent with the estimated fuel surface temperature for that conductance value, and the resultant fuel and gas conductivities. No dimensional changes are considered, only conductivity effects.

The second method of adjustment has also been employed to smooth the transition between time steps. The new value of gap conductance passed to the thermal routines of SAS4A is an average of the new calculated value and the previous time step value. Experience has shown that using the new calculated value leads to oscillations in the temperatures and dimensions, while this averaging technique produces smoother transitions. In the pre-transient calculation this procedure usually produces less than a 2% difference between the calculated and used gap conductances. This can become much larger during pretransient power changes, but the values reconverge quickly after a new constant level is attained. The differences are primarily due to dimensional changes not considered in HGAP. In the transient state, the time steps are so short that the dimensional changes are small, resulting in less than a 1% difference in the calculated and used values of gap conductance. These differences are quite acceptable, especially when weighed against the large savings in computational effort.

A final check is made to see if the new value is between the minimum and maximum values allowed, which are input parameters. If the calculated value is outside the bounds, then the appropriate bound is used as the new value. This is useful if a constant gap conductance is required in order to study parametric effects from other models. In ordinary circumstances, these bounds should be set very wide to allow the model to calculate its own value and not be restricted.

#### 8.3.8.2 SAS3D Parametric Model

In the SAS3D code [8-22], a parametric model was employed to determine the gap conductance. This equation is based on the consideration that the gap conductance has some minimum value plus a term that is related to the fuel-cladding gap size and the gas conductivity.

$$h_{\text{gap}} = c_1 + \frac{c_2}{c_3 + (r_c - r_f)} \quad (8.3-151)$$

where

$c_1, c_2, c_3$  = Constants

$r_c$  = Inner cladding radius, m

$r_f$  = Outer fuel radius, m

The second term on the right-hand side of Eq. 8.3-151 approximates the conduction term in the model discussed above (see Section 8.3.8.1.2). If the fuel and cladding are in contact, there still exists a residual gap through which conduction occurs, i.e.,  $c_3$  in Eq. 8.3-101. By dividing the numerator and denominator of this conduction term by the constant  $c_2$ , the equation form coded in the function HBFND is developed.

$$h_{\text{gap}} = A + \frac{1}{\{B + [(r_c - r_f) + C]/H\}} \quad (8.3-152)$$

where

A, B, C, H = Input empirical constants

While this model does resemble parts of the model described in Section 8.3.8.1, it also has disadvantages. It is only dependent on the gap size and there is no ability to model the effects of solid-to-solid contact or temperature and gas mixture effects on gas conductivity. Its inclusion in SAS4A does allow for a comparison with SAS3D results while using the same gap conductance parameters.

The values calculated by this model are also restricted by upper and lower bounds.

### 8.3.8.3 SAS3D Simple Model

The final model depends only on the fuel-cladding gap size. It is included for parametric comparisons with previous SAS3D results. If there is no fuel-cladding gap, the upper bound on the gap conductance is used. If a gap does exist, the conductance is calculated from

$$h_{\text{gap}} = \frac{H}{(r_c - r_f)} \quad (8.3-153)$$

where

H = Input constant, W m<sup>-1</sup> K<sup>-1</sup>

r<sub>c</sub> = Inner cladding surface radius, m

r<sub>f</sub> = Outer fuel surface radius, m

If this value falls below the lower bound, the lower bound is used for the next thermal calculation.

### 8.3.9 Fuel Axial Expansion Reactivity Model

One of the important reactivity feedbacks in reactor safety analysis is the density change caused by the thermal expansion of the fuel and cladding of the pin. Because the magnitude of this effect can depend on the conditions existing at the fuel-cladding interface, a number of options were made available in DEFORM to study this phenomenon. In the previous release version of SAS4A several options were made available; (1) the fuel could be assumed to expand freely, (2) the fuel could be assumed to be constrained against the cladding requiring a force balance between the fuel and cladding, and (3) a mixture of the two could be assumed depending the actual fuel-cladding conditions.

Results from experiments carried out in RAPSODIE [8-23] with oxide fuel have indicated another possibility. Modifications have been made to the EXPAND subroutine of DEFORM to allow for the inclusion of the assumption that the fuel expansion is controlled by the cladding expansion.

If the DEFORM-4 module is used in a calculation, it will perform the calculation for the transient mass redistribution effects from the axial expansion of the fuel and cladding. It is assumed that the fuel and cladding masses within an axial segment remain constant throughout

the transient DEFORM-4 calculation. Although axial expansion is calculated for both the upper and lower axial blankets, as well as the active core region, the fuel reactivity is calculated only over the axial segments in the active core region. It is also assumed that the location of the bottom interface of the lower axial blanket does not change. All elevation changes are related to this fixed location.

#### 8.3.9.1 Free Fuel Expansion Controlled Feedback

If the fuel and cladding are assumed to behave independently of each other because of an open fuel-cladding gap or interface conditions that allow the fuel to slip freely along the cladding, the reactivity feedback from axial expansion of the pin will be dominated by the thermal expansion, and thus the temperatures, of the fuel. In oxide fuels where the thermal conductivity of the fuel is low and the fuel-cladding gap conductance is low, this assumption effectively decouples the fuel response from the coolant or cladding temperatures and directly relates the reactivity feedback to the power level.

The consequence of this assumption for TOP transients is an increased negative feedback as the power level increases. In a loss of flow (LOF) transient where the power level may drop during the initial stages, there would be a positive reactivity addition due to the cooling of the fuel as the power decreases. In later stages when boiling produces larger positive reactivity additions, the expansion reactivity would again become negative, particularly during a transient-over-power (TOP) event.

The metal fuel pins would behave in much the same manner, except on a more reduced scale. The high thermal conductivity of the fuel and sodium in the gap produces a much closer coupling between the fuel and coolant temperatures.

#### 8.3.9.2 Free Cladding Expansion Controlled Feedback

The opposite assumption to that discussed in Section 8.3.9.1 above would be to assume that the expansion of the cladding controlled the axial movement of the fuel. the condition

necessary for this to be plausible would be an oxide fuel that contains many transverse cracks and fuel connected to the cladding, or a metal fuel connected to the cladding that contains no strength to resist the cladding changes. Some tests and analyses performed with the RAPSODIE reactor [8-23] seem to indicate this type of behavior for oxide fuel.

The consequence of this assumption is to connect the fuel expansion feedback with the coolant, and thereby cladding, temperatures and decouple the feedback from the power level except through its effect on the coolant temperatures. In a TOP scenario, this reduces the magnitude of the reactivity feedback significantly. In the early stages of a LOF event, the effect is to change the magnitude and sign of the feedback from that discussed in Section 8.3.9.1. The feedback would actually be negative as the cladding responded to the heatup of the coolant. However, during the later LOF'd'TOP scenario, the feedback would be less negative as the feedback reached an asymptotic level in a fully voided channel. Differences in magnitude would again occur between the metal and oxide fuels due to the rate of energy transfer to the coolant and the different thermal expansion properties.

This assumption was not included in original version of the SAS4A code but has been added. Since DEFORM calculates both the cladding and fuel response separately under the free expansion assumption (see Section 8.2.4) this assumption was easily added by allowing the cladding expansion to control the expansion of the axial segments.

### 8.3.9.3 Constrained Fuel/Cladding Expansion Controlled Feedback

The final option available in DEFORM for the calculation of the axial expansion assumes that the fuel and cladding are locked together. The expansion is then determined from the required force balance at the fuel-cladding interface. This model is discussed in Section 8.2.4.

Unlike either of the two previous options, this one requires that both the fuel and cladding responses to the specified transient be considered. It would be expected that the results from these assumptions would fall somewhere between those of the previous two sections since elements of both are included in the considerations. In practice this has been found to be the case. In the situations where the fuel and cladding can be assumed to be in contact, such as high

burnups with low swelling cladding or medium burnups with the metal fuels, this option would be expected to yield the most credible results. Even when the oxide fuel can be assumed to be heavily cracked, this option may be most accurate because the bowing or twisting of the pin due to the interaction with wire step may cause the cracked fuel to be wedged within the cladding and therefore act as constrained rather than following the cladding expansion, particularly if the number of transverse cracks is small compared to the length of the fuel segments or the pellets can be assumed to have sintered together.

### 8.3.10 Metal Fuel Modeling

With the renewed interest in uranium metal fuels for breeder reactor applications, there is a need to provide modeling to handle this type of fuel. An initial effort has been made to include important phenomenological features of the metal fuel. This effort involved the use of available DEFORM modeling and incorporation of necessary material properties. Which this effort is not complete, it does provide a basis for evaluating the consequences of the use of metal fuel.

#### 8.3.10.1 Fission Gas Behavior

The buildup of fission gas within the metal fuel produces considerably more fuel swelling than is seen in oxide fuels. In oxide fuels, the strength of the fuel matrix is such that the fission gas bubbles remain small during the irradiation. There is collection of gas on grain boundaries, which leads to fuel swelling, and boundary bubble connecting which produces a local "tunneling" effect that leads to fission gas release.

With the metal fuels, there exists considerably more swelling of the fission bubbles which results from the considerably weaker fuel structure. As the steady state irradiation proceeds, the fission gas is initially all retained in the fuel matrix. Grain boundary bubbles gradually form, producing fuel swelling. As the porosity continues to increase, the grain boundary bubbles can become interlinked, producing a long-range interlinked porosity offering a path for fission gas release.

Recent studies on the growth mechanisms in the analyses of metal fuel swelling [8-24] have indicated that the transient swelling is dominated by grain boundary bubbles, so a single bubble model in an amorphous medium would not be adequate. These grain boundary bubbles also appear to be important for the development of the interlinked porosity in metal fuels. The early work with metal fuels allowed for only low-burnup irradiations because of the extensive swelling, but once it was determined that this "breakway" swelling appeared to be self-limiting, and if enough space was fabricated into the fuel-cladding gap, the result was very little stress on the cladding and high burnups could be achieved [8-25, 8-26]. In order to calculate the steady state behavior of the metal fuel, it is therefore necessary to model this swelling and associated gas release in a consistent manner.

The study of this phenomenon is still underway and not yet developed to the state where an appropriate model could be developed for inclusion into DEFORM. It was therefore necessary to use a more empirical model based on the observed relationship between fuel swelling and fission gas release.

#### 8.3.10.1.1 Closed and Connected Porosity Description

Initially, all created fission gas is assumed to go into fission gas bubbles within the fuel matrix. These bubbles are then allowed to swell in response to any overpressure produced by the bubble pressure acting against the surface tension and hydrostatic pressure [8-27, 8-28]. The amount of swelling allowed is controlled by a time constant determined from the creep rate of the fuel in response to the bubble overpressure. This produces a system of closed porosity within the fuel matrix. The modeling for this creation of closed porosity already existed in DEFORM and the modifications made were to introduce the correct material properties for the metal fuel.

As the closed porosity fraction increases, a point is reached where release would occur. It is assumed that fission gas release is associated with the formation of connected porosity. The release fraction defines the amount of porosity and fission gas that is transferred from closed to open porosity. The calculation of open porosity changes is tied directly to the fission gas release calculation and is explained in more detail below.

### 8.3.10.1.2 Fission Gas Release

The calculation for the amount of fission gas released from the closed porosity is determined directly from the swelling of the fuel cell. First the volumetric swelling fraction is determined from the fully dense theoretical volume and the actual cell volume, which includes porosity.

$$S_f = \frac{V_c - V_{th}}{V_{th}} \quad (8.3-154)$$

where

$S_f$  = Volumetric swelling fraction

$V_c$  = Actual volume of the fuel cell,  $m^3$

$V_{th}$  = Theoretical volume of the mass of fuel in the cell,  $m^3$

By fitting the swelling vs gas release data from Ref. 8-25 and 8-26, see Fig. 8.3-3 the following equation was generated, defining the gas release fraction  $R_f$ . A least 22.78% swelling is required before the gas is released.

$$R_f = 0.57535 \exp(0.33238 S_f) - 9.77836 \exp(-12.10443 S_f) \quad (8.3-155)$$

where

$R_f$  = Fraction of total fission gas released

The total amount of gas released is therefore the release fraction from Eq. 8.3-155 times the total generated in the node. The amount released during a computational time step is the difference between the total released and the amount released previously.

$$G_r = R_f G_t - (G_t - G_f) \quad (8.3-156)$$

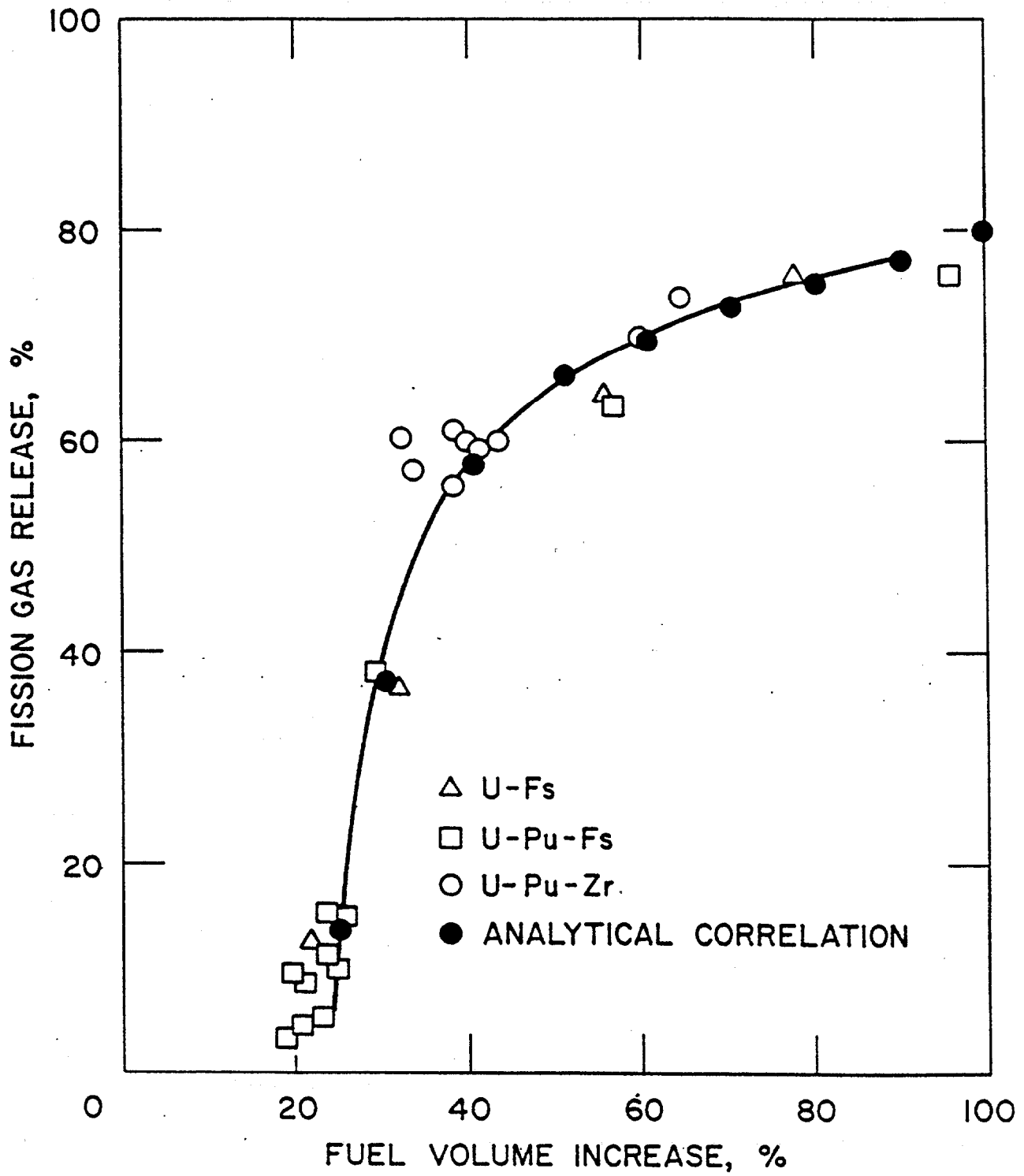


Fig. 8.3-3. Effect of Fuel Swelling on Fission Gas Release in Metal Fuels

where

$G_r$  = Gas released during the time step, kg

$G_t$  = Total amount of gas produced in the cell, kg

$G_f$  = Gas retained in the fuel assuming no release during the time step, kg

It is then assumed that the release of this amount of gas moves an equivalent fraction of the closed porosity volume to the open porosity.

$$V_r = \frac{G_r}{G_f} V_f \quad (8.3-157)$$

where

$V_r$  = Volume moved from closed to open porosity, m<sup>3</sup>

$V_f$  = Volume of fission gas in closed porosity, m<sup>3</sup>

These calculations are carried out in the subroutine RELGAS.

### 8.3.10.2 Metal Fuel Behavior During Melting

#### 8.3.10.2.1 Molten Cavity

The melting of a cell begins as the temperature reaches an input determined temperature, between the solidus and liquidus temperatures. The incremental melt fraction approach developed in Section 8.3.7 is then used to move fuel, gas, and volumes between the solid and molten state. As the temperature of the cell rises above the initial melting temperature, increasing fractions of the cell become associated with the molten cavity. When the cell temperature reaches the fuel liquidus temperature, the whole cell is associated with the molten cavity. Since each radial cell is treated separately, an annular melt zone would be correctly treated if it existed in a U-Pu-Zr fuel pin.

### 8.3.10.2.2 Connected Porosity

Upon melting the connected porosity is released to the molten cavity instantaneously. It is assumed that the bubble morphology associated with this interlinked porosity is such that upon melting, there is no time delay between melting and release of the gas and associated volume to the molten cavity free volume. The connected porosity acts in the same manner as the grain boundary gas in the oxide fuel as far a melting is concerned see (Section 8.3.7.2.2). Table 8.3-1 illustrates the similarities and difference between the types of gas associated with the metal fuel and those of the oxide fuel.

### 8.3.10.2.3 Closed Porosity

The closed porosity consisting of fission gas in constrained bubbles is assumed to act like the retained gas in the oxide fuel. Upon melting, these bubbles must move to the free volume in order to coalesce into the molten cavity. This is treated through the use of a time constant for bubble coalescence. Only the retained gas in the molten fuel can undergo this coalescence process (see Section 8.3.7.2.3). Recent results with the model have indicated a need for further refinement by breaking this closed porosity into an intragranular component and a grain boundary component, that would be released immediately on melting.

Table 8.3-1. Comparison between Oxide and Metal Fuel Models for Fission Gas Porosity Behavior

Behavior	Oxide Fuel Porosity	Metal Fuel Porosity
Causes fuel swelling	Grain boundary	Closed
Released immediately to molten cavity upon fuel melting	Grain boundary	Connected
Release to molten cavity other coalescence delay	Intra-granular	Closed

### 8.3.10.3 Axial Extrusion in Solid Fuel

One of the reasons for interest in metal fuels is the possibility for axial relocation within the intact cladding. While recent preliminary experimental evidence from the TREAT M2 and M3 tests [8-29] indicate that axial relocation occurs primarily upon fuel melting, the study of solid fuel swelling and extrusion possibilities are valuable for they add to the understanding of the fundamental properties of metal fuel. These phenomena include porosity formation and behavior, fuel creep, fission gas swelling, and fuel-cladding chemical interaction.

#### 8.3.10.3.1 Fission Gas Induced Swelling

DEFORM, for both oxide and metal fuel, calculates the increase or decrease in bubble volume containing trapped fission gas in response to the bubble pressure, the local hydrostatic pressure, the bubble surface tension, and the fuel creep rate. This is described in Section 8.3.4 for the oxide fuel.

In the metal fuel the porosity is divided into open and closed porosity, as described in Section 8.3.10.1.1 above, with the closed porosity assumed to produce the fuel swelling. The same basic approach adopted for the oxide fuel is used for the metal fuel swelling modeling. The amount of retained fission gas and the volume available at the beginning of a time step determine the gas pressure in the closed porosity. This force is counteracted by the local hydrostatic pressure and the bubble surface tension. The mismatch between the bubble pressure and restraining forces is the driving force for expansion (bubble pressure greater than restraining pressure) or contraction (bubble pressure less than restraining pressure) of the closed porosity. If the bubble pressure is the same as the restraining pressure, a state of equilibrium would exist. Therefore, given that the amount of retained gas and the restraining pressure are known, an equilibrium closed porosity volume can be determined that would give a bubble pressure equal to the restraining pressure. This is the volume the closed porosity will tend towards during the time step. However, an instantaneous volume change does not occur because the fuel has a finite creep rate dependent on the mismatch between the initial bubble pressure and restraining pressure, the fuel temperature, and the fission rate. This creep rate defines a time constant associated with the change in bubble volume. The time constant and the current computational

time step determine the magnitude of the volume change that takes place as the bubble volume changes from its current volume toward the equilibrium volume.

In the development of the model for the metal fuel, it was found that one of the most sensitive parameters influencing the fuel swelling was the fission gas bubble size used to calculate the surface tension. Because of the low strength of the metal fuel, and the assumption that the interlinked porosity is connected to the fission gas plenum, the stress state in the fuel is assumed to equal the plenum pressure. Under these conditions the surface tension restraint becomes a critical parameter in the control of fuel swelling. If bubble sizes are small, the surface tension is high and effectively limits the amount of swelling. If bubble sizes are large, then the bubbles expand rapidly to near equilibrium values, introducing rapid swelling of the fuel.

Because there currently exists little information on the development of bubble morphology during the early irradiation of metal fuels, it was necessary to devise a method of providing a bubble size that produced results consistent with the observation that the fuel-cladding gap closes, in metal fuel pins, in the 2-3 atom percent burnup range. This was achieved by providing a bubble radius dependent on the burnup level and then determining a calibration constant to obtain the desired behavior.

$$R_B = C_R B \quad (8.3-158)$$

where

$R_B$  = Fission gas bubble radius of closed porosity, m

$C_R$  = Calibration constant

$B$  = Burnup, atom percent

While this formulation does not fully adhere to the principle of using mechanistic models employed in DEFORM, it does produce a reasonable initiation to the calculation and provides for development of other models in a consistent fashion.

### 8.3.10.3.2 Axial Swelling Fraction

Section 8.3.4.1 gives the development of the plane axial swelling strain used in DEFORM. This same approach is used when considering the metal fuels. However, when the metal fuel comes into contact with the cladding, it is assumed that the fuel strength is not great enough to cause fuel-cladding mechanical interaction. Instead, the volume must be added through axial elongation if the fuel-cladding interface is in such a state that movement can occur, i.e., the temperature of the fuel-cladding interface is above the local eutectic temperature. This movement restriction does not currently exist in DEFORM, but will be operational when DEFORM and SSCOMP are coupled.

After the initial calculation in FSHELL, the outer fuel radius may be greater than the inner cladding radius. The volume that must be accounted for by extra axial expansion is determined by the mismatch between the locations of these two surfaces.

$$\Delta V_{exc} = \pi A_H (r_{fo}^2 - r_{ci}^2) \quad (8.3-159)$$

where

- $\Delta V_{exc}$  = Volume of fuel outside the allowed volume, m<sup>3</sup>
- $A_H$  = Axial segment height including all strains, m
- $r_{fo}$  = Outer radius of the fuel including all strains, m
- $r_{ci}$  = Inner radius of the cladding including all strains, m

The total volume change calculated to take place radially and that calculated to take place axially, from the initial calculation, are then modified by this volume discrepancy of Eq. 8.3-159

$$\Delta V_{r,n} = \Delta V_{r,o} - \Delta V_{exc} \quad (8.3-160)$$

$$\Delta V_{a,n} = \Delta V_{a,o} + \Delta V_{exc} \quad (8.3-161)$$

where

$\Delta V_{r,n}$  = New total change in radial volume,  $m^3$

$\Delta V_{r,o}$  = Old total change in radial volume,  $m^3$

$\Delta V_{a,o}$  = New total change in axial volume,  $m^3$

$\Delta V_{a,n}$  = Old total change in axial volume,  $m^3$

These are then used to calculate the new fraction of volume change taking place axially.

$$F_{as} = \frac{\Delta V_{a,n}}{\Delta V_{r,n} + \Delta V_{a,n}} \quad (8.3-162)$$

where

$F_{as}$  = Fraction of volume change taking place axially

This new factor is then used to determine the radial and axial volume changes for each radial cell, and a new generalized axial swelling strain is calculated following the procedure in Section 8.3.4.1. The new node structure is then determined and the fuel and cladding surfaces are again examined. If a mismatch again occurs, the procedure is repeated until a match is formed within a tolerance of  $1.0 \times 10^{-12}$  m. This procedure converges within three to five iterations. Separate thermal/mechanical and swelling strains are maintained for the purpose of comparison. Those calculations are performed in the subroutine FSWELL.

#### 8.3.10.4 Sodium Bond

As the fuel-cladding gap changes, the liquid sodium that fills this gap must move to other locations. A new subroutine, NABOND, has been developed which carries out the accounting of the available volumes and calculates the sodium slug level in the plenum. The temperature of the sodium at a particular elevation is assumed to be the average of the fuel and cladding surface temperatures. The mass of sodium at each axial location is determined from the gap volume and sodium density.

$$M_{s,j} = \pi A_H (r_{ci}^2 - r_{fo}^2) \rho_{s,j} \quad (8.3-163)$$

where

$M_{s,j}$  = Mass of sodium in fuel-cladding gap at axial segment j, kg

$\rho_{s,j}$  = Density of liquid sodium at axial segment j, kg/m<sup>3</sup>

The total sodium mass in the gap is then determined by summing over all axial segments.

$$M_{st} = \sum_{j=1}^{MZ} M_{s,j} \quad (8.3-164)$$

where

$M_{st}$  = Total mass of sodium in fuel-cladding gap, kg

$MZ$  = Total number of axial segments in the pin

The sodium mass in the plenum is then found by subtracting the result of Eq. 8.3-164 from the total sodium initially loaded into the pin.

$$M_{sp} = M_{sl} - M_{st} \quad (8.3-165)$$

where

$M_{sp}$  = Mass of bond sodium in the plenum, kg

$M_{sl}$  = Mass of bond sodium initially loaded in the pin, kg

The sodium level in the plenum is then determined.

$$H_{sp} = \frac{M_{sp}}{\rho_{sp} \pi r_p^2} \quad (8.3-166)$$

where

- $H_{sp}$  = Height of sodium in the plenum, m
- $\rho_{sp}$  = Density of sodium at the plenum temperature,  $\text{kg/m}^3$
- $r_p$  = Inner cladding radius in the plenum, m

In the calculation of the plenum pressure, this sodium filled volume is removed from the plenum volume available for the released fission gas.

#### 8.4 Fuel-pin Failure Criteria

DEFORM-4 contains a number of methods for the determination of fuel-pin failure and failed pin model initiation. These can be divided into two major areas: (1) failure based on specified conditions, and (2) calculated failure correlations. The first method is currently used to produce failure initiation because of the limited amount of integral code validation with the failure correlations. Since these use parameters such as stress and temperature to produce the predictions, it is essential that these be checked against experimental tests to assure the accuracy and appropriateness of their use under various transient conditions. The first method involves parameters used previously with the SAS3D code system, so some familiarity with their use and limitations is assumed. Although these are simple, they can be used in a manner consistent with the SAS3D implementation and available experimental data.

All criteria are cast into the form of a failure fraction which is the current value for the parameter being used as a failure indicator, i.e., melt fraction, time, etc., divided by the value which would produce failure. If this failure fraction becomes 1, then failure is assumed to occur and the failed pin modeling is initiated. In addition to satisfying the parameter under consideration, the fuel melt fraction must be above a specified level, FMELTM, before PLUTO2 or LEVITATE will be initiated. These calculations are performed in the subroutine CLDFAL.

### 8.4.1 Input Specified Failure Criteria

Through the use of the input parameters MFAIL, IFAIL, JFAIL, FSPEC, and FMELTM the code can be controlled to initiate failure with the conditions discussed below. MFAIL selects the meaning of FSPEC, IFAIL and JFAIL specify the radial and axial location of the test for failure, and FMELTM is the minimum melt fraction necessary at the location of failure for PLUTO2 or LEVITATE to be initiated. Table 8.4-1 gives the selections currently available in conjunction with DEFORM-4. If IFAIL and JFAIL are not specified, the location of the parameter maximum is selected.

The use of MFAIL with a value of 7 initiates the failure with a criteria that is consistent with the LEVITATE and PLUTO2 rip propagation considerations, see Sections 16.3.1 and 14.3.3, respectively. This criterion checks the cladding hoop stress introduced by a molten cavity pressure, for fully cracked fuel, or fuel-cladding mechanical interaction, when solid fuel is present, against the ultimate tensile strength of the cladding to determine if failure has occurred. If the cladding does fail, then the routine checks to see if the molten fuel has reached the crack boundary. Both conditions are necessary for the initiation of the failed fuel routines.

Table 8.4-1. Failure Initiation Options

MFAIL	FSPEC	IFAIL	JFAIL
1	Time	-	Nec*
2	Temperature	Nec	Opt**
3	Melt fraction	-	Opt
4	Cavity pressure	-	Opt
5	Hoop stress	-	Opt
7	Rip propagation	-	Opt

\* Nec = Necessary parameter that must be specified.

\*\*Opt = Optional parameter. If not specified, the axial level with the maximum value will be chosen.

When other failure criteria are used, there may be extensive rip propagation after initiation of the failed fuel model because of the change in criterion.

## 8.4.2 Calculated Failure Correlations

In DEFORM-4, there exist a number of failure correlations which may be used to determine the time and location of cladding failure. Care should be taken when drawing any conclusions based on these correlations, since the validation effort is in its initial stages with these correlations. In addition, the method of determining cladding stress is not totally consistent between DEFORM-4, a more mechanistic approach, and the correlations, which were based on initial cold dimensions and fill-gas pressures. DEFORM-4 also considers fuel-cladding mechanical interaction rather than just gas pressure.

The use of these failure correlations currently involves an iterative approach, using the failure fractions printed by SAS4A and one of the failure conditions described in Section 8.4.1. First, the case is run with no failure conditions specified and restart files produced at selected intervals. The output is then studied to determine when the failure fraction of interest reaches one, and at which axial segment. One of the conditions discussed above is then selected to initiate failure at the appropriate time and axial segment. A restart case is then run from a restart file produced before the correlation failure condition was reached. In this case, one of the simple failure criteria will be used to initiate failure. The values used in the simple criteria should be chosen to produce failure initiation at the same time and place as was predicted by the correlation criterion during the initial run.

The various correlations are given below. Although the units are inconsistent in many cases, the code has taken this into account and made the necessary adjustments.

### 8.4.2.1 Biaxial Stress Rupture

This correlation is from the Nuclear Systems Material Handbook [8-17] and is based on unirradiated, 20% cold-worked type 316 SS developmental cladding.

$$\text{Log } \theta = -15.22 + 9.5342 \text{ Log } [\text{Log } (\sigma^*/\sigma)] \quad (8.4-1)$$

where

$\theta$  = Dorn parameter =  $t_r \exp(-Q/RT)$

$t_r$  = Rupture time, hr

$T$  = Temperature, K

$Q$  = 83,508 cal/mole

$R$  = Universal gas constant

$\sigma$  = Hoop stress =  $\frac{r_o^2 + r_i^2}{r_o^2 - r_i^2} P$ , ksi

$\sigma^*$  = 135 ksi

$r_o$  = Clad outer radius

$r_i$  = Clad inner radius

$P$  = Internal gas pressure (or interface pressure), ksi

#### 8.4.2.2 Burst Pressure

This correlation is from the NSMH [8-17] for unirradiated FTR cladding.

$$P = \sum_{i=0}^{10} a_i \sigma^i \quad (8.4-2)$$

where

$P$  = Burst pressure, ksi

$\sigma$  = Hoop stress, as defined above

$a_0$  =  $1.799988 \times 10^1$

$a_1$  =  $2.866442 \times 10^{-2}$

$a_2$  =  $-3.986012 \times 10^{-4}$

$a_3$  =  $2.408207 \times 10^{-6}$

$a_4$  =  $-8.090292 \times 10^{-9}$

$$\begin{aligned}
a_5 &= 1.607218 \times 10^{-11} \\
a_6 &= -1.962158 \times 10^{-14} \\
a_7 &= 1.487159 \times 10^{-17} \\
a_8 &= -6.821934 \times 10^{-21} \\
a_9 &= 1.735220 \times 10^{-24} \\
a_{10} &= 1.879417 \times 10^{-28}
\end{aligned}$$

#### 8.4.2.3 Transient Burst Temperature

This correlation is from the NSMH [8-17] for unirradiated cladding. It involves two temperature ramp rates, 5.56 and 111.1 K/s. If the rate is between these, a linear interpolation is performed.

$$\begin{aligned}
T_f &= 2358.4 - 36.41 \sigma + 0.5649 \sigma^2 - 3.455 \times 10^{-3} \sigma^3 \\
&\text{for } \dot{T} \leq 5.56 \text{ K/s}
\end{aligned} \tag{8.4-3}$$

$$\begin{aligned}
T_f &= 2484.8 - 37.80 \sigma + 0.5827 \sigma^2 - 3.585 \times 10^{-3} \sigma^3 \\
&\text{for } \dot{T} \geq 111.1 \text{ K/s}
\end{aligned} \tag{8.4-4}$$

where

$T_f$  = Failure temperature, °F  
 $\sigma$  = Hoop stress, as defined above

#### 8.4.2.4 Larson-Miller Life Fraction

This correlation is the LMP life fraction incorporated in the TEMECH computer code [8-30].

$$\text{Log} \left( \frac{t_r}{3600} \right) = \frac{\text{LMP}}{1.8 T} - C \tag{8.4-5}$$

where

- $t_r$  = Time to rupture, in seconds
- $C$  = Material-dependent constant = 20
- LMP = Experimentally determined Larson-Miller parameter
- $T$  = Cladding temperature, K

For 20% CW 316 SS cladding, the following correlation is used.

$$\begin{aligned} \text{LMP}' &= 4.6402 - 5.1218 \times 10^{-2} \sigma_m + 7.0417 \times 10^{-4} \sigma_m^2 \\ &\quad - 4.1349 \times 10^{-6} \sigma_m^3 \end{aligned} \tag{8.4-6}$$

for  $0 < \text{fluence} \leq 1.0 \times 10^{22}$

$$\begin{aligned} \text{LMP}' &= 4.2281 - 2.0469 \times 10^{-2} \sigma_m \end{aligned} \tag{8.4-7}$$

for  $1.0 \times 10^{22} < \text{fluence} \leq 3 \times 10^{22}$

$$\begin{aligned} \text{LMP}' &= 7.488 - 0.138 \sigma_m \end{aligned} \tag{8.4-8}$$

for 5.56 K/s temperature ramp and fluences between  
 $3.0 - 4.0 \times 10^{22}$

$$\begin{aligned} \text{LMP}' &= 5.285 - 7.778 \times 10^{-2} \sigma_m + 6.027 \times 10^{-4} \sigma_m^2 \end{aligned} \tag{8.4-9}$$

for 111.1 K/s temperature ramp and fluences between  
 $3.0 - 4.0 \times 10^{22}$

where

$$\begin{aligned} \text{LMP} &= \text{LMP}' \times 10^4 \\ \sigma_m &= \text{Modulus modified hoop stress in ksi,} \\ &= \sigma_c \frac{E (1033^\circ\text{C})}{E (T)} \end{aligned}$$

These rupture times are then used in the life fraction form as

$$\text{life fraction} = \sum_i \frac{\Delta t_i}{t_{r,i}} \quad (8.4-10)$$

where

$$\begin{aligned} i &= \text{Time-step number} \\ \Delta t_i &= \text{Time-step length} \\ t_{r,i} &= \text{Time for cladding rupture} \end{aligned}$$

### 8.4.3 Preliminary Metal Fuel Failure Criteria

The consideration of a new fuel type in the context of DEFORM and SAS4A raises the question of the type of failure these pins will experience. Because metal fuel does not produce the same magnitude of fuel-cladding mechanical interaction as the oxide fuel, it is reasonable to assume that the cladding failure will result from a different phenomenon.

Metal uranium forms a low melting point eutectic alloy with both iron and nickel, constituent materials in the cladding alloys used. As the steady state irradiation proceeds, the iron and nickel can be leached out of the cladding, leading to the formation of a low melting point alloy layer adjacent to the cladding surface. Under transient conditions the temperature in this outer layer, at a certain axial location, may become high enough to melt this material. This in turn can produce a failure at this location by accelerating the further thinning of the load

bearing cladding. A number of tests with UF<sub>6</sub> rods were performed and analyzed to develop a correlation for the time to cladding failure [8-31]. This correlation has been incorporated into the FAILUR routine for preliminary use until a more mechanistic model is developed which handles the cladding thinning and subsequent failure from the local pressure.

$$T_f = 9.142 \times 10^4 \left[ \frac{T_a}{T_{eut}} \right]^{-28.495} (1+B)^{-0.54669} \quad 8.4-11$$

where

- $T_f$  = Time to failure at the current conditions, s
- $T_a$  = Temperature at the fuel-cladding interface, °C
- $T_{eut}$  = Input eutectic temperature, °C
- $B$  = Burnup, atom percent

Once this time has been determined, a life fraction approach is used by dividing the current time step by this failure time and adding it to the previously calculated fractions. When the fraction reaches 1, failure is assumed.

$$F_{f,n} = F_{f,o} + \frac{\Delta t}{T_f} \quad 8.4-12$$

where

- $F_{f,n}$  = New life fraction value
- $F_{f,o}$  = Sum of previous life fraction values
- $\Delta t$  = Time step, s

This correlation was developed over a narrow range of temperatures so its use should be considered preliminary until a more mechanistic approach is developed.

#### 8.4.4 Failure Modeling Coupling to Fuel Motion Models

In order to correctly assess the accident scenario in a transient that leads to fuel pin failure and subsequent fuel motion, there should be a high degree of consistency between the methods for predicting the initial failure and that used to predict the axial propagation of this failure. This consistency has now been incorporated in the FAILUR subroutine for the option with MFAIL equal to 7. While the actual criterion used is preliminary in nature, the fact that consistency exists between failure and rip propagation is important in order to study how this affects the accident scenario. It is noted that this consistent failure model has been implemented only for an oxide-fuel type failure. A similar consistent failure model for the metal fuel pins will be added in the future.

PLUTO2 and LEVITATE use a rip propagation model that compares the circumferential cladding stress, induced by a pressurized moten cavity acting on cracked fuel, to the ultimate tensile strength of the cladding. A stress greater than the ultimate tensile strength produces failure at the axial location. This same approach has been followed in this failure prediction.

First, the SAS4A/DEFORM cladding node structure is converted to one compatible with the failed fuel modeling routines. PLUTO2 and LEVITATE divide the cladding into an inner cladding node containing three-fourths of the cladding thickness, and an outer node containing the rest.

$$r_{c1} = r_{ci} + 0.25 (r_{co} - r_{ci}) \quad (8.4-13)$$

$$r_{c2} = r_{ci} + 0.75 (r_{co} - r_{ci}) \quad (8.4-14)$$

where

- $r_{c1}$  = Outer boundary of old inner cladding cell, m
- $r_{c2}$  = Outer boundary of old central cladding cell, m
- $r_{co}$  = Outer radius of the cladding, m
- $r_{ci}$  = Inner radius of the cladding, m

The new inner cladding cell energy is then determined form weighting factors based on the old cell radii

$$E_{c,a} = [E_c(T_{ci}) \cdot W_1 + E_c(T_{cc}) \cdot W_2]/[W_1 + W_2] \quad (8.4-15)$$

where

$$\begin{aligned} E_{c,a} &= \text{Average energy content of the new inner cladding node, J/kg} \\ E_c(T) &= \text{Cladding energy as a function of temperature, J/kg} \\ T_{ci} &= \text{Inner temperature of the cladding, K} \\ T_{cc} &= \text{central temperature of the cladding, K} \\ W &= r_{c1}^2 - r_{ci}^2 \\ W_2 &= r_{c2}^2 - r_{c1}^2 \end{aligned}$$

The temperature of the new inner cladding node is then determined.

$$T_{c1} = T_c(E_{c,a}) \quad (8.4-16)$$

where

$$\begin{aligned} T_{c1} &= \text{Temperature of modified inner cladding node, K} \\ T_c(E) &= \text{Cladding temperature as a function of energy, K} \end{aligned}$$

The ultimate tensile strength is then determined on the basis of the new node structure.

$$U_{ts} = [3 U_t(T_{c1}) + U_t(T_{co})]/4 \quad (8.4-17)$$

where

$$\begin{aligned} U_{ts} &= \text{Average ultimate tensile strength of the cladding, Pa} \\ U_t(T) &= \text{Ultimate tensile strength as a function of temperature, Pa} \\ T_{co} &= \text{Cladding outer surface temperature, K} \end{aligned}$$

This is the value that determines if failure occurs. If the calculated circumferential stress exceeds  $U_{ts}$ , failure is assumed to occur.

The calculated stress is determined in two ways, depending on the relationship between the melt boundary and cracked region of the fuel. If a solid annulus of fuel exists between the melted and cracked regions, the calculated fuel-cladding interface pressure is used

$$\sigma_c = [P_{fci}r_{ci} - P_{ext}r_{co}]/[r_{co} - r_{ci}] \quad (8.4-18)$$

where

$\sigma_c$  = Calculated circumferential stress based on a force balance, Pa

$P_{fci}$  = Pressure that exists at the fuel-cladding interface, Pa

$P_{ext}$  = Pressure that exists on the outer cladding surface,

If the melting has proceeded to the cracked boundary, then the cladding stress is determined from a force balance on the cladding assuming an inverse  $r$  drop-off in pressure through the solid, cracked fuel.

$$\sigma_c = [P_{cav}r_{cav} - P_{ext}r_{co}]/[r_{co} - r_{ci}] \quad (8.4-19)$$

where

$P_{cav}$  = Central molten cavity pressure, PA

$r_{cav}$  = Radius of the central molten region, m

The failure fraction is then calculated from the cladding stress and ultimate tensile strength.

$$F_f = \sigma_c/U_{ts} \quad (8.4-20)$$

where

$F_f$  = Cladding failure fraction at current time

When this fraction reaches 1, failure of the cladding at the axial segment is assumed to occur. However, this does not mean the ejection of fuel into the coolant channel will take place. Besides cladding failure, the molten fuel radius must have reached the cracked fuel radius. Therefore, there are two conditions to satisfy prior to initiation of the post failure fuel motion modeling; (1) cladding failure, and (2) complete solid fuel cracking.

Once the post failure fuel motion modeling has been initiated, DEFORM is not used. Control is transferred to PLUTO2 or LEVITATE and the same procedure given above is employed by these modules to determine if the cladding failure propagates to other axial segments.

#### 8.4.5 Time-step Control on Approach to Failure

As the conditions necessary for the failure are approached, the maximum time step is reduced to specified levels. This is controlled through the input parameters FIRLIM, SECLIM, and THRLIM, and the associated time steps DTFAL1, DTFAL2, and DTFAL3. When the failure fraction reaches FIRLIM, the main time step will be reduced to DTFAL1 or the current time step, whichever is smaller. This same procedure continues through SECLIM and THRLIM. If

$$0 \leq F_f < \text{FIRLIM} \quad (8.4-11)$$

where

$F_f$  = Failure fraction for the failure condition being used

then the maximum allowable time step is that defined by the initial transient time-step input parameter DT0.

$$\Delta t = \text{DT0} \quad (8.4-22)$$

where

$\Delta t_m$  = Maximum allowable time-step length, s

If

$$FIRLIM \leq F_f < SECLIM \quad (8.4-23)$$

then

$$\Delta t_m = DTFAL1 \quad (8.4-24)$$

Similarly, if

$$SECLIM \leq F_f < THRLIM \quad (8.4-25)$$

then

$$\Delta t_m = DTFAL2 \quad (8.4-26)$$

or, if

$$THRLIM \leq F_f \leq 1 \quad (8.4-27)$$

then

$$\Delta t_m = DTFAL3 \quad (8.4-28)$$

This procedure serves two functions. First, the reduction in main time step produces a corresponding reduction in the PRIMAR time step, thereby allowing the loop model to continue a stable calculation on the initiation of pin failure. Second, the reduced time step on initiation of failure avoids excessive fuel motion in PLUTO2 and LEVITATE prior to the time these failed pin models can initiate their own time-step control procedures.

## 8.5 General Method of Solution

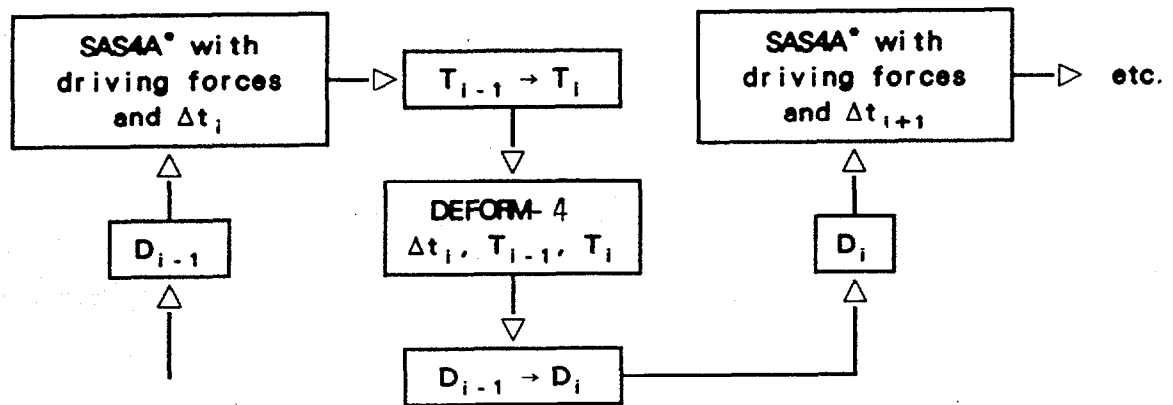
DEFORM-4 is coupled to the rest of SAS4A through two main driver subroutines; SSFUEL for the pre-transient calculation, and DFORM3 for the transient-state calculations. In this manner, the DEFORM-4 subroutines can be considered a separate code module which uses results from the SAS4A thermal/hydraulic calculation, temperatures and coolant pressures, and returns a new set of pin dimensions and properties. A general outline of this interaction scheme is shown in Fig. 8.5-1.

In the integration of DEFORM-4 into SAS4A, one of the primary considerations was to minimize the core storage and computational effort necessary when running a multichannel case with a long pre-transient and transient sequence. Based on these considerations, it was decided to avoid the thermalmechanical iteration process and, instead, provide time-step control for up to eight separate pre-transient irradiation periods. This will be discussed in more detail below. In the transient state, the time steps are short enough to avoid the problem of inconsistent results between the thermal and mechanical calculations.

As Fig. 8.5-1 shows, SAS4A performs thermal/hydraulic calculations over a specific time step in response to power and coolant conditions. During this time step, the dimensions are assumed to remain constant. SAS4A then passes to DEFORM-4 the temperatures at the beginning and end of the time step, the final coolant pressures, and the length of the time step. DEFORM-4 uses this information to calculate the fuel-pin response to the temperature changes and returns to SAS4A a new set of dimensions consistent with the final thermal/hydraulic conditions. These new dimensions are then used in the calculation of the temperatures at the end of the next time step. In this manner SAS4A and DEFORM-4 march through the entire pre-transient and transient calculation.

The flowchart shown in Fig. 8.5-2 illustrates the calling sequence in the pre-transient driver, SSFUEL, and Fig. 8.5-3 shows it in the transient driver, DFORM3. Each phenomenon considered is modularized into a separate subroutine. This makes the inclusion of new models and phenomena a very straightforward process of replacing or modifying specific subroutines.

$D_i$  = Dimension state of the fuel pin at the end of timestep  $i$   
 $T_i$  = Temperatures at the end of timestep  $i$   
 $\Delta t_i$  = Length of timestep  $i$



\* SAS4A refers to the thermal/hydraulic calculation

Fig. 8.5-1. DEFORM-4 - SAS4A Time Step Interaction Scheme

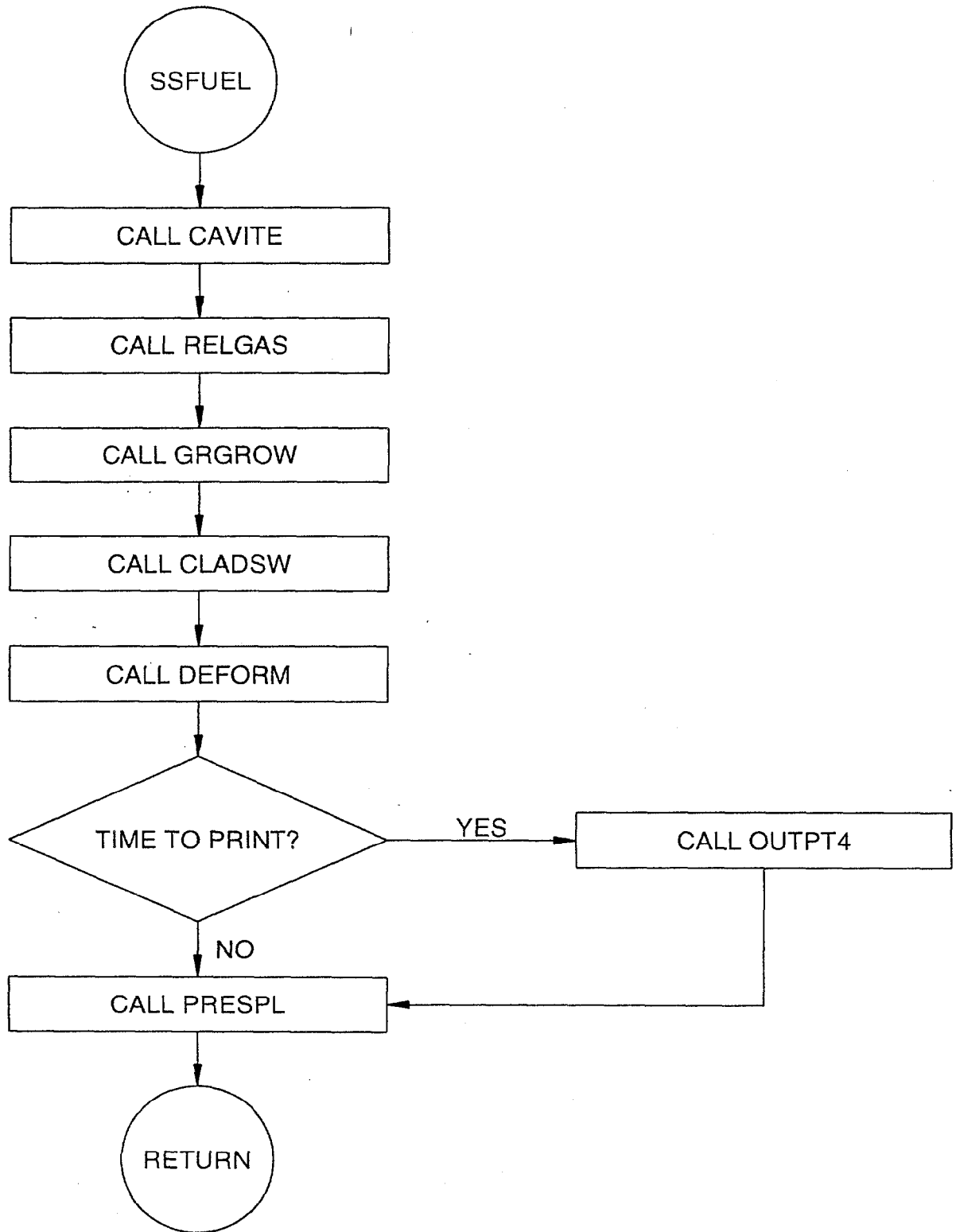


Fig. 8.5-2. Pretransient DEFORM-4 Driver (SSFUEL) Flow Chart

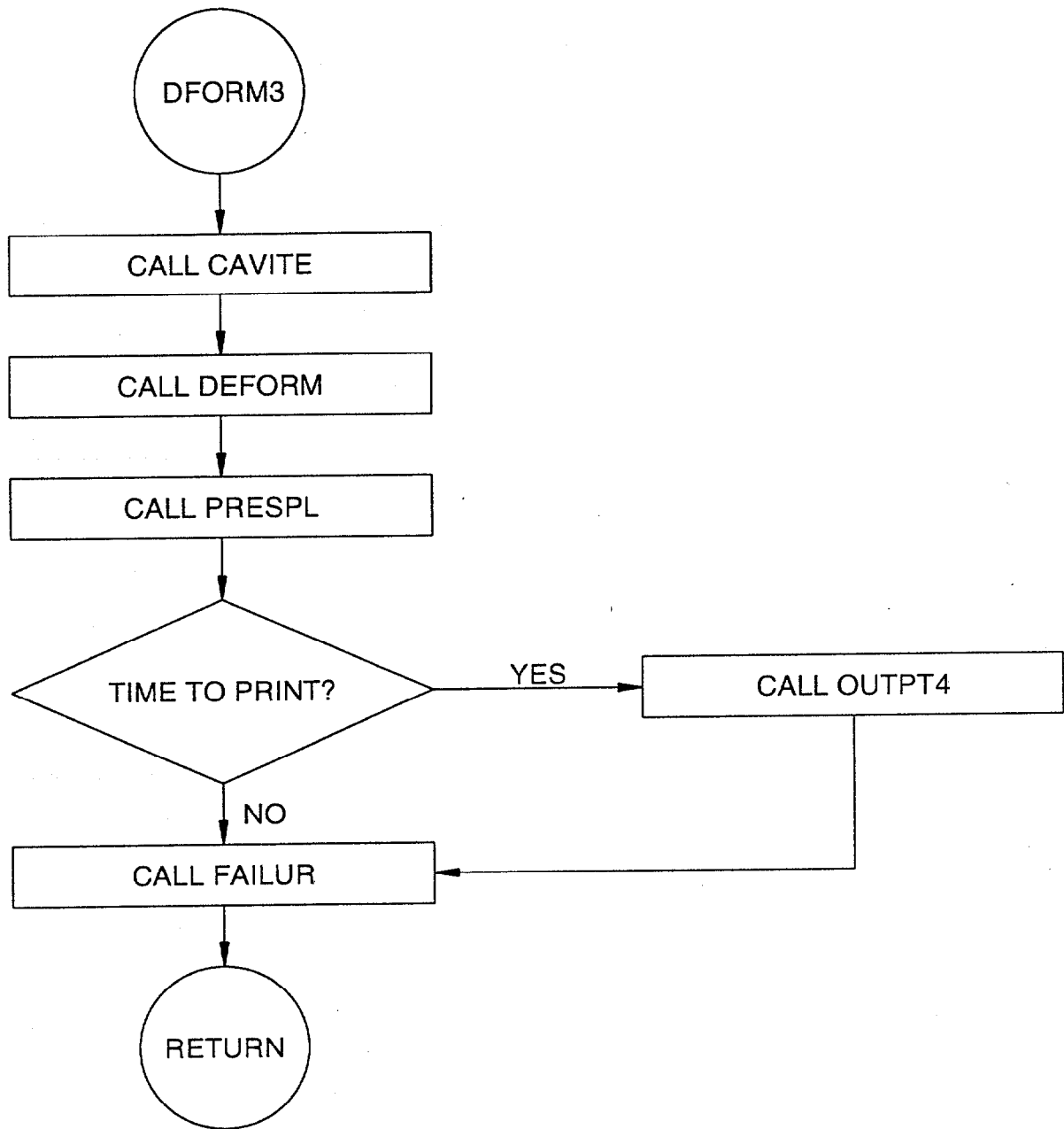


Fig. 8.5-3. Transient DEFORM-4 Driver (DFORM3) Flow Chart

This same procedure has been followed in the incorporation of material properties, as outlined in Section 8.7. A number of the phenomena used in the pre-transient calculation are not included in the transient calculation. Since the time scale of the transient is orders of magnitude less than the pre-transient, phenomena such as pore migration and irradiation-induced cladding swelling are assumed to be inactive, or less than second-order effects. In this manner, the transient calculation is streamlined. If a particular case needs to include these phenomena in the transient, their inclusion is merely a matter of including the appropriate "CALL" statements in the transient driver routine.

For the mechanics calculation, the same routines are used in both the pre-transient and transient calculation. In this way, the pre-transient is considered an extended transient calculation. Since both states use the same routines, the use of computer storage is minimized. Also, since phenomenological changes take place that impact temperatures and dimensions, the pretransient is a special transient. In order to take maximum advantage of this basic structure, the ability to input up to eight different ramps or steady-state levels is incorporated into the SAS4A pre-transient calculation. It is therefore possible to follow a simplified power history prior to the start of the transient.

In the current version of DEFORM-4, an approach has been adopted which separates the elastic and plastic deformation. These are linked through the fuel-cladding interface pressure. The basic mechanics approach is through a generalized plane strain representation with an elastic cladding. The plastic deformation is derived from two sources. If the fuel-cladding interface pressure produces cladding stresses below the flow stress, plastic deformation can occur through the process of creep. If the stresses induced exceed the flow stress, the cladding is assumed to behave in a perfectly plastic manner and the outer boundary condition on the fuel becomes the pressure that produces cladding stresses equal to the flow stress. In this situation, the radial deformation is determined by the fuel displacement until conditions return to the elastic state.

The calculations are performed on an axial segment by segment basis, starting at the lower axial blanket and continuing upward to the top axial blanket. A complete set of calculations for the response of the axial segment is performed before proceeding to the next segment.

### 8.5.1 Thermal-mechanical Solution

The thermal-hydraulic routines in SAS4A provide DEFORM-4 with the new coolant pressures and temperature in the fuel, cladding, coolant, and structure. DEFORM-4 must then calculate the thermal-mechanical response of the fuel-cladding system to the changes during the time step. With the temperature changes and coolant pressure now from SAS4A, only one additional boundary condition remains as input to the calculation, the central cavity pressure. If no fuel melting has occurred, or the axial segment is not in the axial region considered to be the molten cavity, this pressure is set equal to the plenum pressure existing at the end of the previous time step. If molten fuel is present, then the axial pressure distribution is determined from the results of the molten cavity pressure subroutine CAVITE, see Section 8.3.7. This is the boundary force acting on the inner surface of the non-molten fuel. The remaining force necessary to completely describe the external force system is the fuel-cladding interface pressure, and this is determined through the iterative procedure described below.

In Fig. 8.5-4, the main sequence of the mechanics driven routine, DEFORM, is illustrated. After initializing certain parameters, such as the thermal expansion strains, moduli of elasticity, etc., the fuel is checked to see if it is fully cracked or molten out to the cracked region. If a solid, noncracked annulus of fuel still exists, the solid fuel elastic solution routine SOLID is called. If it is determined in this routine that the fuel becomes completely cracked during the time step, the crack fuel elastic solution routine MKDRIV is called. This routine would have been called initially if the fuel was completely cracked at the beginning of the time step.

The sequence of operations within the subroutine SOLID is shown in Fig. 8.5-5. The main purpose of this routine is to determine the correct fuel-cladding interface pressure when a solid, uncracked fuel annulus exists at the beginning of the time step. Since the coolant pressure and central cavity pressure have been determined, SOLID must determine the fuel-cladding interface pressure that produces consistency between the outer fuel surface and inner cladding surface locations.

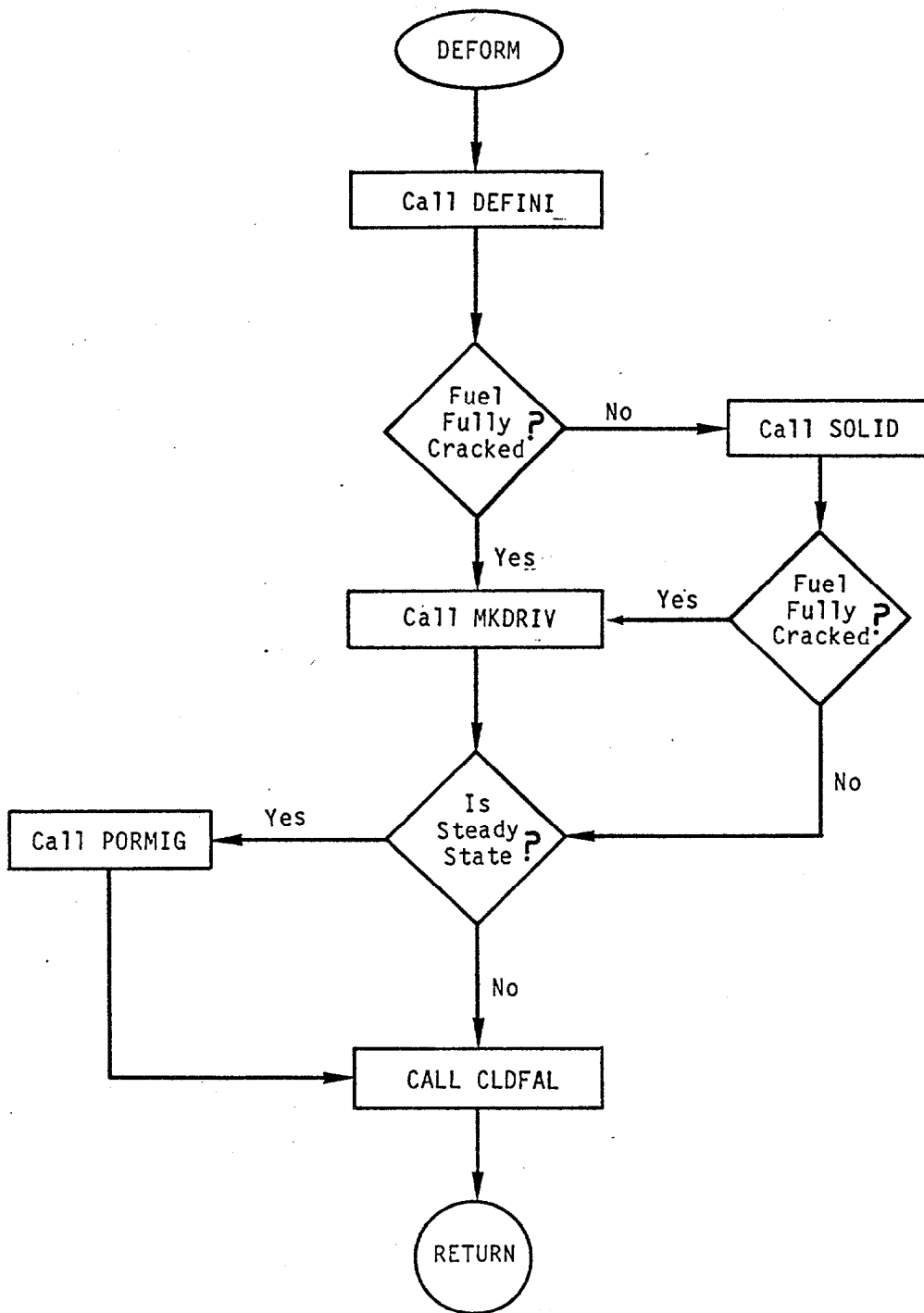


Fig. 8.5-4. DEFORM-4 Mechanics driver (DEFORM) Flow Chart

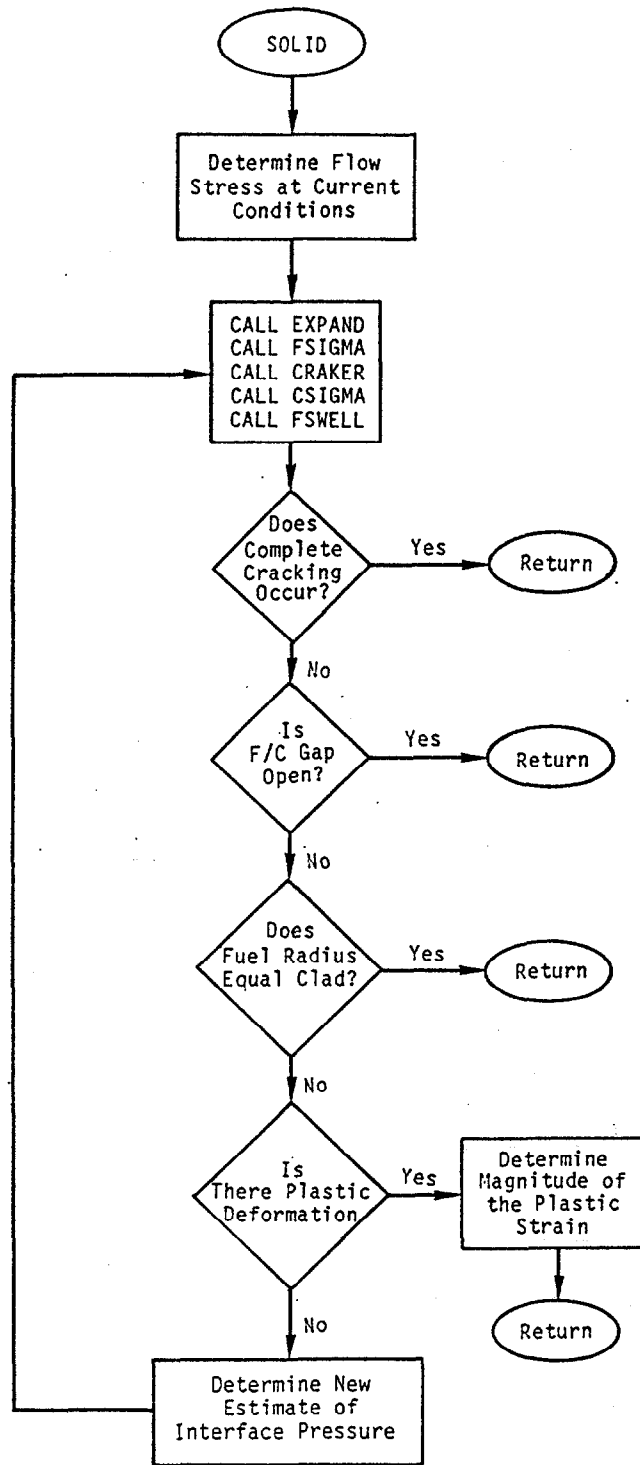


Fig. 8.5-5. DEFORM-4 Mechanics Interaction Solution (SOLID) Flow Chart

The approach used in the solution procedure in SOLID is to recognize that the fuel-cladding interface pressure is a bounded variable. It is, at least, the plenum pressure, but cannot exceed the value that would produce plastic flow in the cladding. SOLID therefore iterates to determine the value between these bounds which produces a consistent set of conditions. As a first estimate, the interface pressure from the previous time step is used. This, together with the thermal expansion in the current time step, is used to calculate the axial expansion in EXPAND, the non-molten fuel stresses and strains in FSIGMA, the crack volume fraction in CRAKER, the cladding stresses and strains in CSIGMA, and the fuel swelling strains in FSWELL. Each of these routines calculate the incremental changes that occur from the previous time step results in response to the changes occurring during the current time step. If complete cracking of the fuel occurs during the time step, control is passed to the subroutine MKDRIV. If part of the fuel remains uncracked, then the new fuel-cladding gap is examined to determine if a consistent set of conditions exists.

If a gap exists and the interface pressure is the plenum pressure, the solution is finished. If there is an interface pressure greater than the plenum pressure and the fuel-cladding gap is zero, then the solution is finished. If there is a negative gap and the interface pressure produces the flow stress, the cladding is in plastic deformation and the fuel determines the deformation, so the solution is finished.

The more interesting case involves a negative gap with an interface pressure below that necessary to cause plastic deformation of the cladding. In this case the interface pressure is first set to that which would cause plastic flow, and the calculations are repeated. This second calculation through EXPAND, FSIGMA, CRAKER, CSIGMA, and FSWELL then provides the upper bound on the interface pressure. If the gap becomes positive, the correct value of the interface pressure is between the initial and the new estimate. Based on the changes in gap size as a function of the change in interface pressure, and the magnitude of the deformation necessary to produce a match of the outer fuel and inner cladding surfaces, a third estimate of the interface pressure is obtained assuming a linear relationship between interface pressure and gap size. This procedure is continued until a fuel-cladding surface match is achieved within the desired tolerance or the fuel cracks completely.

When the applied interface pressure, cavity pressure, and thermal stresses produce a stress state in the fuel sufficient to cause the circumferential stress to exceed the fuel crack strength in a previously uncracked fuel cell, then the routine FSIGMA will redo its internal calculation with the new distribution of uncracked and cracked fuel cells. This routine will allow cracking to occur in all nodes where the circumferential stress exceeds the fracture strength. Prior to each invocation of EXPAND, FSIGMA, CRAKER, CSIGMA, and FSWELL, the crack state of the fuel is reset to the condition at the beginning of the time step.

In the case where all non-molten fuel is cracked, the thermal-mechanical solution is controlled by the subroutine MKDRIV. The sequence of operations for this routine is shown in Fig. 8.5-6. There is no iteration because the fuel-cladding interface pressure must be consistent with the cavity pressure and the solid fuel geometry. Knowing these two boundary conditions, the strains and fission gas induced swelling can be determined. If the fuel-cladding interface is open and the cavity pressure is equal to the plenum pressure, no movement of the cracked fuel takes place beyond the thermal-elastic and swelling strains. If the cavity is pressurized, the cracked fuel is translated radially to the cladding location. If the fuel-cladding gap is negative, the fuel is moved inward to provide a match at the cladding location. In both cases, the crack volumes are adjusted to be consistent with the radial translation.

In the pre-transient calculation, the cracked fuel is allowed to heal if the temperature is high enough. A healing temperature is determined based on the fuel solidus temperature.

$$T_H = f_H T_s \quad (8.5-1)$$

where

$T_H$  = Crack healing temperature, K

$f_H$  = Input fraction

$T_s$  = Fuel solidus temperature, K

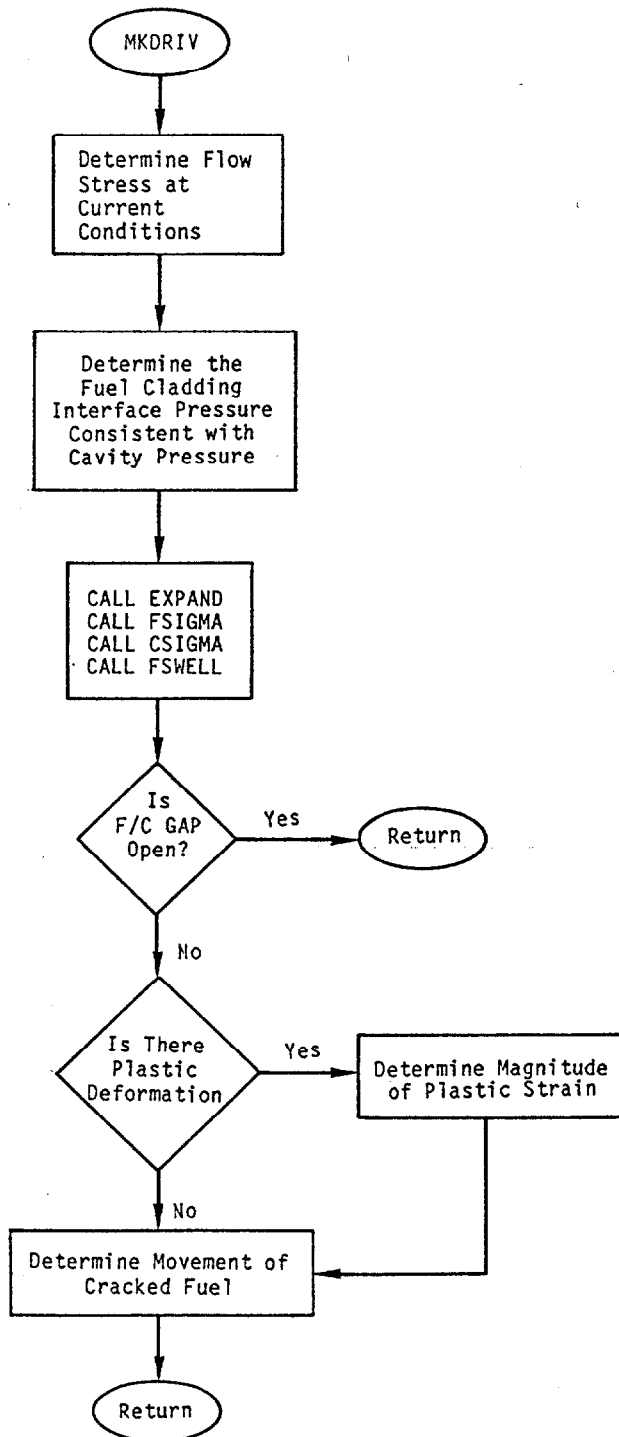


Fig. 8.5-6. DEFORM-4 Mechanics Interaction Solution with Fully Cracked Fuel (MKDRIV) Flow Chart

If the fuel cell temperature is higher than this healing temperature, the cell is assumed to become solid again. This healing does not take place in the transient calculation where the time scale is too short.

### 8.5.2 Plastic Fuel Deformation Solution

The routine FS WELL handles all plastic fuel deformations. The basic equations for the non-equilibrium fission-gas bubbles are given in Section 8.3.4.

First, the fuel hydrostatic pressure in each radial fuel node is calculated. The fission-gas bubble swelling or hot pressing in each node is then determined. Once the swelling strains are known, the new fuel node boundaries are calculated.

In determining whether a fuel cell will move radially outward or inward, the concept of a plasticity temperature is used. If the fuel temperature is above the plasticity temperature,  $T_{sep}$ , it is assumed that the fuel is soft enough to be easily deformed and will move radially inward in response to the restriction of the cooler fuel. This softening temperature is defined as

$$T_{sep} = T_{s1} + T_{s2} \sigma_{fci} \quad (8.5-2)$$

where

- $T_{s1}$  = Input base softening temperature, K
- $T_{s2}$  = Pressure effect constant, K Pa<sup>-1</sup>
- $\sigma_{fci}$  = Fuel-cladding interface stress, Pa

The cooler fuel cells move radially outward. If the central void closes, the inner radius is fixed to a nominal zero value,  $1 \times 10^{-6}$ , and all movement is radially outward. If the fuel is cracked across its entire radial extent, the movement is determined as described above.

In the molten cavity region, the volume changes calculated by CAVITE (see Section 8.3.7) are included in the redefinition of the node boundaries. In the solid nodes, the remaining as-fabricated porosity and any fuel crack volume are included with the fission-gas porosity in determining the new cell volumes. Once all the new node boundaries have been determined, the variation from the original is calculated and these node deformations are passed to the controlling solution routine.

Once a solution is obtained, all dimensions and stresses are updated to their final values, and the final plastic strain calculated (if any).

### 8.5.3 Final DEFORM-4 Calculations

After the thermal-mechanical calculations are finished, DEFORM-4 calculates the fuel axial expansion reactivity effects (see Section 8.3.9). The new plenum pressure, based on the new dimensions, temperatures, and fission gas release is then calculated in the subroutine PRESPL. The new gap conductance values for use in the next time step are determined. Control of the calculation is then returned to the SAS4A thermal/hydraulic routines for the calculation of the temperatures and coolant state for the next time step.

## 8.6 Computer Code Implementation

The DEFORM-4 module is implemented in SAS4A as a group of subroutines. Section 8.6.1 gives a list of these subroutines and a brief description of the calculation performed by each. The direct coupling with SAS4A is through the subroutine SSFUEL for the pre-transient calculation, and DFORM3 for the transient calculation.

The input parameters necessary for DEFORM-4 to perform its calculations are given in Table 8.6-2. This table also includes cross-references to the equation or section number where the parameter is used, the input location and variable name, a suggested value (assuming mixed-oxide fuel with 20, % cold-worked, stainless-steel cladding), and the external reference where the suggested value originated. Further information on the input parameters is given in the Input Description (see Chapter 2 Appendix 2.2).

In Section 8.6.3 a brief description of the output generated by DEFORM-4 is given. The sample output given in Figures 8.6-1 through 8.6-13 are included for illustration only, and should not be used as a sample case.

### 8.6.1 Subroutine and Function List

Table 8.6-1 DEFORM-4 Associated Subroutines and Functions

ALPHC	Mean thermal expansion coefficient of the cladding
ALPHF	Mean thermal expansion coefficient of the fuel
CAVITE	Molten cavity gas release and pressurization
CLADSW	Irradiation-induced cladding swelling
CLDFAL	Cladding failure fraction calculations
CRAKER	Volume fraction of cracks in fuel
CSIGMA	Thermal-elastic calculation in the cladding
DEFINI	Initial setup routine
DEFORM	Main mechanics driver routine
DFORM3	DEFORM-4 interface to SAS4A for transient calculation
ECLADF	Cladding modulus of elasticity function
EFUELF	Fuel modulus of elasticity function
EXPAND	Thermal-mechanical axial expansion routine
FAILUR	Determination of reaching failure criterion
FK	Fuel thermal conductivity function
FSIGMA	Thermal-elastic calculation in the fuel
FSWELL	Fission-gas bubble swelling/compaction routine
GRGROW	Grain growth in the fuel
HGAP	Fuel-cladding gap conductance function
KFUEL	Thermal conductivity of the fuel
MKDRIV	Thermal-elastic and interface pressure control routine when solid fuel is completely cracked
NABOND	Fuel-cladding gap conductance for sodium-bonded metal fuel

Table 8.6-1 DEFORM-4 Associated Subroutines and Functions (Cont'd)

OUTPT3	Short form output routine
OUTPT4	Standard output routine
PORMIG	As-fabricated porosity migration routine
PRESPL	Plenum pressure calculation
RELAX	Stress relaxation in the fuel (not operational)
RELGAS	Fission gas release in the fuel
RHOF	Theoretical density of fuel, solid and liquid
RHOL	Density of liquid fuel (not currently used)
RHOS	Density of solid fuel (not currently used)
SOLID	Thermal-elastic and interface pressure iteration control routine
SIGFRA	Fracture strengths of the fuel
SSFUEL	DEFORM-4 interface to SAS4A for pre-transient irradiation
UTS	Ultimate tensile strength of the cladding
YLDCF	Yield point of the cladding

8.6.2 Input Variables

Table 8.6-2 DEFORM-4 Input Variables

Equation Variable	Reference Eq. or Section No.	SAS4A Input Variable	Location Block	Location	Suggested Value	External Reference
-	-	IPROPT	1	6	0	-
-	-	IYLD	1	26	2	-
-	8.3.7	IMELTV	1	28	1	-
-	-	IXSTPC	1	32	0	-
-	-	IXSTPF	1	33	0	-
-	-	IMCVTY	1	34	0	-
-	-	IAREXT	1	40	0	-
-	-	POW	12	1	-	-
-	8.3-166	BETADN	12	4-9	-	-

Table 8.6-2 DEFORM-4 Input Variables (Cont'd)

Equation Variable	Reference Eq. or Section No.	SAS4A Input Variable	Location Block	Location	Suggested Value	External Reference
$\rho_0$	8.7-1	COEFDS(1)	13	1	11.08D+3	8-17
$C_1$	8.7-1	COEFDS(2)	13	2	2.04D-5	8-17
$C_2$	8.7-1	COEFDS(3)	13	3	8.70D-9	8-17
$C_1$	8.7-13	COEFK(1)	13	4	2.10D+0	8-32
$C_2$	8.7-13	COEFK(2)	13	5	2.88D-3	8-32
$C_3$	8.7-13	COEFK(3)	13	6	2.52D-5	8-32
$C_4$	8.7-13	COEFK(4)	13	7	5.83D-10	8-32
$C_5$	8.7-14	COEFK(5)	13	8	5.75D-2	8-32
$C_6$	8.7-14	CEOFK(6)	13	9	5.03D-4	8-32
$C_7$	8.7-14	COEFK(7)	13	10	2.91D-11	8-32
$T_r$	8.2-5	TR	13	419	300.	-
$MW_{fg}$	8.3-24	FGMM	13	600	131.	-
$f_g$	8.3-22	GATPF	13	601	0.246	8-17
$E_f$	8.3-23	ENPF	13	602	197.	-
$R_{eq}$	8.3-7	RLEQ	13	603	0.6	-
$R_{ueq}$	8.3-21	RUEQ	13	604	1.2	-
-	8.3.1	PRSMIN	13	605	0.02	-
$T_s$	8.3-87	TFSOL	13	786-793	-	-
$T_\ell$	8.3-87	TFLIQ	13	794-801	-	-
$P_0$	8.3-7	PRSTY	13	1073-1080	-	-
Not currently used		AC	13	1081	-	-
Not currently used		QSWL	13	1082	-	-
$A_p$	8.3-1	APORE	13	1083	20.704	8-6
$Q_p$	8.3-1	QPORE	13	1084	4.5281D+5	8-6
$A$	8.3-1	ABC	13	1085	1.5	8-6
$R$	-	RGASSI	13	1086	8.31433	-
$\gamma$	8.3-45	GAMMA	13	1087	0.45	8-6

Table 8.6-2 DEFORM-4 Input Variables (Cont'd)

Equation Variable	Reference Eq. or Section No.	SAS4A Input Variable	Location Block	Location	Suggested Value	External Reference
$A_{pg}$	8.3-44	APG	13	1088	5.0D+4	8-6
$Q_{pg}$	8.3-44	QPG	13	1089	56506.5	8-6
$G_k$	8.3-11	GK	13	1090	1.717D+10	8-11
$Q_v$	8.3-11	QV	13	1091	3.87D+5	8-11
$G$	8.3-13	GK1	13	1092	1.4556D-8	8-12
$Q$	8.3-13	QV1	13	1093	2.67D+5	8-12
$G_m$	8.3-12	GRAINK	13	1094	2.23D-3	8-12
$Q_m$	8.3-12	GRAINQ	13	1095	6.3375D+4	8-12
$C_v$	8.3-145	CVXE	13	1096	94.69	8-30
$C_v$	8.3-145	CVHE	13	1097	3.13D+3	8-30
$\delta_f$	8.3-143	ROFF	13	1098	3.30D-06	-
$\delta_c$	8.3-143	ROFC	13	1099	1.78D-06	-
Not currently used		AZEROX	13	1100	-	-
$\gamma$	8.3-145	GAMGS	13	1101	1.66	8-30
Not currently used		HARDNS	13	1102	-	-
Not currently used		ET	13	1103	1.0	8-30
$a_i$	8.3-144	ACCHE	13	1104	0.15	8-19
$a_i$	8.3-144	ACCXE	13	1105	0.85	8-19
$C_o$	8.3-146	CZERO	13	1106	1.98	8-30
$\sigma$	8.3-135	STEBOL	13	1107	5.69D-8	-
$\epsilon_f$	8.3-135	EMSF	13	1108	0.9	8-19
$\epsilon_c$	8.3-135	EMSC	13	1109	0.8	8-19
$Q_{A1}$	8.3-42	QA1	13	1110	6.92D+3	8-16
$Q_{A2}$	8.3-42	QA2	13	1111	33.95	8-16
$Q_{A3}$	8.3-43	QA3	13	1112	0.338	8-16
$Q_{A4}$	8.3-43	QA4	13	1113	1.48D+4	8-16
$Q_{A5}$	8.3-43	QA5	13	1114	9.575	8-16

Table 8.6-2 DEFORM-4 Input Variables (Cont'd)

Equation Variable	Reference Eq. or Section No.	SAS4A Input Variable	Location Block	Location	Suggested Value	External Reference
$A_\alpha$	8.3-33	ALFSS	13	1115	2.0D-04	-
$Q_\alpha/R$	8.3-33	BETSS	13	1116	1.1D+04	-
$\nu_c$	8.2	CNU	13	1117	0.3	8-17
$\nu_f$	8.2	FNU	13	1118	0.3265	8-17
Not currently used		AM	13	1119	-	-
Not currently used		QLAX	13	1120	-	-
Not currently used		QLAX2	13	1121	-	-
Not currently used		DDX	13	1122	-	-
Not currently used		DDX2	13	1123	-	-
$f_{gb}$	8.3-29	FIFNGB	13	1148	0.10	-
$f_m$	8.3-81	FNMELT	13	1169	0.30	-
$\tau_g$	8.3-107	CIRTFS	13	1170	16.67	-
$C_3$	8.7-2	COEFDL(2)	13	1201	9.3D-5	8-17
Not currently used		QSTAR	13	1202	-	-
Not currently used		ABCDU	13	1203	-	-
Not currently used		QPU	13	1204	-	-
Not currently used		DPUO	13	1205	-	-
Not currently used		TMIDFG	13	1218	-	-
Not currently used		FGSPRD	13	1219	-	-
Not currently used		FGPORX	13	1220	-	-
Not currently used		FGMIN	13	1221	-	-
Not currently used		HECOND	13	1222	1.58D-3	8-38
Not currently used		FGCOND	13	1223	7.2D-5	8-38
Not currently used		AKCOND	13	1224	0.75	8-38
$M_n$	8.3-140	HEMM	13	1225	4	-
$\dot{\epsilon}_{sfp}$	8.3-62	EPSSFP	13	1226	2.46D-3	8-17
Not currently input		HEMASX	13	1227	-	-
Not currently input		ZSWFAC	13	1228	-	-

Table 8.6-2 DEFORM-4 Input Variables (Cont'd)

Equation Variable	Reference Eq. or Section No.	SAS4A Input Variable	Location Block	Location	Suggested Value	External Reference
$A_f$	8.2-57	FAXFAL	13	1258	1.0	-
$\epsilon_{cw}$	8.3-62	FCLDWK	13	1259	-	-
Not currently used		FMELTD	13	1260	-	-
Not currently used		FSTRAN	13	1261	-	-
$f_H$	8.5-1	FTMPCH	13	1262	0.6	-
$f_a$	8.3-116	EXPCOF	13	1263	1.0	-
-	-	PRTSTR	13	1264	0.0	-
-	-	PRTDEL	13	1265	0.0	-
-	8.4.3	FIRLIM	13	1266	0.80	-
-	8.4.3	SECLIM	13	1267	0.95	-
-	8.4.3	THRLIM	13	1268	0.98	-
-	8.4.3	DTFAL1	13	1269	0.020	-
-	8.4.3	DTFAL2	13	1270	0.010	-
-	8.4.3	DTFAL3	13	1271	0.002	-
Not currently used		AKD	13	1272	-	-
Not currently used		CKD	13	1273	-	-
Not currently used		QKD	13	1274	-	-
-	8.3.6	FGFI	13	1275	-	-
-	8.7.4	IRHOK	51	3	3	-
N	8.3-27	NT	51	14	11	-
-	-	IFUELV	51	15	-	-
-	-	IFUELB	51	16	-	-
-	-	ICLADV	51	17	-	-
-	8.3.3	KTING	51	19	0	-
-	-	NAXOP	51	20	25	-
-	-	MSTEP	51	21	-	-
-	8.3.5	ITAU	51	22	0	8-17
-	8.3.5	IRATE	51	23	0	8-17

Table 8.6-2 DEFORM-4 Input Variables (Cont'd)

Equation Variable	Reference Eq. or Section No.	SAS4A Input Variable	Location Block	Location	Suggested Value	External Reference
-	8.3.8	IHGAP	51	24	1	-
$N_{pps}$	8.3-166	NPIN	51	25	-	-
$N_{spc}$	8.3-166	NSUBAS	51	26	-	-
-	8.1	MZUB	51	27	-	-
-	8.1	MZLB	51	28	-	-
-	-	FRELAX	51	30	0	-
n	8.3-11	NGRAIN	51	31	4	8-11
-	-	ISSFUE	51	32	1	-
-	-	NPLIN	51	37-44	-	-
-	-	JPRNT1	51	46	0	-
-	-	JPRNT2	51	47	0	-
-	-	NNBUG1	51	48	0	-
-	-	NNBUG2	51	49	0	-
-	-	IDBUGF	51	50	0	-
-	-	NSKIP	51	51-58	-	-
-	-	MFAIL	51	86	3	-
-	-	IFAIL	51	87	0	-
-	-	JFAIL	51	88	0	-
-	8.3.4.1	IPSIG	51	95	3	-
-	-	IHTPRS	51	96	0	-
-	-	IPRD	51	97	3	-
-	8.1	IEQMAS	51	118	1	-
-	-	ISSFU2	51	122	1	-
-	-	IHEALC	51	123	2	-
-	-	IAXTHF	51	124	1	-
A	8.3.9	AXHI	61	8-31	-	-
-	-	PLENL	61	53	-	-
-	-	RBR	61	54-77	-	-

Table 8.6-2 DEFORM-4 Input Variables (Cont'd)

Equation Variable	Reference Eq. or Section No.	SAS4A Input Variable	Location Block	Location	Suggested Value	External Reference
-	-	RER	61	78-101	-	-
-	-	RBRPL	61	102	-	-
-	-	RERPL	61	103	-	-
-	-	RINFP	61	104-127	-	-
-	-	ROUTFP	61	128-151	-	-
-	-	RBR0	61	180	-	-
-	-	RER0	61	181	-	-
-	-	PSHAPE	62	6-29	-	-
S	8.3-27	PSHAPR	62	30-44	-	-
-	-	PLIN	62	45-52	-	-
-	-	TPLIN	62	53-60	-	-
-	-	FLTPOW	62	61	-	-
-	8.3.9	FUELRA	62	208-231	-	-
A	8.3-152	AHBPAP	63	2	0.0	8-22
B	8.3-152	BHBPAP	63	3	0.0	8-22
C	8.3-152	CHBPAP	63	4	0.0	8-22
-	8.3.8	HBMAX	63	5	4.0D+4	8-22
-	8.3.8	HBMIN	63	6	1.0D+2	-
H	8.3-152, 153	HBPAR	63	7	0.0	-
D <sub>o</sub>	8.3-21	DGO	63	26	1.0D-5	-
P <sub>ogas</sub>	8.3-6	POGAS	63	27	-	-
		FCLOP	63	68	-	-
T <sub>s1</sub>	8.5-2	TSEP1	63	69	2.2D+3	-
T <sub>s2</sub>	8.5-2	TSEP2	63	70	1.0D-8	-
		BONDNA	63	71	-	-
		REFDEN	63	72	-	-
-	8.4	FSPEC	65	1	-	-
-	8.4	FMELTM	65	2	0.20	-

### 8.6.3 Output Specific to DEFORM-4

Figures 8.6-1 through 8.6-13 show a sample of the output generated by DEFORM-4. This sample is for a section of pre-transient output, but the same output is generated in the transient case. What follows is a very brief discussion of the output format for each page.

Figure 8.6-1

The standard SAS4A coolant temperature/pressure summary.

Figure 8.6-2

Fuel node boundary locations and cell temperatures. Radial and axial node numbers are shown. Under "IZ" is the node number of the first non-molten cell. Under "IETA" is the node number of the last solid, i.e., uncracked, cell. Therefore, IZ to IETA defines the extent of the solid annular fuel region.

Figure 8.6-3

Fuel/cladding summary information is presented. The titles are self explanatory except for the third one in the bottom section. This column shows the ratio of the calculated gap conductance to that used for the next timestep thermal calculation. Since there is no iteration between the DEFORM-4 mechanics calculation and the SAS4A thermal calculation, a scheme has been employed to avoid gross oscillations in the gap conductances and temperatures. This is to use the average of the calculated and previously used gap conductance for the next time step. In order to determine how close the values are to those calculated, this ratio is printed.

Figure 8.6-4

The radial stress at each fuel and cladding node. Also printed is the fuel-cladding gap, GAP, the fuel-cladding interface pressure, PFCI, and the coolant pressure, PEXT. All stresses and pressures are in pascal and the gap is in meters.

Figure 8.6-5

The circumferential stress at each fuel and clad node boundary, in pascal.

Figure 8.6-6

The axial stress at each fuel and clad node boundary in pascal.

Figure 8.6-7

The fission-gas retention fraction in each fuel cell. The column titled 'FG RET (KG)' is the retained fission-gas total in kg, 'FG PRD (KG)' is the total kg of fission gas produced, 'M-FG/M-FUEL' is the kg of fission gas retained divided by the mass of fuel, 'FRAC RELS' is the fractional release, and 'NUET/M2' is the fluence, for each axial segment.

Figure 8.6-8

The total porosity fraction in the fuel cells, i.e., retained fission-gas porosity plus remaining as-fabricated porosity.

Figure 8.6-9

The fission-gas-induced porosity in each fuel cell.

Figure 8.6-10

The grain size in each fuel cell, in meters.

Figure 8.6-11

The crack volume fraction in each fuel cell.

Figure 8.6-12

Mesh points in the fuel and the inner and outer clad dimensions. Also shown are the boundaries between the unrestructured and equiaxed region, IUNEQA, and between the equiaxed and columnar regions, IEQCOL.

Figure 8.6-13

Short summary output from DEFORM-4 showing the values calculated for various failure parameters. The hoop stress values are a simple average based on the inner and outer pressures and thickness of the clad.

If a failure criterion has a value greater than 1.0, then that criterion predicts failure. Currently, only the MFAIL parameters are used to automatically initiate failure of the pin.

The amount of output can be controlled through the use of NSKIP and IPRD in block 51 of the input. In the transient state the output from DEFORM-4 is printed at the end of a heat-transfer time step, as controlled by IPO and IPOBOI.

## 8.7 Material Properties

All material property data are cast as functions or subroutines to allow for modularization and ease of making changes. This also allows for the incorporation of different materials data in a straightforward manner. In a number of the correlations used, the units are inconsistent with the SI unit system adopted by SAS4A. The routines that use these correlations carry out appropriate units conversions internally.

### 8.7.1 Mixed Oxide Fuel Density

The solid fuel density is assumed to have the functional form

$$\rho_f = \frac{\rho_o}{1 + C_1(T-273) + C_2(T-273)^2} \quad (8.7-1)$$

\*\*\* STEADY STATE \*\*\*

FLOWRATE (KG/S) 0.1336690

COOLANT PROFILE

AXIAL LOCATION ( M )	COOLANT TEMPERATURE ( K )	SATURATION TEMPERATURE ( K )	PRESSURE ( MPA )
VESSEL OUTLET			0.1526
2.99720	817.973	1206.415	0.1526
2.78130	817.973	1231.720	0.1873
2.56540	817.973	1253.546	0.2221
2.34950	817.973	1272.830	0.2568
2.13360	817.973	1290.166	0.2916
1.93040	817.973	1305.067	0.3243
1.72720	817.973	1318.840	0.3570
1.64254	817.693	1324.617	0.3714
1.55787	817.245	1330.223	0.3859
1.47320	816.527	1335.671	0.4003
1.42240	815.604	1338.869	0.4090
1.37160	814.378	1342.017	0.4177
1.30387	806.591	1346.168	0.4294
1.23614	797.065	1350.239	0.4411
1.16840	785.948	1354.263	0.4529
1.10067	773.836	1358.212	0.4647
1.03294	760.735	1362.087	0.4765
0.96520	746.886	1365.887	0.4883
0.89747	732.732	1369.613	0.5001
0.82973	718.434	1373.270	0.5119
0.76200	704.246	1376.862	0.5237
0.69427	690.342	1380.390	0.5354
0.62653	677.144	1383.853	0.5472
0.55880	664.883	1387.255	0.5589
0.49107	653.529	1390.597	0.5706
0.42333	643.629	1393.878	0.5823
0.35560	635.284	1397.102	0.5940
0.30480	633.788	1399.472	0.6027
0.25400	632.586	1401.816	0.6113
0.12700	631.055	1407.562	0.6330
0.00000	630.150	1413.159	0.6547
-0.16933	630.150	1420.156	0.6826
-0.33867	630.150	1426.940	0.7105
-0.50800	630.150	1433.525	0.7384
-0.67733	630.150	1439.924	0.7663
-0.84667	630.150	1446.151	0.7942
-1.01600	630.150	1452.214	0.8221
-1.24460	630.150	1460.159	0.8597
-1.47320	630.150	1467.847	0.8974
-1.70180	630.150	1475.297	0.9351
VESSEL INLET			0.9351

8-152

Fig. 8.6-1. SAS4A Steady-state Coolant Condition Output

AXIAL LOCATION ( M )	RADIAL FUEL TEMPERATURE MESH ( K )										
	1	2	3	4	5	6	7	8	9	10	11
1.68487	919.938	918.387	916.838	915.292	913.748	912.207	910.667	909.130	907.595	906.063	904.533
1.60020	974.584	971.982	969.385	966.795	964.211	961.632	959.060	956.494	953.934	951.380	948.832
1.51554	1056.018	1051.545	1047.089	1042.649	1038.225	1033.817	1029.426	1025.051	1020.692	1016.349	1012.023
1.44780	1268.195	1257.046	1245.973	1234.975	1224.049	1213.190	1202.400	1191.689	1181.058	1170.507	1160.039
1.39700	1378.112	1362.331	1346.674	1331.131	1315.664	1300.284	1285.036	1269.945	1255.042	1240.306	1225.709
1.33774	1992.826	1953.113	1895.702	1833.187	1765.621	1690.942	1608.179	1521.167	1435.302	1353.289	1275.610
1.27000	1897.194	1856.771	1793.062	1720.878	1643.399	1556.907	1459.309	1357.685	1260.613	1170.430	1087.026
1.20227	2000.403	1954.640	1881.257	1797.141	1707.806	1608.194	1492.694	1371.410	1257.044	1152.386	1057.565
1.13454	2072.057	2022.771	1944.006	1853.988	1758.661	1653.148	1527.902	1393.572	1266.755	1151.276	1047.883
1.06680	2128.644	2076.085	1991.918	1895.951	1794.430	1684.888	1553.904	1408.759	1270.104	1144.294	1032.849
0.99907	2154.229	2099.197	2010.880	1910.265	1803.921	1691.239	1557.123	1405.786	1259.788	1127.792	1011.713
0.93133	2152.705	2096.253	2005.882	1903.118	1794.671	1679.878	1543.230	1389.485	1241.894	1109.036	992.606
0.86360	2145.721	2088.237	1996.582	1892.577	1782.999	1666.373	1527.196	1372.031	1224.462	1092.228	976.611
0.79587	2124.080	2065.937	1974.092	1870.306	1761.253	1642.634	1500.723	1346.671	1202.545	1073.893	961.359
0.72813	2092.632	2034.383	1943.352	1840.952	1733.586	1612.910	1469.283	1319.012	1180.377	1056.930	948.659
0.66040	2038.440	1981.046	1892.933	1794.371	1689.212	1565.772	1423.945	1283.620	1155.522	1041.365	940.428
0.59267	1957.616	1902.173	1818.608	1725.203	1621.401	1497.796	1364.154	1238.188	1123.800	1021.297	929.573
0.52493	1870.819	1816.410	1736.540	1646.934	1544.664	1426.674	1305.507	1193.335	1091.446	999.406	916.173
0.45720	1773.812	1717.565	1641.100	1556.645	1461.874	1358.456	1256.271	1161.448	1074.356	994.508	921.355
0.38947	1861.437	1796.060	1720.881	1640.102	1551.913	1459.418	1368.681	1282.924	1202.534	1127.278	1057.094
0.33020	1353.173	1334.003	1315.031	1296.250	1277.643	1259.169	1240.870	1222.822	1205.015	1187.433	1170.077
0.27940	1252.789	1238.265	1223.874	1209.615	1195.484	1181.479	1167.590	1153.827	1140.209	1126.740	1113.414
0.19050	1006.549	1000.387	994.258	988.163	982.099	976.069	970.070	964.105	958.171	952.270	946.400
0.06350	875.822	872.593	869.374	866.165	862.967	859.779	856.602	853.435	850.278	847.132	843.996

FUEL NODE	RADIAL FUEL MESH (CM)													
	1	2	3	4	5	6	7	8	9	10	11	12	IZ	IETA
24	0.0001	0.0671	0.1162	0.1500	0.1775	0.2013	0.2225	0.2419	0.2598	0.2766	0.2924	0.3000	1	12
23	0.0001	0.0671	0.1163	0.1501	0.1776	0.2014	0.2226	0.2420	0.2600	0.2768	0.2926	0.3002	1	12
22	0.0001	0.0672	0.1164	0.1503	0.1778	0.2016	0.2229	0.2423	0.2602	0.2770	0.2929	0.3005	1	12
21	0.0001	0.0674	0.1168	0.1507	0.1783	0.2022	0.2235	0.2430	0.2610	0.2779	0.2938	0.3014	1	11
20	0.0001	0.0675	0.1170	0.1510	0.1787	0.2026	0.2240	0.2435	0.2616	0.2785	0.2944	0.3020	1	8
19	0.0624	0.0907	0.1304	0.1602	0.1854	0.2080	0.2290	0.2488	0.2672	0.2844	0.3006	0.3083	1	2
18	0.0689	0.0947	0.1321	0.1614	0.1863	0.2086	0.2296	0.2495	0.2679	0.2851	0.3013	0.3090	1	2
17	0.0711	0.0964	0.1332	0.1624	0.1871	0.2091	0.2300	0.2499	0.2684	0.2857	0.3018	0.3095	1	2
16	0.0722	0.0973	0.1340	0.1628	0.1873	0.2091	0.2298	0.2497	0.2683	0.2856	0.3018	0.3095	1	2
15	0.0733	0.0982	0.1347	0.1634	0.1877	0.2093	0.2296	0.2495	0.2681	0.2855	0.3017	0.3095	1	2
14	0.0740	0.0988	0.1352	0.1637	0.1880	0.2095	0.2295	0.2493	0.2679	0.2853	0.3016	0.3093	1	2
13	0.0738	0.0986	0.1351	0.1636	0.1879	0.2094	0.2294	0.2492	0.2678	0.2852	0.3014	0.3092	1	2
12	0.0733	0.0983	0.1348	0.1634	0.1876	0.2092	0.2293	0.2491	0.2677	0.2851	0.3014	0.3091	1	2
11	0.0721	0.0973	0.1341	0.1628	0.1871	0.2087	0.2291	0.2491	0.2677	0.2851	0.3013	0.3090	1	2
10	0.0707	0.0963	0.1333	0.1621	0.1865	0.2082	0.2290	0.2491	0.2677	0.2850	0.3011	0.3088	1	2
9	0.0681	0.0944	0.1319	0.1609	0.1855	0.2076	0.2290	0.2491	0.2676	0.2849	0.3010	0.3087	1	2
8	0.0651	0.0921	0.1301	0.1595	0.1845	0.2074	0.2292	0.2492	0.2677	0.2848	0.3009	0.3085	1	2
7	0.0615	0.0895	0.1285	0.1584	0.1839	0.2074	0.2293	0.2493	0.2677	0.2847	0.3007	0.3084	1	2
6	0.0528	0.0844	0.1259	0.1570	0.1834	0.2074	0.2293	0.2492	0.2675	0.2845	0.3005	0.3082	1	2
5	0.0397	0.0788	0.1233	0.1555	0.1827	0.2069	0.2287	0.2486	0.2669	0.2840	0.3000	0.3077	1	2
4	0.0001	0.0675	0.1170	0.1510	0.1787	0.2026	0.2240	0.2435	0.2616	0.2785	0.2944	0.3020	1	7
3	0.0001	0.0674	0.1168	0.1508	0.1784	0.2023	0.2236	0.2431	0.2611	0.2779	0.2938	0.3014	1	9
2	0.0001	0.0672	0.1164	0.1502	0.1778	0.2015	0.2228	0.2422	0.2602	0.2770	0.2928	0.3004	1	12
1	0.0001	0.0671	0.1162	0.1500	0.1775	0.2012	0.2225	0.2418	0.2598	0.2765	0.2923	0.2999	1	12

Fig. 8.6-2. SAS4A Fuel Temperature and Node Location Map

8-153

AXIAL LOCATION ( M )	CLAD TEMPERATURES ( K )			AVERAGE COOLANT TEMPERATURE ( K )	STRUCTURE TEMPERATURE ( K )		AVERAGE FUEL TEMPERATURE ( K )	RADIAL LOCATION ( CM )			
	INNER	MIDPOINT	OUTER		INNER	OUTER		INNER FUEL	OUTER FUEL	INNER CLAD	OUTER CLAD
1.685	818.549	818.267	818.006	817.833	817.903	817.962	912.216	0.0001	0.3000	0.3090	0.3654
1.600	818.612	818.161	817.744	817.469	817.580	817.675	961.658	0.0001	0.3002	0.3090	0.3654
1.516	818.719	817.996	817.328	816.886	817.065	817.216	1033.886	0.0001	0.3005	0.3090	0.3654
1.448	819.992	818.444	817.011	816.066	816.448	816.772	1213.500	0.0001	0.3014	0.3090	0.3654
1.397	820.206	818.149	816.246	814.991	815.498	815.929	1300.832	0.0001	0.3020	0.3090	0.3654
1.338	835.290	825.508	816.447	810.484	812.900	814.954	1669.072	0.0624	0.3083	0.3091	0.3655
1.270	832.169	820.193	809.095	801.828	804.782	807.295	1531.116	0.0689	0.3090	0.3090	0.3655
1.202	826.827	812.870	799.930	791.506	794.953	797.887	1575.156	0.0711	0.3095	0.3095	0.3659
1.135	818.376	803.146	789.023	779.892	783.645	786.843	1613.205	0.0722	0.3095	0.3095	0.3658
1.067	808.933	792.423	777.111	767.285	771.344	774.805	1640.108	0.0733	0.3095	0.3095	0.3658
0.999	797.885	780.382	764.144	753.811	758.100	761.761	1644.896	0.0740	0.3093	0.3093	0.3656
0.931	784.919	766.971	750.315	739.809	744.192	747.937	1633.610	0.0738	0.3092	0.3092	0.3655
0.864	771.211	753.021	736.137	725.583	730.009	733.796	1620.385	0.0733	0.3091	0.3091	0.3654
0.796	756.686	738.571	721.755	711.340	715.732	719.492	1598.077	0.0721	0.3090	0.3090	0.3653
0.728	741.813	723.991	707.449	697.294	701.598	705.287	1571.143	0.0707	0.3088	0.3088	0.3651
0.660	726.085	709.099	693.336	683.743	687.829	691.333	1531.722	0.0681	0.3087	0.3087	0.3649
0.593	710.427	694.585	679.886	671.014	674.810	678.068	1475.621	0.0651	0.3085	0.3085	0.3648
0.525	695.777	681.049	667.389	659.206	662.722	665.742	1415.441	0.0615	0.3084	0.3084	0.3646
0.457	680.538	667.644	655.692	648.579	651.645	654.281	1356.981	0.0528	0.3082	0.3082	0.3644
0.389	666.438	655.536	645.434	639.456	642.041	644.265	1460.906	0.0397	0.3077	0.3080	0.3642
0.330	640.996	638.382	635.962	634.536	635.154	635.685	1259.986	0.0001	0.3020	0.3079	0.3641
0.279	638.382	636.279	634.333	633.187	633.684	634.111	1182.018	0.0001	0.3014	0.3079	0.3641
0.191	634.467	633.395	632.404	631.820	632.073	632.291	976.207	0.0001	0.3004	0.3079	0.3641
0.064	632.168	631.534	630.947	630.602	630.752	630.881	859.823	0.0001	0.2999	0.3079	0.3641

AXIAL FUEL NODE	FUEL-CLAD GAP		C/U RATIO	LENGTH (M)	ELEV (M)	MASS (KG)	POWER (W)	LINEAR POWER (KW/M)	LINEAR POWER (KW/FT)	BURNUP (A %)	BURNUP (MWD/MT)	FLUENCE (N/CM2)
	CONDUCTANCE W/(M**2-K)	HGAP										
24	3.35731D+02	0.99571	0.08467	1.6849	2.2764D-02	4.7408D+01	5.5994D-01	1.7067D-01	0.143	1.3714D+03	2.3729D+19	
23	3.53776D+02	0.99599	0.08467	1.6002	2.2764D-02	7.5683D+01	8.9389D-01	2.7246D-01	0.229	2.1893D+03	3.7866D+19	
22	3.82014D+02	0.99614	0.08467	1.5155	2.2764D-02	1.2141D+02	1.4340D+00	4.3708D-01	0.367	3.5122D+03	6.0709D+19	
21	4.64418D+02	0.99722	0.05080	1.4478	1.3659D-02	1.5608D+02	3.0725D+00	9.3649D-01	0.786	7.5252D+03	1.2986D+20	
20	5.16480D+02	0.99774	0.05080	1.3970	1.3659D-02	2.0731D+02	4.0810D+00	1.2439D+00	1.045	9.9953D+03	1.7233D+20	
19	2.23063D+03	1.00274	0.06773	1.3377	1.8211D-02	1.3169D+03	1.9442D+01	5.9258D+00	4.976	4.7617D+04	8.1574D+20	
18	4.76914D+03	1.01598	0.06773	1.2700	1.8211D-02	1.6113D+03	2.3789D+01	7.2510D+00	6.089	5.8265D+04	9.9844D+20	
17	6.03762D+03	0.99934	0.06773	1.2023	1.8211D-02	1.8814D+03	2.7777D+01	8.4664D+00	7.109	6.8032D+04	1.1660D+21	
16	6.61786D+03	0.99955	0.06773	1.1345	1.8211D-02	2.0508D+03	3.0277D+01	9.2284D+00	7.749	7.4155D+04	1.2708D+21	
15	7.35372D+03	1.00106	0.06773	1.0668	1.8211D-02	2.2194D+03	3.2767D+01	9.9875D+00	8.387	8.0254D+04	1.3751D+21	
14	8.16626D+03	1.00312	0.06773	0.9991	1.8211D-02	2.3477D+03	3.4661D+01	1.0565D+01	8.871	8.4893D+04	1.4545D+21	
13	8.61735D+03	1.00467	0.06773	0.9313	1.8211D-02	2.4014D+03	3.5454D+01	1.0806D+01	9.074	8.6834D+04	1.4878D+21	
12	8.82084D+03	1.00571	0.06773	0.8636	1.8211D-02	2.4277D+03	3.5842D+01	1.0925D+01	9.174	8.7785D+04	1.5043D+21	
11	8.79815D+03	1.00614	0.06773	0.7959	1.8211D-02	2.4110D+03	3.5596D+01	1.0850D+01	9.111	8.7183D+04	1.4943D+21	
10	8.54499D+03	1.00635	0.06773	0.7281	1.8211D-02	2.3650D+03	3.4917D+01	1.0643D+01	8.937	8.1520D+04	1.4662D+21	
9	7.83035D+03	1.00534	0.06773	0.6604	1.8211D-02	2.2469D+03	3.3173D+01	1.0111D+01	8.490	8.1248D+04	1.3934D+21	
8	7.11295D+03	1.00369	0.06773	0.5927	1.8211D-02	2.0893D+03	3.0847D+01	9.4020D+00	7.895	7.5550D+04	1.2961D+21	
7	6.55780D+03	1.00358	0.06773	0.5249	1.8211D-02	1.9365D+03	2.8590D+01	8.7142D+00	7.317	7.0023D+04	1.2016D+21	
6	5.27962D+03	1.01079	0.06773	0.4572	1.8211D-02	1.6900D+03	2.4950D+01	7.6049D+00	6.386	6.1109D+04	1.0487D+21	
5	2.74499D+03	1.00916	0.06773	0.3895	1.8211D-02	1.4255D+03	2.1046D+01	6.4149D+00	5.387	5.1547D+04	8.8471D+20	
4	4.88023D+02	0.99786	0.05080	0.3302	1.3659D-02	2.5555D+02	5.0305D+00	1.5333D+00	1.288	1.2321D+04	2.1269D+20	
3	4.37721D+02	0.99747	0.05080	0.2794	1.3659D-02	2.0549D+02	4.0451D+00	1.2330D+00	1.035	9.9074D+03	1.7117D+20	
2	3.40364D+02	0.99648	0.12700	0.1905	3.4146D-02	2.6167D+02	2.0604D+00	6.2800D-01	0.527	5.0463D+03	8.7335D+19	
1	2.96597D+02	0.99588	0.12700	0.0635	3.4146D-02	1.5470D+02	1.2181D+00	3.7128D-01	0.312	2.9835D+03	5.1677D+19	

Fig. 8.6-3. SAAS4A Fuel-pin Condition Summary Output

8-154

\*\*\* STEADY STATE TIME (SEC,HRS) = 5.04576D+07 1.40160D+04 \*\*\*

NODE	ELEVATION (M)	RADIAL STRESSES - SIGR - PA								
		1	2	3	4	5	6	7	8	9
24	1.70318	-2.6343D+06	-8.5459D+06	-7.9197D+06	-7.2943D+06	-6.6698D+06	-6.0463D+06	-5.4237D+06	-4.8022D+06	-4.1816D+06
23	1.61805	-2.6343D+06	-1.2796D+07	-1.1716D+07	-1.0637D+07	-9.5615D+06	-8.4884D+06	-7.4181D+06	-6.3504D+06	-5.2853D+06
22	1.53285	-2.6343D+06	-2.0693D+07	-1.8761D+07	-1.6836D+07	-1.4918D+07	-1.3007D+07	-1.1104D+07	-9.2089D+06	-7.3211D+06
21	1.46462	-2.6343D+06	-4.8788D+07	-4.3503D+07	-3.8254D+07	-3.3045D+07	-2.7877D+07	-2.2748D+07	-1.7659D+07	-1.2610D+07
20	1.41335	-2.6343D+06	-4.8471D+07	-4.0664D+07	-3.2920D+07	-2.5248D+07	-1.7642D+07	-1.0103D+07	-2.6343D+06	-2.6343D+06
19	1.35332	-2.6343D+06	-2.6343D+06	-2.6343D+06	-2.6343D+06	-2.6343D+06	-2.6343D+06	-2.6343D+06	-2.6343D+06	-2.6343D+06
18	1.28463	-2.6343D+06	-2.6343D+06	-2.6343D+06	-2.6343D+06	-2.6343D+06	-2.6343D+06	-2.6343D+06	-2.6343D+06	-2.6343D+06
17	1.21598	-2.6343D+06	-2.2050D+07	-1.6685D+07	-1.4162D+07	-1.2638D+07	-1.1583D+07	-1.0770D+07	-1.0122D+07	-9.6064D+06
16	1.14730	-2.6343D+06	-3.8150D+07	-2.8429D+07	-2.3860D+07	-2.1081D+07	-1.9159D+07	-1.7672D+07	-1.6470D+07	-1.5513D+07
15	1.07858	-2.6343D+06	-5.9458D+07	-4.4046D+07	-3.6786D+07	-3.2353D+07	-2.9285D+07	-2.6929D+07	-2.4991D+07	-2.3440D+07
14	1.00985	-2.6343D+06	-8.3686D+07	-6.1834D+07	-5.1515D+07	-4.5203D+07	-4.0830D+07	-3.7497D+07	-3.4727D+07	-3.2497D+07
13	0.94112	-2.6343D+06	-9.8688D+07	-7.2745D+07	-6.0519D+07	-5.3043D+07	-4.7865D+07	-4.3917D+07	-4.0633D+07	-3.7994D+07
12	0.87239	-2.6343D+06	-1.0721D+08	-7.8847D+07	-6.5521D+07	-5.7383D+07	-5.1752D+07	-4.7440D+07	-4.3866D+07	-4.1000D+07
11	0.80369	-2.6343D+06	-1.1038D+08	-8.0825D+07	-6.7055D+07	-5.8674D+07	-5.2884D+07	-4.8399D+07	-4.4729D+07	-4.1803D+07
10	0.73500	-2.6343D+06	-1.0727D+08	-7.8189D+07	-6.4768D+07	-5.6631D+07	-5.1018D+07	-4.6609D+07	-4.3070D+07	-4.0263D+07
9	0.66633	-2.6343D+06	-9.1078D+07	-6.5919D+07	-5.4491D+07	-4.7611D+07	-4.2818D+07	-3.9058D+07	-3.6125D+07	-3.3806D+07
8	0.59769	-2.6343D+06	-7.3833D+07	-5.3028D+07	-4.3738D+07	-3.8181D+07	-3.4252D+07	-3.1243D+07	-2.8944D+07	-2.7130D+07
7	0.52908	-2.6343D+06	-6.1019D+07	-4.3282D+07	-3.5616D+07	-3.1035D+07	-2.7814D+07	-2.5411D+07	-2.3588D+07	-2.2150D+07
6	0.46051	-2.6343D+06	-2.4708D+07	-1.7434D+07	-1.4505D+07	-1.2795D+07	-1.1621D+07	-1.0764D+07	-1.0115D+07	-9.6029D+06
5	0.39194	-2.6343D+06	-2.6343D+06	-2.6343D+06	-2.6343D+06	-2.6343D+06	-2.6343D+06	-2.6343D+06	-2.6343D+06	-2.6343D+06
4	0.33203	-2.6343D+06	-4.8579D+07	-3.9178D+07	-2.9878D+07	-2.0689D+07	-1.1610D+07	-2.6343D+06	-2.6343D+06	-2.6343D+06
3	0.28082	-2.6343D+06	-4.9168D+07	-4.2318D+07	-3.5530D+07	-2.8813D+07	-2.2166D+07	-1.5587D+07	-9.0770D+06	-2.6343D+06
2	0.19139	-2.6343D+06	-2.6802D+07	-2.4198D+07	-2.1607D+07	-1.9030D+07	-1.6467D+07	-1.3920D+07	-1.1387D+07	-8.8681D+06
1	0.06378	-2.6343D+06	-1.4599D+07	-1.3322D+07	-1.2049D+07	-1.0780D+07	-9.5149D+06	-8.2543D+06	-6.9980D+06	-5.7460D+06

NODE	(M)	10	11	12	13	14	15	GAP	PFCI	PEXT
		24	1.70318	-3.5619D+06	-2.9433D+06	-2.6343D+06	-2.6343D+06	-1.4767D+06	-4.8080D+05	9.0104D-05
23	1.61805	-4.2229D+06	-3.1632D+06	-2.6343D+06	-2.6343D+06	-1.5153D+06	-4.9241D+05	8.8267D-05	-2.6343D+06	3.7865D+05
22	1.53285	-5.4408D+06	-3.5680D+06	-2.6343D+06	-2.6343D+06	-1.5739D+06	-5.0402D+05	8.5360D-05	-2.6343D+06	3.9310D+05
21	1.46462	-7.6018D+06	-2.6343D+06	-2.6343D+06	-2.6343D+06	-1.7381D+06	-5.1563D+05	7.6460D-05	-2.6343D+06	4.0467D+05
20	1.41335	-2.6343D+06	-2.6343D+06	-2.6343D+06	-2.6343D+06	-1.8417D+06	-5.2724D+05	7.0105D-05	-2.6343D+06	4.1336D+05
19	1.35332	-2.6343D+06	-2.6343D+06	-2.6343D+06	-2.6343D+06	-3.3231D+06	-5.3889D+05	7.5047D-06	-2.6343D+06	4.2354D+05
18	1.28463	-2.6343D+06	-2.6343D+06	-2.6343D+06	-2.6343D+06	-3.7505D+06	-5.5061D+05	4.9918D-07	-2.6343D+06	4.3521D+05
17	1.21598	-9.1859D+06	-8.8355D+06	-8.6812D+06	-8.6812D+06	-6.7844D+06	-5.6238D+05	0.0000D+00	-8.6812D+06	4.4695D+05
16	1.14730	-1.4733D+07	-1.4084D+07	-1.3799D+07	-1.3799D+07	-9.2769D+06	-5.7422D+05	0.0000D+00	-1.3799D+07	4.5875D+05
15	1.07858	-2.2174D+07	-2.1122D+07	-2.0660D+07	-2.0660D+07	-1.2534D+07	-5.8606D+05	0.0000D+00	-2.0660D+07	4.7057D+05
14	1.00985	-3.0677D+07	-2.9165D+07	-2.8502D+07	-2.8502D+07	-1.6164D+07	-5.9645D+05	0.0000D+00	-2.8502D+07	4.8238D+05
13	0.94112	-3.5839D+07	-3.4050D+07	-3.3265D+07	-3.3265D+07	-1.8341D+07	-6.0538D+05	0.0000D+00	-3.3265D+07	4.9418D+05
12	0.87239	-3.8663D+07	-3.6723D+07	-3.5872D+07	-3.5872D+07	-1.9539D+07	-6.2079D+05	0.0000D+00	-3.5872D+07	5.0597D+05
11	0.80369	-3.9419D+07	-3.7441D+07	-3.6573D+07	-3.6573D+07	-1.9845D+07	-6.4270D+05	0.0000D+00	-3.6573D+07	5.1776D+05
10	0.73500	-3.7978D+07	-3.6081D+07	-3.5248D+07	-3.5248D+07	-1.9224D+07	-6.6771D+05	0.0000D+00	-3.5248D+07	5.2954D+05
9	0.66633	-3.1920D+07	-3.0353D+07	-2.9664D+07	-2.9664D+07	-1.6635D+07	-6.9582D+05	0.0000D+00	-2.9664D+07	5.4130D+05
8	0.59769	-2.5655D+07	-2.4428D+07	-2.3887D+07	-2.3887D+07	-1.3902D+07	-7.2390D+05	0.0000D+00	-2.3887D+07	5.5305D+05
7	0.52908	-2.0979D+07	-2.0004D+07	-1.9574D+07	-1.9574D+07	-1.1814D+07	-7.5197D+05	0.0000D+00	-1.9574D+07	5.6478D+05
6	0.46051	-9.1854D+06	-8.8368D+06	-8.6830D+06	-8.6830D+06	-6.7106D+06	-7.8001D+05	0.0000D+00	-8.6830D+06	5.7648D+05
5	0.39194	-2.6343D+06	-2.6343D+06	-2.6343D+06	-2.6343D+06	-3.6958D+06	-8.0801D+05	3.1913D-06	-2.6343D+06	5.8815D+05
4	0.33203	-2.6343D+06	-2.6343D+06	-2.6343D+06	-2.6343D+06	-2.1250D+06	-8.4085D+05	5.9128D-05	-2.6343D+06	5.9832D+05
3	0.28082	-2.6343D+06	-2.6343D+06	-2.6343D+06	-2.6343D+06	-2.0483D+06	-8.7852D+05	6.4626D-05	-2.6343D+06	6.0701D+05
2	0.19139	-6.3639D+06	-3.8741D+06	-2.6343D+06	-2.6343D+06	-1.8724D+06	-9.1620D+05	7.4914D-05	-2.6343D+06	6.2219D+05
1	0.06378	-4.4982D+06	-3.2546D+06	-2.6343D+06	-2.6343D+06	-1.5362D+06	-4.6731D+05	7.9379D-05	-2.6343D+06	6.4388D+05

Fig. 8.6-4. DEFORM-4 Radial Stress Map

8-155

\*\*\* STEADY STATE TIME (SEC,HRS) = 5.04576D+07 1.40160D+04 \*\*\*

NODE	ELEVATION (M)	CIRCUMFERENTIAL STRESSES - SIGC - PA								
		1	2	3	4	5	6	7	8	9
24	1.70318	-1.5084D+07	-7.9191D+06	-6.0415D+06	-4.1689D+06	-2.3012D+06	-4.3835D+05	1.4196D+06	3.2728D+06	5.1212D+06
23	1.61805	-2.4040D+07	-1.1714D+07	-8.4753D+06	-5.2506D+06	-2.0392D+06	1.1587D+06	4.3435D+06	7.5149D+06	1.0673D+07
22	1.53285	-4.0688D+07	-1.8756D+07	-1.2970D+07	-7.2224D+06	-1.5131D+06	4.1583D+06	9.7923D+06	1.5389D+07	2.0948D+07
21	1.46462	-1.0025D+08	-4.3477D+07	-2.7673D+07	-1.2083D+07	3.3007D+06	1.8490D+07	3.3487D+07	4.8283D+07	6.2872D+07
20	1.41335	-1.0216D+08	-4.0616D+07	-1.7288D+07	5.6521D+06	2.8262D+07	5.0564D+07	7.2511D+07	9.4047D+07	-2.6343D+06
19	1.35332	-2.7797D+07	2.2532D+07	-2.6343D+06						
18	1.28463	-2.5393D+07	2.0125D+07	-2.6343D+06						
17	1.21598	-1.1311D+08	-4.2562D+07	-2.6343D+06						
16	1.14730	-1.8672D+08	-9.5993D+07	-2.6343D+06						
15	1.07858	-2.8333D+08	-1.7014D+08	-2.6343D+06						
14	1.00985	-3.9417D+08	-2.5488D+08	-2.6343D+06						
13	0.94112	-4.6143D+08	-3.0510D+08	-2.6343D+06						
12	0.87239	-4.9711D+08	-3.3135D+08	-2.6343D+06						
11	0.80369	-5.0305D+08	-3.3477D+08	-2.6343D+06						
10	0.73500	-4.7986D+08	-3.1508D+08	-2.6343D+06						
9	0.66633	-3.9935D+08	-2.4961D+08	-2.6343D+06						
8	0.59769	-3.1566D+08	-1.8540D+08	-2.6343D+06						
7	0.52908	-2.5164D+08	-1.3555D+08	-2.6343D+06						
6	0.46051	-1.0580D+08	-2.2383D+07	-2.6343D+06						
5	0.39194	-4.1093D+07	3.5825D+07	-2.6343D+06						
4	0.33203	-1.0400D+08	-3.9105D+07	-1.1047D+07	-1.6411D+07	4.3313D+07	6.9717D+07	9.5626D+07	-2.6343D+06	-2.6343D+06
3	0.28082	-1.0260D+08	-4.2274D+07	-2.1813D+07	-1.7245D+06	1.8009D+07	3.7400D+07	5.6461D+07	7.5196D+07	9.3583D+07
2	0.19139	-5.3583D+07	-2.4189D+07	-1.6395D+07	-8.6769D+06	-1.0331D+06	6.5376D+06	1.4036D+07	2.1462D+07	2.8818D+07
1	0.06378	-2.7843D+07	-1.3320D+07	-9.4938D+06	-5.6903D+06	-1.9083D+06	1.8523D+06	5.5916D+06	9.3099D+06	1.3007D+07

NODE	(M)	10	11	12	13	14	15
		24	1.70318	6.9647D+06	8.8035D+06	9.7215D+06	1.1139D+07
23	1.61805	1.3818D+07	1.6950D+07	1.8513D+07	1.0256D+07	1.1279D+07	1.2236D+07
22	1.53285	2.6470D+07	3.1955D+07	3.4688D+07	8.8793D+06	1.1254D+07	1.3361D+07
21	1.46462	7.7254D+07	9.1431D+07	-2.6343D+06	4.8685D+06	1.1331D+07	1.6916D+07
20	1.41335	-2.6343D+06	-2.6343D+06	-2.6343D+06	2.3674D+06	1.1350D+07	1.9077D+07
19	1.35332	-2.6343D+06	-2.6343D+06	-2.6343D+06	-3.4469D+07	1.2704D+07	5.2899D+07
18	1.28463	-2.6343D+06	-2.6343D+06	-2.6343D+06	-4.5042D+07	1.3038D+07	6.2498D+07
17	1.21598	-2.6343D+06	-2.6343D+06	-2.6343D+06	-1.8175D+07	4.6389D+07	1.0161D+08
16	1.14730	-2.6343D+06	-2.6343D+06	-2.6343D+06	6.4475D+06	7.4536D+07	1.3295D+08
15	1.07858	-2.6343D+06	-2.6343D+06	-2.6343D+06	4.1522D+07	1.1220D+08	1.7307D+08
14	1.00985	-2.6343D+06	-2.6343D+06	-2.6343D+06	8.3826D+07	1.5512D+08	2.1683D+08
13	0.94112	-2.6343D+06	-2.6343D+06	-2.6343D+06	1.1022D+08	1.8114D+08	2.4273D+08
12	0.87239	-2.6343D+06	-2.6343D+06	-2.6343D+06	1.2458D+08	1.9532D+08	2.5685D+08
11	0.80369	-2.6343D+06	-2.6343D+06	-2.6343D+06	1.2896D+08	1.9899D+08	2.5994D+08
10	0.73500	-2.6343D+06	-2.6343D+06	-2.6343D+06	1.2218D+08	1.9153D+08	2.5183D+08
9	0.66633	-2.6343D+06	-2.6343D+06	-2.6343D+06	9.2345D+07	1.6068D+08	2.1987D+08
8	0.59769	-2.6343D+06	-2.6343D+06	-2.6343D+06	6.2858D+07	1.2873D+08	1.8558D+08
7	0.52908	-2.6343D+06	-2.6343D+06	-2.6343D+06	4.2063D+07	1.0477D+08	1.5875D+08
6	0.46051	-2.6343D+06	-2.6343D+06	-2.6343D+06	-1.4877D+07	4.4775D+07	9.5714D+07
5	0.39194	-2.6343D+06	-2.6343D+06	-2.6343D+06	-4.1896D+07	1.1203D+07	5.6342D+07
4	0.33203	-2.6343D+06	-2.6343D+06	-2.6343D+06	-2.4976D+06	9.4299D+06	1.9644D+07
3	0.28082	-2.6343D+06	-2.6343D+06	-2.6343D+06	-3.2322D+05	9.0916D+06	1.7169D+07
2	0.19139	3.6103D+07	4.3318D+07	4.6906D+07	4.3254D+06	8.6571D+06	1.2412D+07
1	0.06378	1.6683D+07	2.0339D+07	2.2161D+07	9.5612D+06	1.1474D+07	1.3191D+07

8-156

Fig. 8.6-5. DEFORM-4 Circumferential Stress Map

\*\*\* STRADY STATE TIME (SEC,HRS) = 5.04576D+07 1.40160D+04 \*\*\*

NODE	ELEVATION (M)	AXIAL STRESSES - SIGZ - PA								
		1	2	3	4	5	6	7	8	9
24	1.70318	-1.5719D+07	-1.4466D+07	-1.1962D+07	-9.4637D+06	-6.9715D+06	-4.4852D+06	-2.0046D+06	4.7009D+05	2.9390D+06
23	1.61805	-2.4647D+07	-2.2483D+07	-1.8163D+07	-1.3860D+07	-9.5734D+06	-5.3024D+06	-1.0473D+06	3.1919D+06	7.4152D+06
22	1.53285	-4.1243D+07	-3.7370D+07	-2.9651D+07	-2.1978D+07	-1.4351D+07	-6.7693D+06	7.6752D+05	8.2594D+06	1.5706D+07
21	1.46462	-1.0392D+08	-9.3300D+07	-7.2210D+07	-5.1372D+07	-3.0779D+07	-1.0421D+07	9.7046D+06	2.9590D+07	4.9227D+07
20	1.41335	-1.3575D+08	-1.2004D+08	-8.8907D+07	-5.8224D+07	-2.7942D+07	1.9657D+06	3.1452D+07	6.0457D+07	-2.6343D+06
19	1.35332	-4.2610D+08	-3.7577D+08	-2.6343D+06						
18	1.28463	-4.0933D+08	-3.6381D+08	-2.6343D+06						
17	1.21598	-5.1971D+08	-4.6858D+08	-2.6343D+06						
16	1.14730	-5.8643D+08	-5.3123D+08	-2.6343D+06						
15	1.07858	-6.2917D+08	-5.7280D+08	-2.6343D+06						
14	1.00985	-6.7108D+08	-6.1284D+08	-2.6343D+06						
13	0.94112	-6.9110D+08	-6.3083D+08	-2.6343D+06						
12	0.87239	-7.0356D+08	-6.4237D+08	-2.6343D+06						
11	0.80369	-6.9983D+08	-6.3929D+08	-2.6343D+06						
10	0.73500	-6.8369D+08	-6.2355D+08	-2.6343D+06						
9	0.66633	-6.4136D+08	-5.8006D+08	-2.6343D+06						
8	0.59769	-5.6113D+08	-5.0207D+08	-2.6343D+06						
7	0.52908	-4.6890D+08	-4.1119D+08	-2.6343D+06						
6	0.46051	-3.6387D+08	-3.0252D+08	-2.6343D+06						
5	0.39194	-4.7179D+08	-3.9488D+08	-2.6343D+06						
4	0.33203	-2.5258D+08	-2.3363D+08	-1.9617D+08	-1.5941D+08	-1.2332D+08	-8.7839D+07	-5.2954D+07	-2.6343D+06	-2.6343D+06
3	0.28082	-2.1416D+08	-2.0037D+08	-1.7306D+08	-1.4618D+08	-1.1973D+08	-9.3692D+07	-6.8052D+07	-4.2807D+07	-1.7977D+07
2	0.19139	-1.1661D+08	-1.1139D+08	-1.0099D+08	-9.0681D+07	-8.0460D+07	-7.0327D+07	-6.0281D+07	-5.0322D+07	-4.0448D+07
1	0.06378	-7.1900D+07	-6.9341D+07	-6.4239D+07	-5.9162D+07	-5.4111D+07	-4.9085D+07	-4.4085D+07	-3.9111D+07	-3.4162D+07

NODE	(M)	10	11	12	13	14	15
		24	1.70318	5.4022D+06	7.8596D+06	9.0866D+06	-2.0518D+06
23	1.61805	1.1623D+07	1.5815D+07	1.7906D+07	-2.8771D+06	-7.3602D+05	1.2446D+06
22	1.53285	2.3109D+07	3.0467D+07	3.4133D+07	-4.1971D+06	-7.6211D+05	2.4153D+06
21	1.46462	6.8618D+07	8.7762D+07	-2.6343D+06	-8.1507D+06	-7.9178D+05	6.0152D+06
20	1.41335	-2.6343D+06	-2.6343D+06	-2.6343D+06	-1.0595D+07	-8.1935D+05	8.2224D+06
19	1.35332	-2.6343D+06	-2.6343D+06	-2.6343D+06	-4.7374D+07	-8.8936D+05	4.2090D+07
18	1.28463	-2.6343D+06	-2.6343D+06	-2.6343D+06	-5.7889D+07	-9.2476D+05	5.1734D+07
17	1.21598	-2.6343D+06	-2.6343D+06	-2.6343D+06	-6.7422D+07	-9.6129D+05	6.0479D+07
16	1.14730	-2.6343D+06	-2.6343D+06	-2.6343D+06	-7.3601D+07	-9.9019D+05	6.6124D+07
15	1.07858	-2.6343D+06	-2.6343D+06	-2.6343D+06	-7.9820D+07	-1.0175D+06	7.1802D+07
14	1.00985	-2.6343D+06	-2.6343D+06	-2.6343D+06	-8.4678D+07	-1.0418D+06	7.6235D+07
13	0.94112	-2.6343D+06	-2.6343D+06	-2.6343D+06	-8.6910D+07	-1.0620D+06	7.8257D+07
12	0.87239	-2.6343D+06	-2.6343D+06	-2.6343D+06	-8.8169D+07	-1.0946D+06	7.9355D+07
11	0.80369	-2.6343D+06	-2.6343D+06	-2.6343D+06	-8.7900D+07	-1.1350D+06	7.9010D+07
10	0.73500	-2.6343D+06	-2.6343D+06	-2.6343D+06	-8.6563D+07	-1.1809D+06	7.7668D+07
9	0.66633	-2.6343D+06	-2.6343D+06	-2.6343D+06	-8.2598D+07	-1.2320D+06	7.3894D+07
8	0.59769	-2.6343D+06	-2.6343D+06	-2.6343D+06	-7.7137D+07	-1.2834D+06	6.8745D+07
7	0.52908	-2.6343D+06	-2.6343D+06	-2.6343D+06	-7.1800D+07	-1.3338D+06	6.3707D+07
6	0.46051	-2.6343D+06	-2.6343D+06	-2.6343D+06	-6.3007D+07	-1.3821D+06	5.5487D+07
5	0.39194	-2.6343D+06	-2.6343D+06	-2.6343D+06	-5.3472D+07	-1.4340D+06	4.6592D+07
4	0.33203	-2.6343D+06	-2.6343D+06	-2.6343D+06	-1.3912D+07	-1.4752D+06	1.0023D+07
3	0.28082	-2.6343D+06	-2.6343D+06	-2.6343D+06	-1.1552D+07	-1.5517D+06	7.6951D+06
2	0.19139	-3.0658D+07	-2.0954D+07	-1.6126D+07	-6.7186D+06	-1.6250D+06	3.0857D+06
1	0.06378	-2.9237D+07	-2.4338D+07	-2.1896D+07	-3.6884D+06	-6.7705D+05	2.1082D+06

8-157

Fig. 8.6-6. DEFORM-4 Axial Stress Map

\*\*\* STEADY STATE TIME (SEC,HRS) = 5.04576D+07 1.40160D+04 \*\*\*

NODE	ELEVATION (M)	FISSION GAS RETENTION								
		1	2	3	4	5	6	7	8	9
24	1.70318	9.7328D-01	9.7381D-01	9.7433D-01	9.7485D-01	9.7535D-01	9.7585D-01	9.7633D-01	9.7681D-01	9.7728D-01
23	1.61805	9.5082D-01	9.5227D-01	9.5367D-01	9.5505D-01	9.5638D-01	9.5769D-01	9.5895D-01	9.6019D-01	9.6139D-01
22	1.53285	8.9132D-01	8.9581D-01	9.0015D-01	9.0434D-01	9.0839D-01	9.1229D-01	9.1606D-01	9.1969D-01	9.2319D-01
21	1.46462	5.4557D-01	5.6917D-01	5.9245D-01	6.1533D-01	6.3773D-01	6.5957D-01	6.8078D-01	7.0128D-01	7.2104D-01
20	1.41335	3.2748D-01	3.5578D-01	3.8529D-01	4.1579D-01	4.4709D-01	4.7890D-01	5.1089D-01	5.4276D-01	5.7421D-01
19	1.35332	2.4669D-02	2.7565D-02	3.2613D-02	3.9618D-02	4.9635D-02	6.5016D-02	9.0242D-02	1.3223D-01	2.0066D-01
18	1.28463	3.1813D-02	3.5839D-02	4.3628D-02	5.5289D-02	7.2578D-02	1.0066D-01	1.5011D-01	2.3517D-01	3.6590D-01
17	1.21598	2.4433D-02	2.7798D-02	3.4654D-02	4.5654D-02	6.3093D-02	9.4473D-02	1.5952D-01	2.8584D-01	4.7457D-01
16	1.14730	2.0185D-02	2.2976D-02	2.8652D-02	3.7760D-02	5.2253D-02	7.8645D-02	1.3850D-01	2.7287D-01	4.8982D-01
15	1.07858	1.7509D-02	1.9952D-02	2.4950D-02	3.2987D-02	4.5815D-02	6.8573D-02	1.2148D-01	2.5562D-01	4.9442D-01
14	1.00985	1.6452D-02	1.8800D-02	2.3641D-02	3.1484D-02	4.4111D-02	6.6181D-02	1.1729D-01	2.5404D-01	5.0901D-01
13	0.94112	1.6500D-02	1.8921D-02	2.3931D-02	3.2095D-02	4.5330D-02	6.8639D-02	1.2321D-01	2.7007D-01	5.3605D-01
12	0.87239	1.6768D-02	1.9293D-02	2.4523D-02	3.3086D-02	4.7042D-02	7.2011D-02	1.3162D-01	2.9113D-01	5.6545D-01
11	0.80369	1.7659D-02	2.0409D-02	2.6087D-02	3.5405D-02	5.0652D-02	7.9002D-02	1.4900D-01	3.2858D-01	6.0647D-01
10	0.73500	1.9076D-02	2.2147D-02	2.8456D-02	3.8816D-02	5.5837D-02	8.9259D-02	1.7420D-01	3.7469D-01	6.4810D-01
9	0.66633	2.1930D-02	2.5609D-02	3.3077D-02	4.5340D-02	6.6122D-02	1.1057D-01	2.2184D-01	4.4072D-01	6.9310D-01
8	0.59769	2.7410D-02	3.2251D-02	4.1986D-02	5.8137D-02	8.7404D-02	1.5257D-01	2.9421D-01	5.1344D-01	7.3182D-01
7	0.52908	3.5481D-02	4.2234D-02	5.5607D-02	7.8051D-02	1.1966D-01	2.0401D-01	3.5396D-01	5.5283D-01	7.4206D-01
6	0.46051	4.7317D-02	5.7169D-02	7.4948D-02	1.0277D-01	1.4893D-01	2.2675D-01	3.4677D-01	5.0530D-01	6.7313D-01
5	0.39194	3.5822D-02	4.4034D-02	5.6730D-02	7.6040D-02	1.0743D-01	1.5907D-01	2.4070D-01	3.5943D-01	5.7775D-01
4	0.33203	3.8697D-01	4.2504D-01	4.6404D-01	5.0348D-01	5.4287D-01	5.8177D-01	6.1967D-01	6.5609D-01	6.9075D-01
3	0.28082	5.9890D-01	6.2884D-01	6.5783D-01	6.8569D-01	7.1231D-01	7.3759D-01	7.6146D-01	7.8387D-01	8.0479D-01
2	0.19139	9.4218D-01	9.4593D-01	9.4947D-01	9.5280D-01	9.5595D-01	9.5890D-01	9.6169D-01	9.6430D-01	9.6676D-01
1	0.06378	9.8828D-01	9.8882D-01	9.8934D-01	9.8984D-01	9.9032D-01	9.9077D-01	9.9121D-01	9.9163D-01	9.9203D-01

NODE	(M)	10	11	FG RET(KG)	FG PRD(KG)	M-FG/M-FUEL	FRAC RELS	NEUT/M**2
		24	1.70318	9.7774D-01	9.7819D-01	3.9269D-06	4.0243D-06	1.7250D-04
23	1.61805	9.6256D-01	9.6370D-01	6.1516D-06	6.4243D-06	2.7023D-04	4.2459D-02	3.7866D+23
22	1.53285	9.2656D-01	9.2980D-01	9.3961D-06	1.0306D-05	4.1275D-04	8.8296D-02	6.0709D+23
21	1.46462	7.4000D-01	7.5815D-01	8.7035D-06	1.3249D-05	6.3722D-04	3.4308D-01	1.2986D+24
20	1.41335	6.0504D-01	6.3506D-01	8.4417D-06	1.7598D-05	6.1805D-04	5.2030D-01	1.7233D+24
19	1.35332	3.0467D-01	4.4168D-01	1.3139D-05	1.1178D-04	7.2147D-04	8.8246D-01	8.1574D+24
18	1.28463	5.3233D-01	6.9802D-01	2.6759D-05	1.3678D-04	1.4694D-03	8.0436D-01	9.9844D+24
17	1.21598	6.7612D-01	8.3116D-01	3.6564D-05	1.5970D-04	2.0078D-03	7.7105D-01	1.1660D+25
16	1.14730	7.1321D-01	8.6714D-01	3.9661D-05	1.7408D-04	2.1778D-03	7.7216D-01	1.2708D+25
15	1.07858	7.3767D-01	8.9101D-01	4.2497D-05	1.8840D-04	2.3335D-03	7.7443D-01	1.3751D+25
14	1.00985	7.6181D-01	9.0933D-01	4.5622D-05	1.9929D-04	2.5051D-03	7.7107D-01	1.4545D+25
13	0.94112	7.8530D-01	9.2225D-01	4.8370D-05	2.0384D-04	2.6560D-03	7.6271D-01	1.4878D+25
12	0.87239	8.0666D-01	9.3244D-01	5.0806D-05	2.0607D-04	2.7898D-03	7.5346D-01	1.5043D+25
11	0.80369	8.3045D-01	9.4182D-01	5.3330D-05	2.0466D-04	2.9284D-03	7.3942D-01	1.4943D+25
10	0.73500	8.5102D-01	9.4884D-01	5.5539D-05	2.0076D-04	3.0497D-03	7.2335D-01	1.4662D+25
9	0.66633	8.6774D-01	9.5246D-01	5.7053D-05	1.9073D-04	3.1328D-03	7.0087D-01	1.3934D+25
8	0.59769	8.7851D-01	9.5280D-01	5.8180D-05	1.7735D-04	3.1947D-03	6.7196D-01	1.2961D+25
7	0.52908	8.7386D-01	9.4605D-01	5.7747D-05	1.6438D-04	3.1709D-03	6.4870D-01	1.2016D+25
6	0.46051	8.1151D-01	9.0329D-01	4.9098D-05	1.4345D-04	2.6960D-03	6.5774D-01	1.0487D+25
5	0.39194	6.5952D-01	7.8689D-01	3.1729D-05	1.2101D-04	1.7422D-03	7.3779D-01	8.8471D+24
4	0.33203	7.2342D-01	7.5393D-01	1.2533D-05	2.1692D-05	9.1757D-04	4.2224D-01	2.1269D+24
3	0.28082	8.2421D-01	8.4216D-01	1.2763D-05	1.7443D-05	9.3446D-04	2.6829D-01	1.7117D+24
2	0.19139	9.6907D-01	9.7123D-01	2.1282D-05	2.2212D-05	6.2326D-04	4.1843D-02	8.7335D+23
1	0.06378	9.9241D-01	9.9278D-01	1.3010D-05	1.3132D-05	3.8099D-04	9.3087D-03	5.1677D+23

Fig. 8.6-7. DEFORM-4 Fission-gas Retention Fraction Map

8-158

\*\*\* STEADY STATE TIME (SEC,HRS) = 5.04576D+07 1.40160D+04 \*\*\*

NODE	ELEVATION (M)	TOTAL POROSITY DISTRIBUTION								
		1	2	3	4	5	6	7	8	9
24	1.70318	1.3202D-01	1.3202D-01	1.3202D-01	1.3202D-01	1.3202D-01	1.3202D-01	1.3202D-01	1.3202D-01	1.3202D-01
23	1.61805	1.3207D-01	1.3207D-01	1.3207D-01	1.3207D-01	1.3207D-01	1.3207D-01	1.3207D-01	1.3207D-01	1.3207D-01
22	1.53285	1.3219D-01	1.3219D-01	1.3219D-01	1.3220D-01	1.3221D-01	1.3221D-01	1.3222D-01	1.3221D-01	1.3221D-01
21	1.46462	1.3261D-01	1.3266D-01	1.3276D-01	1.3289D-01	1.3310D-01	1.3353D-01	1.3359D-01	1.3360D-01	1.3360D-01
20	1.41335	1.3285D-01	1.3299D-01	1.3326D-01	1.3380D-01	1.3534D-01	1.3566D-01	1.3588D-01	1.3530D-01	1.3447D-01
19	1.35332	5.2549D-02	6.6479D-02	5.5996D-02	6.4395D-02	8.6003D-02	1.1896D-01	1.4594D-01	1.5611D-01	1.5662D-01
18	1.28463	2.1670D-02	2.9835D-02	4.9599D-02	5.5559D-02	7.8304D-02	1.2085D-01	1.5392D-01	1.6089D-01	1.5780D-01
17	1.21598	2.0440D-02	2.1067D-02	4.5085D-02	5.0732D-02	6.5068D-02	1.1486D-01	1.5724D-01	1.6272D-01	1.5961D-01
16	1.14730	2.0324D-02	2.0773D-02	3.5146D-02	4.1401D-02	5.0121D-02	1.0178D-01	1.5618D-01	1.6310D-01	1.6149D-01
15	1.07858	2.0259D-02	2.0597D-02	2.9350D-02	3.3833D-02	4.0486D-02	8.0354D-02	1.4998D-01	1.6254D-01	1.6271D-01
14	1.00985	2.0220D-02	2.0498D-02	2.6504D-02	3.0205D-02	3.5561D-02	6.5817D-02	1.4355D-01	1.6141D-01	1.6253D-01
13	0.94112	2.0208D-02	2.0468D-02	2.5675D-02	2.9182D-02	3.4235D-02	6.5203D-02	1.4380D-01	1.6109D-01	1.6193D-01
12	0.87239	2.0204D-02	2.0459D-02	2.5424D-02	2.8898D-02	3.3965D-02	6.9608D-02	1.4637D-01	1.6111D-01	1.6137D-01
11	0.80369	2.0211D-02	2.0477D-02	2.5676D-02	2.9364D-02	3.4802D-02	8.4782D-02	1.5185D-01	1.6110D-01	1.6026D-01
10	0.73500	2.0229D-02	2.0522D-02	2.6502D-02	3.0637D-02	3.7093D-02	1.0490D-01	1.5652D-01	1.6112D-01	1.5892D-01
9	0.66633	2.0278D-02	2.0648D-02	2.9212D-02	3.4691D-02	5.7722D-02	1.3237D-01	1.5992D-01	1.6061D-01	1.5664D-01
8	0.59769	2.0379D-02	2.0916D-02	3.4889D-02	4.4879D-02	9.3050D-02	1.5274D-01	1.6085D-01	1.5858D-01	1.5331D-01
7	0.52908	2.2446D-02	3.2177D-02	4.4542D-02	6.7245D-02	1.2018D-01	1.5947D-01	1.6071D-01	1.5645D-01	1.5096D-01
6	0.46051	5.3857D-02	6.2117D-02	7.3953D-02	9.8206D-02	1.3984D-01	1.6051D-01	1.5989D-01	1.5550D-01	1.5118D-01
5	0.39194	1.1919D-01	9.4656D-02	9.7040D-02	1.2005D-01	1.4692D-01	1.5798D-01	1.5779D-01	1.5466D-01	1.5219D-01
4	0.33203	1.3286D-01	1.3298D-01	1.3321D-01	1.3356D-01	1.3427D-01	1.3579D-01	1.3561D-01	1.3501D-01	1.3484D-01
3	0.28082	1.3270D-01	1.3276D-01	1.3286D-01	1.3299D-01	1.3317D-01	1.3347D-01	1.3394D-01	1.3394D-01	1.3378D-01
2	0.19139	1.3220D-01	1.3220D-01	1.3220D-01	1.3220D-01	1.3220D-01	1.3220D-01	1.3221D-01	1.3221D-01	1.3221D-01
1	0.06378	1.3205D-01	1.3205D-01	1.3204D-01						

NODE	(M)	10	11
		24	1.70318
23	1.61805	1.3206D-01	1.3206D-01
22	1.53285	1.3220D-01	1.3220D-01
21	1.46462	1.3358D-01	1.3349D-01
20	1.41335	1.3437D-01	1.3426D-01
19	1.35332	1.5432D-01	1.5236D-01
18	1.28463	1.5459D-01	1.5025D-01
17	1.21598	1.5445D-01	1.4762D-01
16	1.14730	1.5565D-01	1.4759D-01
15	1.07858	1.5658D-01	1.4753D-01
14	1.00985	1.5621D-01	1.4672D-01
13	0.94112	1.5514D-01	1.4565D-01
12	0.87239	1.5403D-01	1.4464D-01
11	0.80369	1.5239D-01	1.4343D-01
10	0.73500	1.5069D-01	1.4232D-01
9	0.66633	1.4851D-01	1.4115D-01
8	0.59769	1.4600D-01	1.3990D-01
7	0.52908	1.4459D-01	1.3938D-01
6	0.46051	1.4606D-01	1.4129D-01
5	0.39194	1.4902D-01	1.4515D-01
4	0.33203	1.3467D-01	1.3450D-01
3	0.28082	1.3352D-01	1.3343D-01
2	0.19139	1.3220D-01	1.3219D-01
1	0.06378	1.3204D-01	1.3204D-01

8-159

Fig. 8.6-8. DEFORM-4 Total Porosity Fraction Map

\*\*\* STEADY STATE TIME (SEC,HRS) = 5.04576D+07 1.40160D+04 \*\*\*

NODE	ELEVATION (M)	FISSION GAS INDUCED POROSITY								
		1	2	3	4	5	6	7	8	9
24	1.70318	2.4347D-05	2.4227D-05	2.4166D-05	2.4103D-05	2.4038D-05	2.3970D-05	2.3894D-05	2.3694D-05	2.3415D-05
23	1.61805	6.6628D-05	6.6572D-05	6.6874D-05	6.7177D-05	6.7481D-05	6.7786D-05	6.7784D-05	6.6609D-05	6.5447D-05
22	1.53285	1.8529D-04	1.8822D-04	1.9386D-04	2.0010D-04	2.0707D-04	2.1495D-04	2.1593D-04	2.1106D-04	2.0618D-04
21	1.46462	6.0741D-04	6.6107D-04	7.5530D-04	8.8888D-04	1.1018D-03	1.5287D-03	1.5927D-03	1.6007D-03	1.5962D-03
20	1.41335	8.4920D-04	9.8778D-04	1.2641D-03	1.7985D-03	3.3396D-03	3.6627D-03	3.8761D-03	3.2958D-03	2.4689D-03
19	1.35332	3.8958D-04	9.1581D-04	2.1654D-02	2.3947D-02	2.5848D-02	2.7576D-02	2.8307D-02	2.7416D-02	2.5179D-02
18	1.28463	5.7163D-04	1.2337D-03	2.9599D-02	3.2159D-02	3.4032D-02	3.4542D-02	3.3570D-02	3.0518D-02	2.5954D-02
17	1.21598	4.3999D-04	1.0674D-03	2.5085D-02	3.0732D-02	3.5379D-02	3.7629D-02	3.6603D-02	3.1807D-02	2.7675D-02
16	1.14730	3.2447D-04	7.7284D-04	1.5146D-02	2.1401D-02	2.8783D-02	3.3531D-02	3.6352D-02	3.2029D-02	2.9536D-02
15	1.07858	2.5898D-04	5.9722D-04	9.3505D-03	1.3833D-02	2.0486D-02	2.5561D-02	3.2957D-02	3.1507D-02	3.0748D-02
14	1.00985	2.2022D-04	4.9825D-04	6.5040D-03	1.0205D-02	1.5561D-02	2.0500D-02	2.8862D-02	3.0413D-02	3.0557D-02
13	0.94112	2.0793D-04	4.6815D-04	5.6751D-03	9.1822D-03	1.4235D-02	1.9012D-02	2.7668D-02	2.9925D-02	2.9946D-02
12	0.87239	2.0414D-04	4.5947D-04	5.4241D-03	8.8983D-03	1.3965D-02	1.8603D-02	2.7673D-02	2.9743D-02	2.9390D-02
11	0.80369	2.1135D-04	4.7724D-04	5.6763D-03	9.3636D-03	1.4802D-02	1.9185D-02	2.8583D-02	2.9475D-02	2.8274D-02
10	0.73500	2.2941D-04	5.2210D-04	6.5024D-03	1.0637D-02	1.6477D-02	2.1412D-02	2.9634D-02	2.9323D-02	2.6925D-02
9	0.66633	2.7779D-04	6.4763D-04	9.2124D-03	1.4691D-02	2.0429D-02	2.8202D-02	3.0348D-02	2.8715D-02	2.4641D-02
8	0.59769	3.7932D-04	9.1624D-04	1.4889D-02	2.2295D-02	2.8385D-02	3.5103D-02	3.0034D-02	2.6639D-02	2.1312D-02
7	0.52908	5.5149D-04	1.3277D-03	2.3957D-02	3.0426D-02	3.5169D-02	3.6314D-02	2.9495D-02	2.4500D-02	1.8960D-02
6	0.46051	8.1213D-04	1.9309D-03	3.3450D-02	3.5594D-02	3.5598D-02	3.3827D-02	2.8481D-02	2.3546D-02	1.9181D-02
5	0.39194	4.8888D-04	1.2909D-03	2.7917D-02	3.0239D-02	3.0709D-02	2.9540D-02	2.6348D-02	2.2735D-02	2.0200D-02
4	0.33203	8.5922D-04	9.8353D-04	1.2071D-03	1.5622D-03	2.2710D-03	3.7887D-03	3.6129D-03	3.0118D-03	2.8415D-03
3	0.28082	7.0451D-04	7.6286D-04	8.6061D-04	9.8953D-04	1.1736D-03	1.4717D-03	1.9449D-03	1.9374D-03	1.7769D-03
2	0.19139	1.9826D-04	1.9798D-04	1.9963D-04	2.0128D-04	2.0292D-04	2.0455D-04	2.0614D-04	2.0763D-04	2.0841D-04
1	0.06378	4.6167D-05	4.5410D-05	4.4775D-05	4.4129D-05	4.3472D-05	4.2805D-05	4.2128D-05	4.1441D-05	4.0742D-05

NODE	ELEVATION (M)	10	11
		24	1.70318
23	1.61805	6.4298D-05	6.3142D-05
22	1.53285	2.0132D-04	1.9624D-04
21	1.46462	1.5807D-03	1.4869D-03
20	1.41335	2.3654D-03	2.2633D-03
19	1.35332	2.2383D-02	2.0387D-02
18	1.28463	2.2599D-02	1.8252D-02
17	1.21598	2.2449D-02	1.5616D-02
16	1.14730	2.3655D-02	1.5589D-02
15	1.07858	2.4585D-02	1.5525D-02
14	1.00985	2.4210D-02	1.4722D-02
13	0.94112	2.3137D-02	1.3645D-02
12	0.87239	2.2035D-02	1.2645D-02
11	0.80369	2.0390D-02	1.1435D-02
10	0.73500	1.8687D-02	1.0322D-02
9	0.66633	1.6514D-02	9.1471D-03
8	0.59769	1.3996D-02	7.9012D-03
7	0.52908	1.2588D-02	7.3845D-03
6	0.46051	1.4058D-02	9.2914D-03
5	0.39194	1.7023D-02	1.3146D-02
4	0.33203	2.6718D-03	2.5021D-03
3	0.28082	1.5216D-03	1.4268D-03
2	0.19139	2.0290D-04	1.9459D-04
1	0.06378	4.0018D-05	3.9153D-05

8-160

Fig. 8.6-9. DEFORM-4 Fission-gas-induced Porosity Fraction Map

\*\*\* STEADY STATE TIME (SEC,HRS) = 5.04576D+07 1.40160D+04 \*\*\*

NODE	ELEVATION (M)	GRAIN SIZE DISTRIBUTION - DGR2 - M								
		1	2	3	4	5	6	7	8	9
24	1.70318	1.0000D-05	1.0000D-05	1.0000D-05	1.0000D-05	1.0000D-05	1.0000D-05	1.0000D-05	1.0000D-05	1.0000D-05
23	1.61805	1.0000D-05	1.0000D-05	1.0000D-05	1.0000D-05	1.0000D-05	1.0000D-05	1.0000D-05	1.0000D-05	1.0000D-05
22	1.53285	1.0000D-05	1.0000D-05	1.0000D-05	1.0000D-05	1.0000D-05	1.0000D-05	1.0000D-05	1.0000D-05	1.0000D-05
21	1.46462	1.0007D-05	1.0005D-05	1.0004D-05	1.0003D-05	1.0002D-05	1.0001D-05	1.0001D-05	1.0001D-05	1.0000D-05
20	1.41335	1.0142D-05	1.0096D-05	1.0064D-05	1.0043D-05	1.0028D-05	1.0019D-05	1.0012D-05	1.0008D-05	1.0005D-05
19	1.35332	1.0398D-04	8.7797D-05	7.1261D-05	5.6385D-05	4.3103D-05	3.1481D-05	2.1956D-05	1.5131D-05	1.1432D-05
18	1.28463	1.1189D-04	9.5018D-05	7.6015D-05	5.8401D-05	4.2774D-05	2.9275D-05	1.8742D-05	1.2416D-05	1.0338D-05
17	1.21598	1.2095D-04	1.0357D-04	8.2085D-05	6.1775D-05	4.3990D-05	2.8777D-05	1.7259D-05	1.1353D-05	1.0112D-05
16	1.14730	1.2962D-04	1.1142D-04	8.7747D-05	6.5235D-05	4.5772D-05	2.9277D-05	1.6886D-05	1.1011D-05	1.0061D-05
15	1.07858	1.4097D-04	1.2138D-04	9.5086D-05	7.0016D-05	4.8613D-05	3.0711D-05	1.7167D-05	1.0881D-05	1.0039D-05
14	1.00985	1.4998D-04	1.2910D-04	1.0066D-04	7.3568D-05	5.0630D-05	3.1711D-05	1.7380D-05	1.0800D-05	1.0028D-05
13	0.94112	1.5193D-04	1.3049D-04	1.0131D-04	7.3597D-05	5.0260D-05	3.1125D-05	1.6832D-05	1.0649D-05	1.0020D-05
12	0.87239	1.5123D-04	1.2953D-04	1.0014D-04	7.2343D-05	4.9038D-05	2.9982D-05	1.6040D-05	1.0497D-05	1.0014D-05
11	0.80369	1.4525D-04	1.2375D-04	9.5113D-05	6.8264D-05	4.5820D-05	2.7455D-05	1.4631D-05	1.0315D-05	1.0009D-05
10	0.73500	1.3701D-04	1.1598D-04	8.8612D-05	6.3192D-05	4.1920D-05	2.4571D-05	1.3282D-05	1.0193D-05	1.0006D-05
9	0.66633	1.2407D-04	1.0399D-04	7.8982D-05	5.5994D-05	3.6562D-05	2.1025D-05	1.2050D-05	1.0118D-05	1.0004D-05
8	0.59769	1.1167D-04	9.2083D-05	6.9446D-05	4.8887D-05	3.1417D-05	1.8099D-05	1.1335D-05	1.0085D-05	1.0004D-05
7	0.52908	1.0378D-04	8.4059D-05	6.2974D-05	4.4125D-05	2.8264D-05	1.6654D-05	1.1108D-05	1.0083D-05	1.0004D-05
6	0.46051	9.4469D-05	7.4785D-05	5.5771D-05	3.9188D-05	2.5572D-05	1.5891D-05	1.1173D-05	1.0122D-05	1.0009D-05
5	0.39194	8.4910D-05	6.5899D-05	4.9290D-05	3.5216D-05	2.3937D-05	1.5901D-05	1.1565D-05	1.0248D-05	1.0030D-05
4	0.33203	1.0067D-05	1.0040D-05	1.0024D-05	1.0014D-05	1.0008D-05	1.0005D-05	1.0003D-05	1.0002D-05	1.0001D-05
3	0.28082	1.0004D-05	1.0002D-05	1.0002D-05	1.0001D-05	1.0001D-05	1.0000D-05	1.0000D-05	1.0000D-05	1.0000D-05
2	0.19139	1.0000D-05	1.0000D-05	1.0000D-05	1.0000D-05	1.0000D-05	1.0000D-05	1.0000D-05	1.0000D-05	1.0000D-05
1	0.06378	1.0000D-05	1.0000D-05	1.0000D-05	1.0000D-05	1.0000D-05	1.0000D-05	1.0000D-05	1.0000D-05	1.0000D-05

NODE	ELEVATION (M)	GRAIN SIZE DISTRIBUTION - DGR2 - M	
		10	11
24	1.70318	1.0000D-05	1.0000D-05
23	1.61805	1.0000D-05	1.0000D-05
22	1.53285	1.0000D-05	1.0000D-05
21	1.46462	1.0000D-05	1.0000D-05
20	1.41335	1.0003D-05	1.0002D-05
19	1.35332	1.0255D-05	1.0035D-05
18	1.28463	1.0032D-05	1.0002D-05
17	1.21598	1.0006D-05	1.0000D-05
16	1.14730	1.0003D-05	1.0000D-05
15	1.07858	1.0001D-05	1.0000D-05
14	1.00985	1.0001D-05	1.0000D-05
13	0.94112	1.0000D-05	1.0000D-05
12	0.87239	1.0000D-05	1.0000D-05
11	0.80369	1.0000D-05	1.0000D-05
10	0.73500	1.0000D-05	1.0000D-05
9	0.66633	1.0000D-05	1.0000D-05
8	0.59769	1.0000D-05	1.0000D-05
7	0.52908	1.0000D-05	1.0000D-05
6	0.46051	1.0001D-05	1.0000D-05
5	0.39194	1.0003D-05	1.0000D-05
4	0.33203	1.0001D-05	1.0000D-05
3	0.28082	1.0000D-05	1.0000D-05
2	0.19139	1.0000D-05	1.0000D-05
1	0.06378	1.0000D-05	1.0000D-05

8-161

Fig. 8.6-10. DEFORM-4 Fuel Grain Size Map

\*\*\* STEADY STATE TIME (SEC,HRS) = 5.04576D+07 1.40160D+04 \*\*\*

NODE	ELEVATION (M)	CRACK VOLUME FRACTION								
		1	2	3	4	5	6	7	8	9
24	1.70318	0.0000D+00	0.0000D+00	0.0000D+00	0.0000D+00	0.0000D+00	0.0000D+00	0.0000D+00	0.0000D+00	0.0000D+00
23	1.61805	0.0000D+00	0.0000D+00	0.0000D+00	0.0000D+00	0.0000D+00	0.0000D+00	0.0000D+00	0.0000D+00	0.0000D+00
22	1.53285	0.0000D+00	0.0000D+00	0.0000D+00	0.0000D+00	0.0000D+00	0.0000D+00	0.0000D+00	0.0000D+00	0.0000D+00
21	1.46462	0.0000D+00	0.0000D+00	0.0000D+00	0.0000D+00	0.0000D+00	0.0000D+00	0.0000D+00	0.0000D+00	0.0000D+00
20	1.41335	0.0000D+00	0.0000D+00	0.0000D+00	0.0000D+00	0.0000D+00	0.0000D+00	0.0000D+00	8.9034D-05	1.3762D-04
19	1.35332	0.0000D+00	8.4941D-06	7.3467D-05	9.0068D-05	7.8064D-05	5.4891D-05	3.8875D-05	3.2034D-05	2.9686D-05
18	1.28463	0.0000D+00	1.8955D-04	6.8431D-04	8.6019D-04	8.7192D-04	7.9414D-04	6.9761D-04	6.2069D-04	1.1111D-03
17	1.21598	0.0000D+00	0.0000D+00	2.0019D-04	3.7953D-04	3.9626D-04	3.0242D-04	2.1719D-04	5.8894D-04	1.4921D-03
16	1.14730	0.0000D+00	0.0000D+00	0.0000D+00	0.0000D+00	0.0000D+00	0.0000D+00	0.0000D+00	0.0000D+00	1.0478D-03
15	1.07858	0.0000D+00	0.0000D+00	0.0000D+00	0.0000D+00	0.0000D+00	0.0000D+00	0.0000D+00	0.0000D+00	1.0203D-03
14	1.00985	0.0000D+00	0.0000D+00	0.0000D+00	0.0000D+00	0.0000D+00	0.0000D+00	0.0000D+00	0.0000D+00	1.1713D-03
13	0.94112	0.0000D+00	0.0000D+00	0.0000D+00	0.0000D+00	0.0000D+00	0.0000D+00	0.0000D+00	0.0000D+00	1.2699D-03
12	0.87239	0.0000D+00	0.0000D+00	0.0000D+00	0.0000D+00	0.0000D+00	0.0000D+00	0.0000D+00	0.0000D+00	7.9978D-04
11	0.80369	0.0000D+00	0.0000D+00	0.0000D+00	0.0000D+00	0.0000D+00	0.0000D+00	0.0000D+00	0.0000D+00	9.2114D-04
10	0.73500	0.0000D+00	0.0000D+00	0.0000D+00	0.0000D+00	0.0000D+00	0.0000D+00	0.0000D+00	3.6966D-04	1.5801D-03
9	0.66633	0.0000D+00	0.0000D+00	0.0000D+00	0.0000D+00	0.0000D+00	0.0000D+00	0.0000D+00	5.5004D-04	1.6250D-03
8	0.59769	0.0000D+00	0.0000D+00	0.0000D+00	0.0000D+00	0.0000D+00	0.0000D+00	0.0000D+00	7.1546D-04	1.6236D-03
7	0.52908	0.0000D+00	0.0000D+00	0.0000D+00	4.1849D-05	8.0314D-05	5.3133D-05	7.0643D-04	1.5155D-03	2.2349D-03
6	0.46051	0.0000D+00	0.0000D+00	5.6047D-04	8.1323D-04	8.3952D-04	7.8326D-04	8.0652D-04	1.4137D-03	2.2897D-03
5	0.39194	0.0000D+00	2.5679D-05	3.5952D-04	4.4061D-04	4.4336D-04	4.2807D-04	4.1031D-04	7.2176D-04	1.2089D-03
4	0.33203	0.0000D+00	0.0000D+00	0.0000D+00	0.0000D+00	0.0000D+00	0.0000D+00	4.4057D-04	4.0202D-04	2.8381D-04
3	0.28082	0.0000D+00	0.0000D+00	0.0000D+00	0.0000D+00	0.0000D+00	0.0000D+00	0.0000D+00	0.0000D+00	4.0847D-04
2	0.19139	0.0000D+00	0.0000D+00	0.0000D+00	0.0000D+00	0.0000D+00	0.0000D+00	0.0000D+00	0.0000D+00	0.0000D+00
1	0.06378	0.0000D+00	0.0000D+00	0.0000D+00	0.0000D+00	0.0000D+00	0.0000D+00	0.0000D+00	0.0000D+00	0.0000D+00

NODE	(M)	10	11
		24	1.70318
23	1.61805	0.0000D+00	0.0000D+00
22	1.53285	0.0000D+00	0.0000D+00
21	1.46462	0.0000D+00	1.5966D-05
20	1.41335	8.1658D-05	9.1073D-05
19	1.35332	2.2579D-04	8.6337D-04
18	1.28463	1.7628D-03	2.4292D-03
17	1.21598	2.2907D-03	3.0595D-03
16	1.14730	1.9966D-03	2.8695D-03
15	1.07858	2.0898D-03	3.0441D-03
14	1.00985	2.3022D-03	3.2930D-03
13	0.94112	2.4027D-03	3.3879D-03
12	0.87239	1.9501D-03	2.9396D-03
11	0.80369	2.0219D-03	2.9716D-03
10	0.73500	2.5833D-03	3.4627D-03
9	0.66633	2.5219D-03	3.3253D-03
8	0.59769	2.3936D-03	3.1052D-03
7	0.52908	2.8592D-03	3.4644D-03
6	0.46051	2.7829D-03	3.2901D-03
5	0.39194	1.9365D-03	2.4460D-03
4	0.33203	1.9989D-04	1.2609D-04
3	0.28082	3.9787D-04	4.0593D-04
2	0.19139	0.0000D+00	0.0000D+00
1	0.06378	0.0000D+00	0.0000D+00

8-162

Fig. 8.6-11. DEFORM-4 Fuel Crack Volume Fraction Map

\*\*\* STEADY STATE TIME (SEC,HRS) = 5.04576D+07 1.40160D+04 \*\*\*

NODE	ELEVATION (M)	RADIAL MESH POINTS - R - M								
		1	2	3	4	5	6	7	8	9
24	1.70318	1.0027D-06	6.7091D-04	1.1620D-03	1.5002D-03	1.7750D-03	2.0127D-03	2.2251D-03	2.4189D-03	2.5983D-03
23	1.61805	1.0032D-06	6.7136D-04	1.1628D-03	1.5012D-03	1.7762D-03	2.0140D-03	2.2265D-03	2.4204D-03	2.5999D-03
22	1.53285	1.0040D-06	6.7207D-04	1.1640D-03	1.5027D-03	1.7780D-03	2.0160D-03	2.2287D-03	2.4228D-03	2.6025D-03
21	1.46462	1.0056D-06	6.7411D-04	1.1675D-03	1.5072D-03	1.7833D-03	2.0220D-03	2.2354D-03	2.4301D-03	2.6103D-03
20	1.41335	1.0120D-06	6.7534D-04	1.1697D-03	1.5100D-03	1.7867D-03	2.0262D-03	2.2402D-03	2.4354D-03	2.6160D-03
19	1.35332	6.2416D-04	9.0732D-04	1.3044D-03	1.6022D-03	1.8543D-03	2.0803D-03	2.2904D-03	2.4876D-03	2.6717D-03
18	1.28463	6.8944D-04	9.4706D-04	1.3210D-03	1.6143D-03	1.8629D-03	2.0864D-03	2.2963D-03	2.4945D-03	2.6791D-03
17	1.21598	7.1117D-04	9.6418D-04	1.3323D-03	1.6236D-03	1.8708D-03	2.0915D-03	2.3003D-03	2.4994D-03	2.6844D-03
16	1.14730	7.2223D-04	9.7330D-04	1.3400D-03	1.6282D-03	1.8733D-03	2.0911D-03	2.2978D-03	2.4973D-03	2.6829D-03
15	1.07858	7.3297D-04	9.8205D-04	1.3473D-03	1.6336D-03	1.8772D-03	2.0932D-03	2.2960D-03	2.4949D-03	2.6810D-03
14	1.00985	7.3975D-04	9.8751D-04	1.3519D-03	1.6371D-03	1.8798D-03	2.0949D-03	2.2950D-03	2.4930D-03	2.6792D-03
13	0.94112	7.3792D-04	9.8621D-04	1.3510D-03	1.6362D-03	1.8788D-03	2.0938D-03	2.2939D-03	2.4921D-03	2.6781D-03
12	0.87239	7.3307D-04	9.8257D-04	1.3481D-03	1.6337D-03	1.8765D-03	2.0916D-03	2.2927D-03	2.4913D-03	2.6775D-03
11	0.80369	7.2104D-04	9.7346D-04	1.3413D-03	1.6279D-03	1.8713D-03	2.0868D-03	2.2911D-03	2.4909D-03	2.6770D-03
10	0.73500	7.0705D-04	9.6287D-04	1.3333D-03	1.6212D-03	1.8654D-03	2.0817D-03	2.2903D-03	2.4908D-03	2.6766D-03
9	0.66633	6.8141D-04	9.4357D-04	1.3186D-03	1.6091D-03	1.8551D-03	2.0762D-03	2.2904D-03	2.4911D-03	2.6765D-03
8	0.59769	6.5147D-04	9.2115D-04	1.3014D-03	1.5953D-03	1.8446D-03	2.0738D-03	2.2919D-03	2.4922D-03	2.6768D-03
7	0.52908	6.1476D-04	8.9485D-04	1.2852D-03	1.5838D-03	1.8392D-03	2.0744D-03	2.2933D-03	2.4929D-03	2.6766D-03
6	0.46051	5.2819D-04	8.4443D-04	1.2595D-03	1.5702D-03	1.8344D-03	2.0740D-03	2.2926D-03	2.4916D-03	2.6748D-03
5	0.39194	3.9737D-04	7.8756D-04	1.2331D-03	1.5554D-03	1.8269D-03	2.0687D-03	2.2870D-03	2.4860D-03	2.6692D-03
4	0.33203	1.0168D-06	6.7549D-04	1.1699D-03	1.5102D-03	1.7868D-03	2.0261D-03	2.2401D-03	2.4353D-03	2.6158D-03
3	0.28082	1.0065D-06	6.7437D-04	1.1680D-03	1.5077D-03	1.7839D-03	2.0226D-03	2.2360D-03	2.4308D-03	2.6110D-03
2	0.19139	1.0036D-06	6.7191D-04	1.1637D-03	1.5023D-03	1.7775D-03	2.0155D-03	2.2281D-03	2.4221D-03	2.6017D-03
1	0.06378	1.0023D-06	6.7079D-04	1.1618D-03	1.4999D-03	1.7746D-03	2.0122D-03	2.2246D-03	2.4183D-03	2.5976D-03

NODE	(M)	10	11	12	R(NR, J)	R(NRP, J)	IEQCOL	IUNEQA
24	1.70318	2.7661D-03	2.9242D-03	3.0002D-03	3.0903D-03	3.6544D-03	1	1
23	1.61805	2.7678D-03	2.9260D-03	3.0020D-03	3.0903D-03	3.6544D-03	1	1
22	1.53285	2.7705D-03	2.9289D-03	3.0049D-03	3.0903D-03	3.6544D-03	1	1
21	1.46462	2.7788D-03	2.9376D-03	3.0138D-03	3.0903D-03	3.6544D-03	1	1
20	1.41335	2.7847D-03	2.9438D-03	3.0202D-03	3.0903D-03	3.6544D-03	1	1
19	1.35332	2.8439D-03	3.0057D-03	3.0832D-03	3.0907D-03	3.6549D-03	6	9
18	1.28463	2.8511D-03	3.0127D-03	3.0899D-03	3.0904D-03	3.6545D-03	6	9
17	1.21598	2.8568D-03	3.0183D-03	3.0953D-03	3.0953D-03	3.6586D-03	7	8
16	1.14730	2.8560D-03	3.0181D-03	3.0952D-03	3.0952D-03	3.6584D-03	7	8
15	1.07858	2.8547D-03	3.0173D-03	3.0946D-03	3.0946D-03	3.6577D-03	7	8
14	1.00985	2.8531D-03	3.0158D-03	3.0932D-03	3.0932D-03	3.6564D-03	7	8
13	0.94112	2.8520D-03	3.0145D-03	3.0917D-03	3.0917D-03	3.6549D-03	7	8
12	0.87239	2.8512D-03	3.0135D-03	3.0907D-03	3.0907D-03	3.6538D-03	7	8
11	0.80369	2.8505D-03	3.0126D-03	3.0897D-03	3.0897D-03	3.6526D-03	7	8
10	0.73500	2.8498D-03	3.0114D-03	3.0884D-03	3.0884D-03	3.6512D-03	6	8
9	0.66633	2.8489D-03	3.0100D-03	3.0868D-03	3.0868D-03	3.6494D-03	6	8
8	0.59769	2.8484D-03	3.0088D-03	3.0854D-03	3.0854D-03	3.6479D-03	6	7
7	0.52908	2.8475D-03	3.0074D-03	3.0838D-03	3.0838D-03	3.6462D-03	5	7
6	0.46051	2.8453D-03	3.0052D-03	3.0816D-03	3.0816D-03	3.6440D-03	5	7
5	0.39194	2.8400D-03	3.0003D-03	3.0770D-03	3.0802D-03	3.6425D-03	4	7
4	0.33203	2.7846D-03	2.9437D-03	3.0200D-03	3.0792D-03	3.6413D-03	1	1
3	0.28082	2.7794D-03	2.9382D-03	3.0144D-03	3.0790D-03	3.6411D-03	1	1
2	0.19139	2.7696D-03	2.9279D-03	3.0040D-03	3.0789D-03	3.6409D-03	1	1
1	0.06378	2.7654D-03	2.9235D-03	2.9994D-03	3.0788D-03	3.6408D-03	1	1

8-163

Fig. 8.6-12. DEFORM-4 Radial Node Locations

\*\*\* STEADY STATE TIME (SEC,HRS) = 0.00000D+00 0.00000D+00 \* 1

***** FAILURE CRITERIA *****																	
AXIAL	AXIAL	FUEL/CLAD	F/C	HOOP	FLOW	CLAD	K-D	NSMH	NSMH	NSMH	INPUT	INPUT	HBDL	HBDL	HBDL	TDC2	
FUEL	ELEV	GAP	PRESS	STRESS	STRESS	STRAIN	FAIL	LIFE	BRST	FAIL	STRAN	MPFAIL	LMP	111	DORN	LIFE	
NODE	(M)	(M)	(MPA)	(MPA)	(MPA)	PERCENT	STRN	FRAC	PRES	TEMP	LIMIT	LIMIT	FRAC	FRAC	FRAC	FRAC	
24	1.7032	9.0104D-05	2.63	13.30	624.10	0.0000	0.0000	0.0000	0.0279	0.5363	0.0000	0.0000	0.0007	0.0007	0.0000	0.0001	
23	1.6180	8.8267D-05	2.63	13.20	624.00	0.0000	0.0000	0.0000	0.0279	0.5362	0.0000	0.0000	0.0007	0.0007	0.0000	0.0001	
22	1.5329	8.5360D-05	2.63	13.10	623.83	0.0000	0.0000	0.0000	0.0279	0.5361	0.0000	0.0000	0.0007	0.0007	0.0000	0.0001	
21	1.4646	7.6460D-05	2.63	13.02	621.84	0.0000	0.0000	0.0000	0.0279	0.5364	0.0000	0.0000	0.0008	0.0008	0.0000	0.0001	
20	1.4133	7.0105D-05	2.63	12.96	621.50	0.0000	0.0000	0.0000	0.0279	0.5362	0.0000	0.0000	0.0007	0.0007	0.0000	0.0001	
19	1.3533	7.5047D-06	2.63	12.88	597.88	0.0000	0.0000	0.0000	0.0281	0.5410	0.0000	0.0000	0.0013	0.0013	0.0000	0.0002	
18	1.2846	4.9918D-07	2.63	12.80	602.77	0.0000	0.0000	0.0000	0.0279	0.5376	0.0000	0.0000	0.0009	0.0009	0.0000	0.0001	
17	1.2160	0.0000D+00	8.68	49.26	611.13	0.0000	0.0000	0.0000	0.0913	0.5328	0.0000	0.0000	0.0005	0.0005	0.0002	0.0007	
16	1.1473	0.0000D+00	13.80	80.08	624.37	0.0002	0.0000	0.0000	0.1438	0.5264	0.0000	0.0000	0.0002	0.0002	0.0007	0.0018	
15	1.0786	0.0000D+00	20.66	121.42	636.73	0.0008	0.0000	0.0000	0.2132	0.5194	0.0000	0.0000	0.0001	0.0001	0.0019	0.0040	
14	1.0098	0.0000D+00	28.50	168.59	640.70	0.0020	0.0000	0.0000	0.2911	0.5115	0.0000	0.0000	0.0001	0.0001	0.0035	0.0065	
13	0.9411	0.0000D+00	33.26	197.17	645.37	0.0016	0.0000	0.0000	0.3362	0.5027	0.0000	0.0000	0.0001	0.0001	0.0028	0.0050	
12	0.8724	0.0000D+00	35.87	212.78	650.31	0.0008	0.0000	0.0000	0.3589	0.4936	0.0000	0.0000	0.0000	0.0000	0.0014	0.0026	
11	0.8037	0.0000D+00	36.57	216.91	655.54	0.0003	0.0000	0.0000	0.3626	0.4841	0.0000	0.0000	0.0000	0.0000	0.0005	0.0009	
10	0.7350	0.0000D+00	35.25	208.80	660.89	0.0001	0.0000	0.0000	0.3467	0.4745	0.0000	0.0000	0.0000	0.0000	0.0001	0.0002	
9	0.6663	0.0000D+00	29.66	175.00	666.55	0.0000	0.0000	0.0000	0.2897	0.4648	0.0000	0.0000	0.0000	0.0000	0.0000	0.0000	
8	0.5977	0.0000D+00	23.89	140.07	672.19	0.0000	0.0000	0.0000	0.2318	0.4552	0.0000	0.0000	0.0000	0.0000	0.0000	0.0000	
7	0.5291	0.0000D+00	19.57	113.96	676.73	0.0000	0.0000	0.0000	0.1889	0.4464	0.0000	0.0000	0.0000	0.0000	0.0000	0.0000	
6	0.4605	0.0000D+00	8.68	48.24	679.48	0.0000	0.0000	0.0000	0.0833	0.4376	0.0000	0.0000	0.0000	0.0000	0.0000	0.0000	
5	0.3919	3.1913D-06	2.63	11.73	682.01	0.0000	0.0000	0.0000	0.0251	0.4296	0.0000	0.0000	0.0000	0.0000	0.0000	0.0000	
4	0.3320	5.9128D-05	2.63	11.66	686.59	0.0000	0.0000	0.0000	0.0250	0.4184	0.0000	0.0000	0.0000	0.0000	0.0000	0.0000	
3	0.2808	6.4626D-05	2.63	11.60	687.07	0.0000	0.0000	0.0000	0.0249	0.4170	0.0000	0.0000	0.0000	0.0000	0.0000	0.0000	
2	0.1914	7.4914D-05	2.63	11.49	687.77	0.0000	0.0000	0.0000	0.0249	0.4151	0.0000	0.0000	0.0000	0.0000	0.0000	0.0000	
1	0.0638	7.9379D-05	2.63	11.34	688.18	0.0000	0.0000	0.0000	0.0249	0.4139	0.0000	0.0000	0.0000	0.0000	0.0000	0.0000	

GAS PLENUM PRESSURE = 2.6343D+06 PA  
 MOLTEN CAVITY PRESSURE = 0.0000D+00 PA  
 TOTAL FISSION GAS PRODUCED = 2.7084D-03 KG  
 FISSION GAS IN SOLID FUEL = 7.6230D-04 KG  
 FISSION GAS IN MOLTEN FUEL = 0.0000D+00 KG  
 FRACTIONAL GAS RELEASE = 0.71853743  
 MOLTEN CAVITY VOLUME = 0.0000D+00 M3  
 MOLTEN CAVITY GAS CONTENT = 0.0000D+00 MOL  
 MOLTEN CAVITY TEMPERATURE = 0.0000D+00 K  
 MASS MOLTEN FUEL IN PIN = 0.0000D+00 KG  
 MASS SOLID FUEL IN PIN = 4.6439D-01 KG  
 PLENUM HELIUM GAS CONTENT = 1.2426D-03 MOL  
 PLENUM FISSION GAS CONTENT = 1.4691D-02 MOL  
 AXIAL EXPANSION REACTIVITY = 0.0000D+00 DOL

8-164

Fig. 8.6-13. DEFORM-4 Short Form Pin Summary Output

where

$\rho_0$  = The theoretical density at 273 K, kg/m<sup>3</sup>

$C_1, C_2$  = Input coefficients

T = Temperature, K

This applies between 273 K and the solidus temperature.

The liquid fuel density is given by

$$\rho_l = \frac{\rho_0}{1 + C_3(T-273)} \quad (8.7-2)$$

where

$C_3$  = Input coefficient

This applies to temperatures above the liquidus. For the range between the solidus and liquidus temperatures, a linear interpolation is performed.

These equations are found in the function RHOF. Suggested values of coefficients are from the Nuclear Systems Materials Handbook [8-17].

$\rho_0$  = COEFDS(1) = 11.05x10<sup>3</sup> kg/m<sup>3</sup> (mixed oxide)

$C_1$  = COEFDS(2) = 2.04x10<sup>-5</sup> K<sup>-1</sup>

$C_2$  = COEFDS(3) = 8.70x10<sup>-9</sup> K<sup>-2</sup>

$C_3$  = COEFDL(2) = 9.30x10<sup>-5</sup> K<sup>-1</sup>

### 8.7.2 Mixed Oxide Fuel Thermal Expansion Coefficient

The thermal expansion coefficient of the fuel is derived from the coefficients of the fuel density function. This assures consistency between the thermal expansion and the density.

The specific volume (inverse of density) at two temperatures is given by

$$v_1 = \frac{1 + C_1(T_1 - 273) + C_2(T_1 - 273)^2}{\rho_0} \quad (8.7-3)$$

$$v_2 = \frac{1 + C_1(T_2 - 273) + C_2(T_2 - 273)^2}{\rho_0} \quad (8.7-4)$$

The change in volume is therefore given by

$$\Delta v = v_2 - v_1 = \frac{1}{\rho_0} \{ [C_1 + C_2(T_2 - 273)](T_2 - 273) - [C_1 + C_2(T_1 - 273)](T_1 - 273) \} \quad (8.7-5)$$

Equation 8.7-5 can be rewritten in terms of the bulk thermal expansion coefficient,  $\beta$ .

$$\Delta v = \frac{1}{\rho_0} \{ \beta(T_2) (T_2 - T_r) - \beta(T_1) (T_1 - T_r) \} \quad (8.7-6)$$

where

$$\begin{aligned} \beta(T) &= C_1 + C_2 T \\ T &= \text{Temperature, K} \\ C_1, C_2 &= \text{Density function coefficients} \\ T_r &= \text{Reference temperature, K} \end{aligned}$$

Since the linear expansion coefficient is assumed to be a third of the bulk expansion coefficient, the linear expansion coefficient can be defined from the density coefficients as

$$\alpha(T) + C'_1 + C'_2 T \quad (8.7-7)$$

where

$$\begin{aligned} \alpha &= \text{Linear thermal expansion coefficient} \\ C'_1 &= C_1/3 \\ C'_2 &= C_2/3 \\ T &= \text{Temperature, K} \end{aligned}$$

This is found in the function ALPHF.

### 8.7.3 Mixed Oxide Fuel Modulus of Elasticity

The modulus of elasticity, Young's Modulus, is determined from the bulk modulus by

$$E = 3(1 - 2\nu) K \quad (8.7-8)$$

where

$$\begin{aligned} E &= \text{Modulus of elasticity, Pa} \\ K &= \text{Bulk modulus, Pa} \\ \nu &= \text{Poisson's ratio} \end{aligned}$$

The bulk modulus is from the NSMH [8-17] and is given by

$$K = 1.38 \times 10^{11} [1 - 0.5 (T/2760)^2] (1 - 2P) \quad (8.7-9)$$

where

$$\begin{aligned} K &= \text{Bulk modulus, Pa} \\ T &= \text{Temperature, } ^\circ\text{C} \\ P &= 1 - \rho_{TD} = \text{Porosity fraction} \\ \rho_{TD} &= \text{Fraction of theoretical density} \end{aligned}$$

Based on the evaluation in MATPRO-10 [8-11], if this calculated modulus of elasticity becomes less than  $7.9 \times 10^8$ , it is fixed at this value.

These equations are solved in the function EFUELF.

#### 8.7.4 Mixed Oxide Fuel Thermal Conductivity

Four different options exist for the fuel thermal conductivity. These are controlled through the input parameter IRHOK.

$$\text{IRHOK} = 0$$

The thermal conductivity as a function of temperature is input in table form through the variable arrays XKTAB and XKTEM.

$$\text{RHOK} = 1$$

For this option, the mixed oxide conductivity equations [8-3] are given by

$$k_1(T) = 1.1 + \frac{1 \times 10^2}{T (.4848 - .4465f_D)} \quad \text{for } 800^\circ\text{C} \leq T \leq 2000^\circ\text{C} \quad (8.7-10)$$

$$k_2(T) = k_1(800) \frac{168.844}{12.044 + (0.196)T} \quad \text{for } T < 800^\circ\text{C} \quad (8.7-11)$$

$$k_3(T) = k_1(2000) \quad \text{for } T > 2000^\circ\text{C} \quad (8.7-12)$$

where

$k_1, k_2, k_3$  = Fuel thermal conductivity, W/m-K

T = Temperature, °C

$f_D$  = Fuel fraction of theoretical density

IRHOK = 2

This form of the mixed oxide conductivity [8-31] is given by

$$k_1(T) = [(C_1 - f_D) f_D - 1] \left[ \frac{1}{(C_2 + C_3 T)} + C_4 T^3 \right] \quad (8.7-13)$$

for  $0.75 \leq f_D \leq 0.95$

$$k_2(T) = (3f_D - 1) \left[ \frac{1}{(C_5 + C_6 T)} + C_7 T^3 \right] \quad \text{for } f_D > 0.95 \quad (8.7-14)$$

where

$C_1, C_2, C_3, C_4, C_5, C_6, C_7$	=	Input variables
$k_1, k_2$	=	Fuel conductivity W/m-K
T	=	Temperature, K

If T is greater than the melting temperature, it is set to the melting temperature.

Suggested values:

$C_1$	=	COEFK(1) = 2.1
$C_2$	=	COEFK(2) = $2.88 \times 10^{-3}$
$C_3$	=	COEFK(3) = $2.52 \times 10^{-5}$
$C_4$	=	COEFK(4) = $5.83 \times 10^{-10}$
$C_5$	=	COEFK(5) = $5.75 \times 10^{-2}$
$C_6$	=	COEFK(6) = $5.03 \times 10^{-4}$
$C_7$	=	COEFK(7) = $2.91 \times 10^{-11}$

IRHOK = 3

This mixed oxide conductivity form is [8-32]

$$k_1(T) = \frac{4.005 \times 10^3}{(T-273) + 402.4} + 0.6416 \times 10^{-10} T^3 \quad (8.7-15)$$

where

- T = Temperature, K  
k = Conductivity in W/m-K

This is the correlation for  $UO_2$  and is converted to mixed oxide by subtracting 0.2.

$$k_2(T) = k_1(T) - 0.2 \quad (8.7-16)$$

The porosity correction term was derived for use in the COMETHE-IIIJ [8-33] code and is given by

$$f_p = 1 - 1.029 \epsilon - 3.2 \epsilon^2 - 40.1 \epsilon^3 + 158 \epsilon^4 \quad (8.7-17)$$

where

- $f_p$  = Porosity multiplier  
 $\epsilon$  =  $1 - \rho_f$  = Fractional porosity  
 $\rho_f$  = Fractional fuel density = actual density/theoretical density

The conductivity is therefore given by

$$k(T) = f_p \times k_2(T). \quad (8.7-18)$$

Two different routines contain the above correlations, FK and KFUEL. The function FK returns a single value of the conductivity for a single invocation and is used in the pre-transient. The subroutine KFUEL returns the conductivity values for each radial node in the current axial segment. It is used in the transient calculational procedure.

### 8.7.5 Mixed Oxide Fuel Fracture Strength

The fracture strength for mixed-oxide fuel is from the NSMH [8-17] and is for unirradiated fuel.

$$\sigma_f = 2.74 \times 10^7 + 5.9 \times 10^4 T \quad (8.7-19)$$

This is coded in the function SIGFRA.

### 8.7.6 Mixed Oxide Fuel Creep Rate

The fuel creep rate function is from the NSMH [8-17] and is used in the subroutine FSWELL. It represents diffusional flow, dislocation creep, fission-enhanced thermal creep, and fission-induced creep.

$$\begin{aligned} \dot{\epsilon}_{\text{total}} = & \frac{A}{d^2} [1 + 2.11(97 - TD)] \sigma \exp(-Q_1/RT) \\ & + B [1 + 0.22(97 - TD)] \sigma^{4.4} \exp(-Q_2/RT) \\ & + C \sigma \dot{F} \exp(-Q_3/RT) \\ & + D \sigma \dot{F} \end{aligned} \quad (8.7-20)$$

where

- $\dot{\epsilon}_{\text{total}}$  = Creep rate,  $s^{-1}$
- A =  $8.97222 \times 10^5$
- d = Grain size,  $\mu\text{m}$
- TD = Fuel percent of theoretical density
- $\sigma$  = Stress, MPa
- $Q_1$  =  $3.87173 \times 10^5$
- R = Gas constant = 8.3169 J/mole-K
- T = Temperature, K
- $\beta$  =  $9.0 \times 10^2$

$$\begin{aligned}
Q_2 &= 5.72598 \times 10^5 \\
C &= 7.8889 \times 10^{-21} \\
\dot{F} &= \text{Fission rate, fissions/cm}^3\text{-s} \\
Q_3 &= 5.7343 \times 10^4 \\
D &= 1.5 \times 10^{-24}
\end{aligned}$$

This is used to calculate the fuel creep for fission-gas bubble expansion or contraction in the routine FSWELL.

### 8.7.7 Cladding Thermal Expansion Coefficient

The mean thermal expansion coefficient of the cladding is taken from the Nuclear Systems Materials Handbook [8-17]. It has the form

$$\alpha_m = C_1 (C_2)^{(C_3)^T} \quad (8.7-21)$$

where

$$\begin{aligned}
\alpha_m &= \text{Mean thermal expansion coefficient, } ^\circ\text{F}^{-1} \\
C_1, C_2, C_3 &= \text{Calibration constants} \\
T &= \text{Temperature, } ^\circ\text{F}
\end{aligned}$$

The values for the calibration are given below:

$$\begin{aligned}
C_1 &= 11.397 \\
C_2 &= 0.71828 \\
C_3 &= 0.99890
\end{aligned}$$

This is calculated in the function ALPHC.

### 8.7.8 Cladding Modulus of Elasticity

The cladding modulus of elasticity is taken from the NSHM [8-17] and is given by

$$E_c = 2.833669 \times 10^1 - 2.882211 \times 10^{-3} T - 3.697849 \times 10^{-6} T^2 + 7.709188 \times 10^{-10} T^3 \quad (8.7-22)$$

where

$$\begin{aligned} E &= \text{Modulus of elasticity, Mpsi} \\ T &= \text{Temperature, } ^\circ\text{F} \end{aligned}$$

This is then converted to Pa by multiplying by  $6.894757 \times 10^9$ . This correlation is coded in the function ECLADF.

### 8.7.9 Cladding Ultimate Tensile Strength

The ultimate tensile strength of unirradiated, 20% cold-worked, 316 SS is taken from the NSMH [8-17].

$$\sigma_u = C_0 + C_1 T + C_2 T^2 + C_3 T^3 + C_4 T^4 + C_5 T^5 + C_6 T^6 + C_7 T^7 \quad (8.7-23)$$

where

$$\begin{aligned} \sigma_u &= \text{Ultimate tensile strength, ksi} \\ T &= \text{Temperature, F} \\ C_0 &= 1.220241 \times 10^2 \\ C_1 &= -1.015998 \times 10^{-1} \end{aligned}$$

$$\begin{aligned}
C_2 &= 8.336636 \times 10^{-4} \\
C_3 &= -3.365737 \times 10^{-6} \\
C_4 &= 6.227377 \times 10^{-9} \\
C_5 &= -5.736229 \times 10^{-12} \\
C_6 &= 2.542064 \times 10^{-15} \\
C_7 &= -4.321098 \times 10^{-19}
\end{aligned}$$

This is then converted to SI units by multiplying by  $6.894757 \times 10^6$ .

This correlation is good for temperatures below 1200 K only. For temperatures above 1200 K, the curve is assumed to go to zero at the cladding solidus according to the following equation.

$$\sigma_u = \sigma_u(1200\text{K}) \left\{ 1 - \left[ \frac{T-1200}{T_{mc}-1200} \right]^2 \right\} \quad (8.7-24)$$

where

$$\begin{aligned}
\sigma_u(1200\text{ K}) &= 1.122 \times 10^8 \text{ Pa} \\
T &= \text{Temperature, K} \\
T_{mc} &= \text{Cladding solidus temperature, K}
\end{aligned}$$

Care should be exercised when using the function UTS since it is for unirradiated cladding and may be inconsistent with the option used for the cladding flow stress.

#### 8.7.10 Cladding Flow Stress

There exist four different options available to control the cladding flow stress calculation in the function YLDCF. These are controlled through the input parameter IYLD.

$$\text{IYLD} = 0$$

The value is calculated from the correlation in the NSMH [8-17] for unirradiated, 20% cold-worked, 316 SS. For temperatures below 1200 K the following form is used. It should be noted that this correlation is for the strain rate of the tensile tests and may not be appropriate in many accident cases with high strain rates.

$$\begin{aligned} \sigma_y = & C_0 + C_1T + C_2T^2 + C_3T^3 + C_4T^4 + C_5T^5 + C_6T^6 + C_7T^7 + C_8T^8 \\ & + C_9T^9 + C_{10}T^{10} \end{aligned} \quad (8.7-25)$$

where

$\sigma_y$	=	Clad flow stress, ksi
T	=	Temperature, °F
$C_0$	=	$9.611825 \times 10^1$
$C_1$	=	$-1.262505 \times 10^{-1}$
$C_2$	=	$1.510991 \times 10^{-3}$
$C_3$	=	$-1.021806 \times 10^{-5}$
$C_4$	=	$3.796623 \times 10^{-8}$
$C_5$	=	$-8.438888 \times 10^{-11}$
$C_6$	=	$1.163911 \times 10^{-13}$
$C_7$	=	$-9.993892 \times 10^{-17}$
$C_8$	=	$5.177194 \times 10^{-20}$
$C_9$	=	$-1.477323 \times 10^{-23}$
$C_{10}$	=	$1.780710 \times 10^{-27}$

The value is then converted to Pa by multiplying by  $6.894757 \times 10^6$ .

For temperatures above 1200 K, a form like Eq. 8.7-24 is used for the extrapolation to the melting temperature.

$$\sigma_y = \sigma_y(1200) \left\{ 1 - \left[ \frac{T-1200}{T_{mc}-1200} \right]^2 \right\} \quad (8.7-26)$$

where

$$\begin{aligned} \sigma_y(1200) &= 7.375 \times 10^7 \text{ Pa} \\ T &= \text{Temperature, K} \\ T_{mc} &= \text{Clad solidus temperature, K} \end{aligned}$$

IYLD = 1,2

For these values of IYLD, a flow stress model developed by DiMelfi and Kramer [8-34] is used. If IYLD = 1, the model is temperature, strain, strain rate, and burnup dependent. If IYLD = 2, a high strain rate approximation is used, removing the strain rate dependence.

The flow stress,  $\sigma$ , is defined by

$$\sigma = \sigma_s - (\sigma_s - \sigma_1) \exp(-\hat{\epsilon}/\epsilon_c) \quad (8.7-27)$$

where

$$\begin{aligned} \sigma_1 &= \text{Yield stress of fully annealed, unirradiated material} \\ \sigma_s &= \text{Saturation flow stress approached as } \hat{\epsilon} \text{ increases} \\ \hat{\epsilon} &= \text{Hardness parameter} \\ \epsilon_c &= \text{Material parameter} \end{aligned}$$

The hardness parameter  $\hat{\epsilon}$  has two components;  $\epsilon_p$ , the accumulated equivalent plastic strain, and  $\hat{\epsilon}_\phi$ , the hardness due to irradiation, which is determined from

$$\hat{\epsilon}_\phi = -\epsilon_c \ln (1 - \{1 - \exp[-B(\phi t - \phi_o t_o)]\}^{1/2}) \quad (8.7-28)$$

where

$$\begin{aligned} B &= 3.5 \times 10^{-27}, \text{ m}^2/\text{n} \\ \phi_0 t_0 &= 4.5 \times 10^{25}, \text{ n/m}^2 \\ \phi t &= \text{Neutron fluence, n/m}^2 \end{aligned}$$

and

$$\bar{\epsilon} = \epsilon_p + \hat{\epsilon}_\phi + \epsilon_{cw} \quad (8.7-29)$$

where

$$\epsilon_{cw} = \text{As-fabricated cold-work strain}$$

The relationship between  $\sigma_s$ ,  $\sigma_1$ , and  $\epsilon_c$  is given by

$$\left[ \frac{\sigma_s}{G} - \frac{\sigma_1}{G} \right] \frac{1}{\epsilon_c} = \frac{\theta_1}{G} \quad (8.7-30)$$

where

$$\begin{aligned} \theta_1/G &= 3.66 \times 10^{-2} \\ G &= 92.0 - 4.02 \times 10^{-2} T, \text{ GPa} \end{aligned}$$

This relationship is equivalent to assuming that the initial work-hardening rate  $\theta_1$ , for annealed material ( $\hat{\epsilon} = 0$ ) is constant.

The functions  $\sigma_s$  and  $\sigma_1$  are chosen to be of the form

$$\frac{\sigma_s}{G} = \frac{\sigma_{s0}}{G} \{1 - \exp[-(\hat{\epsilon}_p/\hat{\epsilon}_{0s})^{nk\gamma}]\}^{1/k} \quad (8.7-31)$$

$$\frac{\sigma_1}{G} = \frac{\sigma_{10}}{G} \{1 - \exp[-(\dot{\epsilon}_p/\dot{\epsilon}_{01})^{nk}]\}^{1/k} \quad (8.7-32)$$

where

$$\begin{aligned} \hat{\epsilon}_p &= \text{Equivalent plastic strain rate} \\ n &= \text{Constant} = 1/5.35 \\ k &= \text{Constant} = 2.0 \end{aligned}$$

The functions  $\sigma_{s0}$ ,  $\sigma_{10}$ ,  $\dot{\epsilon}_{0s}$ ,  $\dot{\epsilon}_{01}$  are all temperature dependent. The constant  $k$  is a nonphysical parameter that governs the sharpness of the transition between strain-rate-dependent and strain-rate-independent behavior.

If  $IYLD = 2$ , then the above relationships for  $\sigma_s$  and  $\sigma_1$  are assumed to have the form

$$\frac{\sigma_s}{G} = \frac{\sigma_{s0}}{G} \quad (8.7-33)$$

and

$$\frac{\sigma_1}{G} = \frac{\sigma_{10}}{G} \quad (8.7-34)$$

In both cases,  $IYLD = 1$  or  $IYLD = 2$ , the following functions are used

$$\frac{\sigma_{s0}}{G} = 2.06 \times 10^{-3} + \frac{7.12 \times 10^{-1}}{T} \quad (8.7-35)$$

$$\frac{\sigma_{10}}{G} = 2.00 \times 10^{-2} - 9.12 \times 10^{-6} T \quad (8.7-36)$$

The functions  $\dot{\epsilon}_{0S}$  and  $\dot{\epsilon}_{01}$  are strong functions of temperature and are related to the dominant creep mechanism. This is assumed to be thermally activated, so Arrhenius relationships are used.

$$\dot{\epsilon}_{0S} = \dot{\epsilon}_{00S} \exp(-Q/RT) \quad (8.7-37)$$

$$\dot{\epsilon}_{01} = \dot{\epsilon}_{001} \exp(-Q/RT) \quad (8.7-38)$$

where

$$Q/R = 38,533, \text{ K}$$

$$\dot{\epsilon}_{00S} = 1.062 \times 10^{14}, \text{ s}^{-1}$$

$$\dot{\epsilon}_{001} = 3.794 \times 10^{12}, \text{ s}^{-1}$$

Given the above constants and relationships, it is then possible to calculate the flow stress of the cladding.

$$IYLD = 3$$

With this selection, the input flow stress table YLDTAB with its corresponding temperature table YLDTEM are searched to find the flow stress as a function of temperature. One table exists for each cladding type.

#### 8.7.11 Thermal Conductivity of Helium

The thermal conductivity of the helium in the fuel pin free volume is temperature dependent and has been fit to the following equation [8-35].

$$K = 1.43 \times 10^{-1} + 3.17 \times 10^{-4} (T-273) - 2.24 \times 10^{-8} (T-273)^2 \quad (8.7-39)$$

where

- K = Thermal conductivity,  $\text{W m}^{-1} \text{K}^{-1}$
- T = Gas temperature, K

This is used in the function routine HGAP.

#### 8.7.12 Thermal Conductivity of Fission Gas

All fission gas is assumed to be xenon. A functional form of the xenon conductivity [8-35] is used in the function routine HGAP.

$$K = 5.15 \times 10^{-3} + 1.69 \times 10^{-5} (T-273) - 3.50 \times 10^{-9} (T-273)^2 \quad (8.7-40)$$

where

- K = Thermal conductivity,  $\text{Wm}^{-1} \text{K}^{-1}$
- T = Gas temperature, K

#### 8.7.13 Mixed Oxide Fuel Hardness

In DEFORM-4 it is assumed that conditions could arise where either the fuel or cladding could be the softer material when considering fuel-cladding contact in the determination of the gap conductance. The following equation is therefore used to determine the oxide fuel hardness [8-21].

$$H = 6.009 \times 10^9 \exp (-T/641) \quad (8.7-41)$$

where

- H = Meyer hardness, Pa
- T = Temperature, K

#### 8.7.14 Cladding Hardness

The cladding hardness is calculated from the following equation [8-21] when comparing with the fuel hardness. The softer of the fuel or cladding is used in the solid-to-solid gap conductance considerations.

$$H = 5.961 \times 10^9 T^{-0.206}, T < 893.92 \text{ K} \quad (8.7-42)$$

$$H = 2.75 \times 10^{22} T^{-6.53}, T > 893.92 \text{ K} \quad (8.7-43)$$

where

H = Meyer hardness, Pa

T = Temperature, K

#### 8.7.15 Cladding Fast Creep

Kramer and DiMelfi [8-34] have shown that the following equation is suitable for plastic strain of cladding at high temperatures.

$$\dot{\epsilon} = \frac{\dot{\epsilon}_{00s}}{\sigma_{so}^n} \sigma^n \exp(-Q_c/T) \quad (8.7-44)$$

where

$\dot{\epsilon}$  = Plastic strain rate,  $s^{-1}$

$\sigma$  = Equivalent stress in the cladding, Pa

T = Temperature, K

$\dot{\epsilon}_{00s}$  =  $1.062 \times 10^{14}$ ,  $s^{-1}$

$\sigma_{so}$  = Material constant defined in Eq. 8.7-35

n = Stress exponent = 5.35

$$Q_c = \text{Creep activation constant} = 38,533 \text{ K}$$

This allows for plastic deformation of the cladding below the flow stress.

#### 8.7.16 Material Properties of Metal Alloy Fuel

Material properties for the metal fuels under consideration for the Integral Fast Reactor concept are currently under investigation in order to prepare a set of recommended values for use by the safety community. Unlike the oxide fuel which has been under study for a number of years, the metal fuel data is fairly sparse and limited to specific fuel types. Therefore, the correlations given below are to be considered preliminary in nature, but they should provide results that are consistent with future results. These have been coded into DEFORM in a manner that makes future modifications a simple replacement task.

Several thermal properties are also used by DEFORM and these have been addressed in Chapter 10 of this document. Most of the properties given below are obtained from a survey of data carried out for the modification of the FPIN code to analyze metal fuels [8-36].

##### 8.7.16.1 Modulus of Elasticity

Although the modulus of elasticity varies with temperature, composition, and phase, a single average value has been used.

$$E_f = 1.4 \times 10^{12} \tag{8.7-45}$$

where

$$E_f = \text{Modulus of elasticity, Pa}$$

##### 8.7.16.2 Poisson's Ratio

Poisson's ratio is an input parameter to the SAS4A code. For both the ternary and fission alloy fuels the currently recommended value is 0.23.

### 8.7.16.3 Fracture Strength

Unlike the oxide fuels, the metal fuel does not exhibit a fracture phenomenon. While there does appear to be a separation between the phases that result in the ternary fuels, there is no radial cracking. This appears to be the result of the softness of the metal matrix and the inherent structural differences that exist between ceramics and metals. When metal fuel has been specified, the function SIGFRA returns a large value for the fracture strength to avoid cracking during the mechanical calculations.

### 8.7.16.4 Fuel Creep Rate

One of the more important correlations used by DEFORM is the creep rate of the fuel because of its influence on the rate of fuel swelling through the process of fission gas bubble volume change. For the metal fuels the creep rate, determined in a study performed by John Kramer [8-37], has been employed for both types of metal fuel currently considered in DEFORM.

For uranium phases existing below 973 K, the rate is dependent on two stress related terms.

$$R_c = (0.5 \times 10^4 \sigma + 6.0 \sigma^{4.5}) \exp(-26168/T) \quad (8.7-46)$$

where

$R_c$  = Fuel creep rate,  $s^{-1}$

$\sigma$  = Stress, MPa

$T$  = Temperature, K

For the high temperature gamma uranium phase, the rate is given by a single stress dependent function.

$$R_c = 8.0 \times 10^{-2} \sigma^3 \exp(-14353/T)$$

(8.7-47)

The time constant for bubble expansion is the inverse of the calculated creep rate. These functions are coded into the subroutine FSWELL.

## REFERENCES

### NOTICE

Several references in this document refer to unpublished information. For a list of available open-literature citations, please contact the authors.





